technische universität
dortmund

rp° | fakultät raumplanung

Assessment of renewable energy potentials based on GIS and RS- A case study in China

by

Jie Zhang

A doctoral dissertation submitted to the Faculty of Spatial Planning at TU Dortmund University in partial fulfilment of the requirements for the degree of Doctor of Engineering

Dissertation Committee:

First supervisor:	**Univ.-Prof. Dr. habil. Nguyen Xuan Thinh**
Second supervisor:	**Univ.-Prof. Dr. Dietwald Gruehn**
Examiner:	**Dr. Jörg Fromme**

Acknowledgement

Foremost, I would like to thank my supervisor Univ.-Prof. Dr. habil. Nguyen Xuan Thinh for providing me a chance to pursue a Dr. degree in the TU Dortmund University. He has given me the scientific suggestions on my study and instructed me to finish my PhD thesis. I am sincerely grateful for his patience, motivation, enthusiasm and immense knowledge in GIS.

I am also very grateful to Univ.-Prof. Dr. Dietwald Gruehn for his support and valuable suggestions on my final thesis.

I will forever be thankful to my colleges in TU Dortmund University, Department of Spatial Information Management and Modelling, who gave me valuable comments and supports during my PhD study.

Without the scholarship from China Scholarship Council it was impossible to do my PhD research.

For the non-scientific side of my thesis, I particularly want to thank my friends (too many to list here but you know who you are!) for providing support and friendship that I needed.

I truly thank my mom, dad and brother for sticking by my side during my good and bad times. They always have faith in me and my intellect even when I felt like digging hole.

Finally, the unique thanks should belong to my husband. As I believe, accompany is the most powerful confession of love. He was always by my side even when I was irritable and depressed. These past several years were not an easy ride, both academically and personally.

Abstract

As increased energy demand, global warming and other environmental problems caused by the use of fossil fuels have brought severe challenges to China, the Chinese government has set targets to improve the share of renewable energy in the energy structure and promote the construction of wind, photovoltaic and other renewable energy power plants. In this study, the researcher develops a geographic information system (GIS) and remote sensing (RS) based methodology to assess renewable energy potentials in a specific study area at a regional scale from the view of spatial planning. The specific aims of the study are: (1) to quantify and map the wind energy, solar energy and bioenergy potential from a theoretical level to an economic level. (2) to define the social and environmental restrictions for wind, photovoltaic and biomass power plants, and (3) to analyze land suitability for wind, photovoltaic power plants and to find the optimal locations for biomass power plants.

The research used the wind speed extrapolation model, Weibull distribution, wind power density and wind energy estimation models to assess theoretical and technical wind energy potential. Theoretical and technical solar energy potential were evaluated using the Bristow and Campbell model, and the solar energy estimation model. Land suitability analysis for wind and Photovoltaic (PV) power plants was implemented using the multi-criteria method. In addition, the unit generation costs of wind power and solar power were calculated, and bioenergy potential was derived from net primary productivity (NPP) through generic model. The optimal locations of biomass power plants were identified using network analysis tools in ArcGIS. One creative research view is that the researcher combined renewable energy policy and economic factors, such as cost and price, to estimate the economic potential of renewable energy. Thus, through the analysis of different scenarios, the effects of incentives contained in renewable energy policy become apparent.

The results of this thesis provide not only the total quantitative amount of renewable energy potential, but also identify the spatial distribution of wind, solar and bioenergy potential. In the study area, including Hebei Province, Beijing and Tianjin, the economic wind potential under current renewable energy policy is 34 TWh, and the economic installed capacity is 32 GW. The eligible area for wind projects

occupies 21,543 km^2, which is enough for 108 GW installed wind power capacity. Maintaining the current energy policy and improving transmission lines and local grids are crucial for further development.

Under current energy policy, solar energy using PV technology has no economic potential. However, the total technical potential over the region is estimated to be 2,379 TWh/year for large-scale PV plants. A slight increase in subsidy and prioritising the decentralisation of small-scale PV plants are suggested for the development or solar energy in the future. Most of the suitable areas are distributed across the north-western part of the study area, on the Bashang Plateau, and cover 10,634 km^2.

Moreover, the technical biomass power potential in the study area is 214 TWh. The economic analysis results based on 12 MW installed capacity and 30 MW installed capacity case studies indicate that biomass power plants can be profitable without subsidy. The incentives offered under the present energy policy are sufficient to stimulate biomass energy development.

The methodology employed in this study can be used in other study area to assess renewable energy potential. Energy project developers can identify new profitable areas based on the land suitability analysis results in this study, and policy makers can define different parameters (such as restricted areas and energy incentive policy) to analyse their effects on power generation.

Table of Contents

List of Tables

List of Figures

List of Abbreviations

AGB	Above Ground Biomass
AHP	Analytic Hierarchy Process
ANN	Artificial Neural Networks
ANP	Analytic Network Process
ARIMA	Autoregressive Integrated Moving Average
AVHRR	Advanced Very High Resolution Radiometer
BGPG	Biomass Gasification and Power Generation
CHP	Combined Heat Power
CI	Consistency Index
CPS	Concentrated Photovoltaic Systems
CR	Consistency Ratio
CSP	Concentrated Solar Power
DSS	Decision Support Systems
EIA	Energy Information Administration
ELECTRE	Elimination and Choice Translating Reality
ETM	Landsat Enhanced Thematic Mapper
FIT	Feed-in-Tariff
GMS5	Geostationary Meteorological Satellite
GPP	Gross Primary Productivity
IEA	International Energy Agency
IPCC	Intergovernmental panel on Climate Chang

MADM	Multi-Attribute Decision Making
MCDM	Multi-Criteria Decision Methods
METEOSAT	Meteorological Satellite
METSTAT	Meteorological/Statistical Solar Radiation Model
MODIS	Moderate Resolution Imaging Spectroradiometer
MODM	Multi-Objective Decision Making
NCAR	National Center for Atmospheric Research
NCEP	National Center for Environmental Prediction
NDRC	National Development and Reform Commission
NOAA	National Oceanic and Atmospheric Administration
NPP	Net Primary Productivity
OECD	Organization for Economic Cooperation and Development
PROMETHEE	Preference Ranking Organization Method for Enrichment Evaluation
PV	Photovoltaic
R&D	Research and Development
RS	Remote Sensing
SAR	Synthetic Aperture Radar
SRTM	Shuttle Radar Topography Mission
TM	Landsat Thematic Mapper
TRMM	Tropical Rainfall Measuring Mission satellite
USGS	US Geology Survey

VAT	Value Added Tax
WAsP	Wind Atlas Analysis and Application Program
WRF	Weather Research and Forecasting

1 Introduction

1.1 Motivation

Based on data from the Population Division of the United Nations and projections from the world's two main energy agencies, the International Energy Agency (IEA) and the Energy Information Administration (EIA), total world energy consumption will increase from 505 quadrillion British thermal units (Btu) in 2008 to 619 quadrillion Btu in 2020 and 770 quadrillion Btu in 2035 (Figure 1.1). Most of the growth in energy consumption occurs in countries outside the Organization for Economic Cooperation and Development (non-OECD nations), where energy demand is driven by strong long-term economic growth. In the reference case, energy use in non-OECD nations is set to increase by 85 percent, compared with 18 percent in OECD economies (EIA, 2011). China, with its economic growth of more than 7% in 2013, continues to face a sharp increase in energy consumption: since 2009, energy consumption in China exceeds that in the United States (Word Energy Council, 2013) and China has become the largest energy consumer in the world.

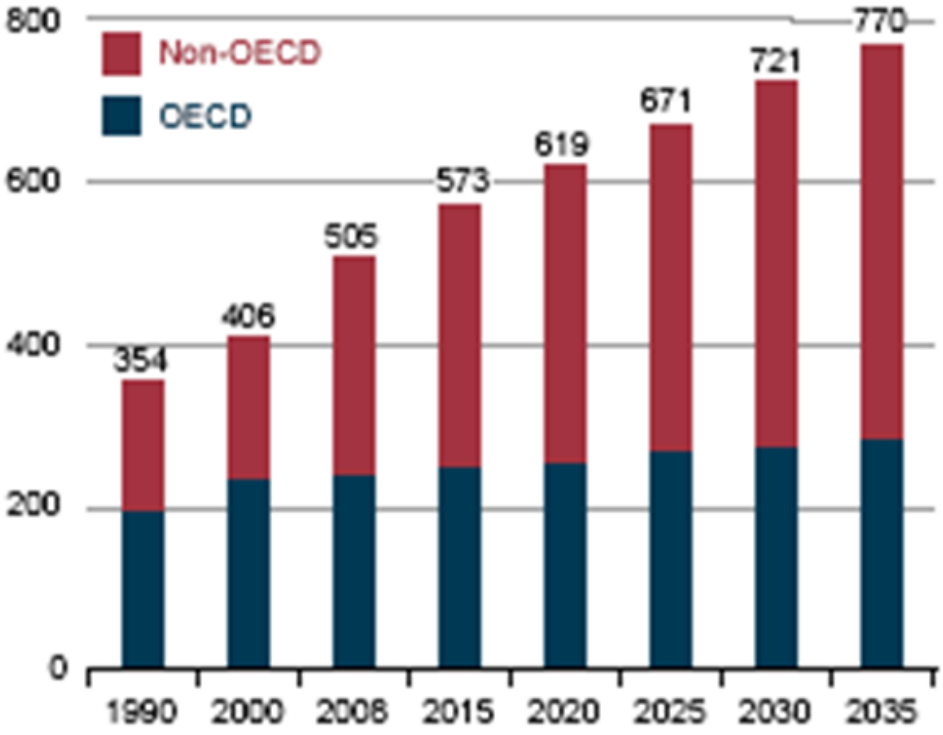

Figure 1.1: World energy consumption, 1990 – 2035 (quadrillion Btu)

Source: International Energy Outlook 2011

Fossil fuels are expected to continue supplying much of the energy used worldwide (Figure 1.2) (IEA, 2011). The use of fossil fuels produces significant negative environmental effects, especially the rise of carbon dioxide (CO_2) emissions. World CO_2 emissions are expected to increase from 30.2 billion metric tons in 2008 to 35.2 billion metric tons in 2020 and 43.2 billion metric tons in 2035 (IEA, 2011). Since 2006, China's CO_2 emissions from fossil fuel use and industrial processes have been the highest in the world and China tops the list of CO_2 emitting countries (IEA, 2011). In 2013, CO_2 emissions reached 10 billion tons, accounting for 30% of global CO_2 emissions (Netherlands Environmental Assessment Agency, 2013). With increased of CO_2 emissions from the use of fossil fuels, the issue of global warming is becoming a great challenge for the international community. According to the Intergovernmental Panel on Climate Change, averaged over all land and ocean surfaces, temperatures increased roughly 1.53 °F (0.85 °C) from 1880 to 2012 (IPCC, 2013).

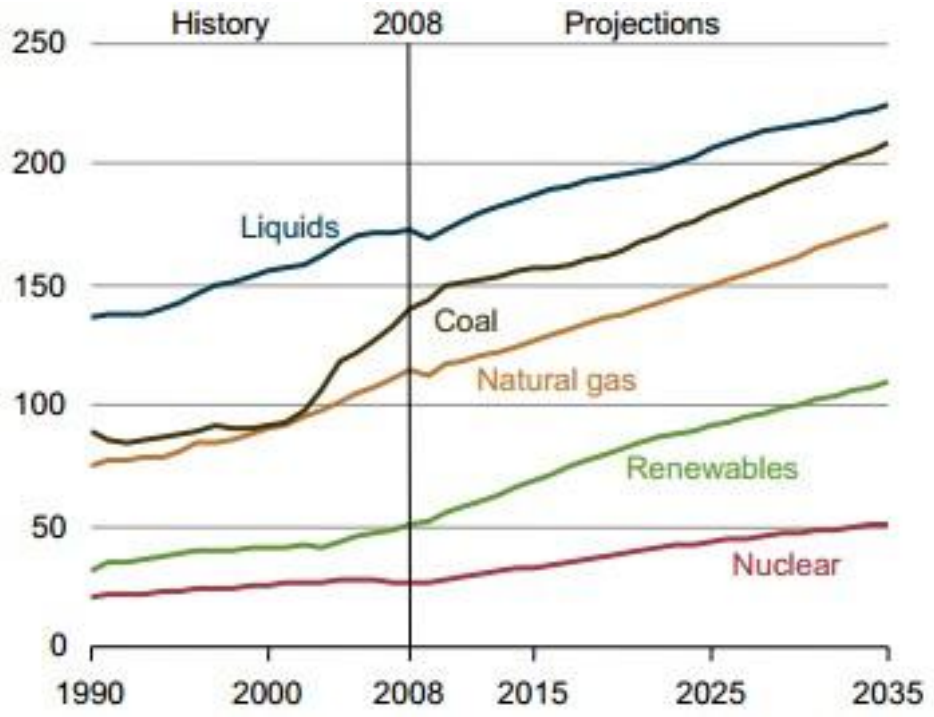

Figure 1.2: World energy consumption by fuel, 1990 - 2035 (quadrillion Btu)

Source: International Energy Outlook 2011

In China, the large population and strong economic growth cause high energy consumption, while large domestic coal reserves lead to the wide use of coal for electricity generation and industrial processes. Total electricity generation in 2013

was 5168.7 TWh, which increased approximately 7% in 2014 (China Statistics Bureau, 2013). More than 70% of electricity is produced using coal power plant; the installed coal-fired capacity in China is set to nearly double from 2008 to 2035, and coal use in China's industrial sector will grow by 67% (EIA, 2011). Hence, greater focus on the environmental problems caused by CO_2 emissions is required.

The increased energy demand and the environmental consequences of greenhouse gas emissions have driven the Chinese government to support a substantial increase in renewable energy sources, as substituting fossil fuels with renewable energy sources is regarded as a significant measure for satisfying the increased demand for energy while reducing global carbon emissions. Full use of renewable energy sources can help to mitigate global warming in environmental terms and also meet energy needs in economic terms (Yue & Wang, 2006). China has set the target that the share of renewable energy in the energy structure shall reach 20% by 2020 according to the 12th national five-year plan (Yue & Wang, 2006). Viable renewable energy sources include wind, solar and biomass energy.

Wind power comprises the largest development and market-oriented utilization of renewable resources. Over the last six years, the wind power industry has formed 30% of global annual installed capacity growth and created 300,000 new jobs worldwide in a global business worth $40 billion annually (Grassi et al., 2012). By the end of June 2012, grid-connected installed wind power capacity in China reached 52.58 GW; the total wind-installed capacity may reach 70 GW by 2015. It is planned that the annual output reached 140 TWh (He et al., 2013).

Solar power is the conversion of sunlight into electricity, directly using photovoltaic (PV) technology or indirectly using concentrated solar power (CSP). PV electricity is one of the sustainable energy options available worldwide, and PV development in China began in 2009 increasing at an annual rate of 200 to 300% (China Electricity Council, 2013). Since 2009, the Chinese government has promoted the constructions of PV power plants, especially in the northwestern region of China because of abundant solar energy and barren land cover. In 2009, China increased the installed PV capacity of 160 MW to a total installed capacity of 300 MV, while in 2013, the 11GW PV capacity increased to a total installed capacity of 17GW (China Electricity Council, 2013). At present, the global PV market is growing at an annual

rate of 35% to 40%, and the total installed capacity in China accounts for 40% of global installed capacity. By 2015, the total installed PV capacity is planned to reach 10 GW (Sun et al., 2013).

Biomass as a renewable and carbon neutral fuel is a sustainable energy source, because when biomass is used for energy, it decreases environmental pollution caused by Sulphur oxides (Sox) and nitrogen oxides (NOx) emissions and net CO_2 emissions (Liao et al., 2004). Biomass resources can be grouped into wood residues generated from wood products industries; agricultural residues generated by crops, agroindustry and animal farms; energy crops (that is, crops and trees dedicated to energy production); and municipal solid waste (Easterly & Burnham. 1996). Biomass is used as fuel for direct heating in industrial or domestic applications, in the production of steam for electricity generation and for the production of gaseous or liquid fuels (Voivontas et al., 2001).

The total output of straw resources in China in 2005 reached 841 million tons, which formed 62% of global straw resources (Bi et al., 2009). Moreover, half the population of China lives in rural areas, according to the data of the 6th national census, and biomass residues are widely used for cooking and heating in rural households, although at low efficiency (MOA/DOE Project Expert Team, 1998). Thus, the Chinese government has focused on the development and utilization of biomass as an energy resource since 1998, and it has conducted long-term and wide-ranging R&D on the latest biomass energy conversion technologies through the National Program for Key Science and Technology projects (MOA/DOE Project Expert Team, 1998).

The deteriorating environment, increasing energy demands, and incentives contained in renewable energy policy provide a promising outlook for renewable energy development in China. Wind, solar and biomass energy all are derived from the sun, which supplies a constant flow of energy to the earth (Hoogwijk, 2004). In addition, wind, solar and biomass energy are endowed with enormous potential to supply energy. To utilize renewable energy in a scientific manner, the assessment of renewable energy potential and mapping of the spatial distribution of renewable energy potential is the first crucial step.

1.2 The potential of wind, solar and biomass energy

The potential availability of wind, solar and biomass energy in different regions varies not only by the theoretical resource availability (theoretical limit) but also by geographical conditions, such as land-use demands; by technology characteristics, such as innovative conversion technologies; and by economic developments, such as investment cost, or operation and maintenance cost, and revenue. When studying the potential of renewable energy sources, aspects such as geographical, technical and economic development must be considered. Therefore, different types of potentials can be defined, such as the categories introduced by Wijk and Coelingh (1993):

• The theoretical potential is the theoretical limit of the primary resource. For solar-driven sources, this is solar energy or solar energy converted to wind or biomass.

• The geographical potential is the theoretical potential reduced by the energy generated in areas considered available and suitable for this production.

• The technical potential is the geographical potential reduced by the losses of the conversion of the primary energy to secondary energy sources. The technological potential is defined by the energy that can be harvested using existing technology.

• The economic potential is the total amount of technical potential derived at cost levels that are competitive compared to those of alternative energy applications. Thus, the economic potential is defined as the energy that can be harvested using economically feasible installations. Infrastructure or technical constraints (road and grid network) and economic aspects (energy production cost and expected profits) fix the limits of economic potential, and subsidies and other policy incentives can boost economic potential.

In this study, the researcher assesses the theoretical, geographical, technical and economic potential of wind and solar energy. Biomass energy potential is determined through the assessment of usable biomass potential and economic analysis, as biomass energy differs from wind and solar energy in that biomass must be transported to power plants. Thus it is impossible to evaluate the spatial distribution of the economic potential of biomass because transport costs must be

calculated based on a specific study and the economic analysis should be based on a specific case study or a specific project.

The Wind and Solar Resource Centre of China Meteorology Administration has published data on wind resource distribution in China in 2009. However, the evaluation is based on the numerical simulation model and the research field is the entire country. Similarly, solar resources were evaluated based on measurement results from meteorological stations. Several researchers focused on wind and solar resource evaluation in specific regions, yet most studies and researches assessed only the theoretical potential; few researchers evaluated technical potential, economic potential considering the technology, economic aspects and energy policies. Bioenergy resource assessment has received little attention, and this gap should be addressed in the near future. In contrast, this study includes an assessment of not only theoretical potential but also technical aspect, the economic potential of renewable energy in light of technology, energy policies and economic factors.

1.3 Research objectives and questions

The main objective of this study is to present a GIS-based method to assess renewable energy potential at a regional scale. The research results provide renewable energy project investors and planners with scientific information regarding renewable energy potential and suggestions for renewable energy development in the near future. To achieve this general objective, specific research objectives have been formulated:

(1) To quantify and map wind energy, solar energy and bioenergy potential

Wind speed, solar radiation, biomass residues, technology, economic factors and renewable energy policies determine renewable energy potential. Wind power density and solar radiation are indicators of the theoretical potential of wind and solar energy; geographic conditions and technology determine technical potential, namely annual energy yield; and the current energy price, cost of renewable energy plants, and renewable energy policies have the influence economic potential.

(2) To define the social and environmental restrictions for wind power, photovoltaic and biomass power plants

Due to the social and environmental restrictions on the construction of power plants, restricted areas identified by social and environmental restrictions should be excluded.

(3) To analyze land suitability for wind and photovoltaic power plants, and to find the optimal locations for biomass power plants.

Several aspects should be considered when planning the locations of power plants: the transportation cost of biomass is a major element in finding the optimal location for biomass power plants and the transportation and installation of wind turbines play an important role for wind power plants. When determining the locations of wind, photovoltaic and biomass power plants, different standards and methods are considered.

Furthermore, the researcher answers the following questions:

a. Which types of renewable energy potential are assessed in this thesis?
b. Which types of renewable energy technologies are adopted in this thesis?
c. What indicators are used to express the theoretical potential, geographical potential, technical potential and economic potential of wind energy and solar energy?
d. What indicators are used to express biological biomass potential and usable biomass potential?
e. How are wind, solar and bioenergy potential based on GIS and RS assessed in the given study area?
f. Which types of restrictions should be considered when positioning power plants?
g. How can one find the optimal sites for biomass power plants and suitable area for wind and PV power plants?
h. How have policies regarding renewable energy incentives influenced the development of renewable energy?

1.4 Outline of the thesis

This consists of six chapters. Chapter 1 introduces the motivation of the research work, concept of renewable energy potential, research objectives and research

questions. In Chapter 2 a review of current research is presented with the research methods related to the assessment of wind, solar energy and biomass energy potential examined separately. Chapter 3 begins with an introduction to the study area before information regarding the renewable energy development situation and energy policy in the study area is supplied. The data used in this study is listed at the end of Chapter 3, and the methodologies used to assess wind, solar and biomass energy potential are described in Chapter 4. The framework of the study includes methods used in the analysis of theoretical potential, the definition of geographical restrictions for power plants, and the analysis of technical energy and economic potential analysis and land suitability analysis for power plants. Chapter 5 contains the results and discussion of the research, including renewable energy potential, sensitive analysis and land suitability levels for power plants. In Chapter 6, the researcher summarizes the main findings of this research and gives an offers suggestions for further study.

2 Review of current research

As renewable energy is the trend for future energy sources, assessing renewable energy potential, locating sites for wind and solar farm installation, and identifying and characterizing the potential for biomass utilization are unavoidable topics. Renewable energy is emerging as a sustainable, environmentally friendly and long-term cost-effective energy. Wind speed, solar radiation and biomass amounts are the major elements that determine the potential of renewable energy resources. Accessibility is limited by geographical conditions, such as terrain conditions, nature reserves; hence, a GIS database that contains data on wind, solar radiation, biomass amounts, topography, urban areas and special activities is essential for the evaluation of renewable energy potential. The main advantages of using GIS technology is its flexibility in handling data the available on different levels of spatial analysis and its ability to highlight the spatial interrelations between data sets (Voivontas, 1998). GIS is used not only for storing and managing digital data, but also for spatial analysis. Moreover, RS technology provides a rapid method to obtain land use information and monitor land use change.

The improvements in GIS technology, the availability of spatial data and the growing interest in renewable energy multiplied the number of studies conducted not only on the estimation of solar (Nguyen & Pearce, 2010) and wind energy potential (Sliz-Szkliniarz & Vogt 2011; Janke, 2010) but also on the estimation of bioenergy potential (Shi et al., 2008). In addition, in recent years, the large-scale integration of renewable energy in the landscape has piqued researchers' interest in the application of GIS in the field of social acceptance (Serwan & Baban 2001; Simão et al., 2009; Grassi et al., 2012).

Renewable energy resources can replace conventional sources of energy. Renewable energy decision making is considered a multiple-criteria decision-making problem because of the increasing complexity of the related social, technological, environmental and economic factors, and traditional single criterion decision-making approaches can't manage the complexity of current systems in addressing this problem (Abu-Taha, 2013). The multi-criteria decision method (MCDM) provides a flexible tool that can manage and bring together a

wide range of variables appraised in different ways and, thus, offers decision makers useful assistance in solving the problem (Abu-Taha, 2013).

Several projects utilize GIS in the field of renewable energy: many of them employ GIS applications in the resolution of localization problems or in resources evaluation for specific sources (Domínguez-Bravo et al, 2007). In this field, studies of wind farm siting, photovoltaic electrification and biomass evaluation stand out (Domínguez-Bravo et al., 2007). In the following paragraphs, the researcher separately examines the current research status of the assessment of wind, solar and biomass energy potential and MCDM.

2.1 Assessment of wind energy potential

Wind power is one form of renewable energy expected to be commercially successful, mainly because wind energy can be economically viable and does not produce any physical pollution (Serwan & Baban, 2001). Voivontas et al. described one of the pioneer projects in 1998, and since then, GIS has been used for renewable energy site selection at the local, regional, and national levels.

Through their research, Voivontas et al. (1998) intended to identify areas with high wind energy potential to site wind farms. Based on the normalization of each potential type and the determination of the restrictions applicable, theoretical, available, technological and economically exploitable potential were selected as the different layers of renewable energy potential concepts. Wind resources determine the theoretical potential for wind energy and the available potential depends on the restrictions imposed by local characteristic. Thus, Voivontas et al. (1998) assessed wind energy potential using sequential steps:

1. Estimation of the existing wind energy system potential

2. Assessment of the restrictions imposed by local characteristics

3. Evaluation of the restrictions imposed by the available technology

4. Assessment of the expected economic profits

Voivontas's research is the first application of GIS in estimating the potential of renewable energy resources over a large area and a GIS database with data on wind, topography, urban areas, and special activities was developed and used

for the evaluation of theoretical potential through the spatially continuous mapping of renewable energy resources (Voivontas, 1998).

In the Uited Kingdom, Serwan & Baban (2001) developed a GIS-assisted approach to siting wind farms. In this model, public participation is implemented through questionnaires about the criteria for locating wind farms: 112 questionnaires were distributed to gather information about the criteria used to locate new areas suitable for wind farms. After collecting responses from the public, the criteria are justified by considering previous research and existing planning principles. Criteria from different constraint factors, such as topography, wind direction, land use, population, access, economy and hydrology as well as historic and cultural resource, determined the final wind farm location. The weight for each criterion is allocated based on a pairwise comparison for the relative importance of the two criteria by rating rows relative to columns and entering the rating into a matrix (Serwan & Baban, 2001). This overlay methodology is different from the steps used in the research of Voivontas et al. However, both methodologies consider physical resources, the accessibility of planning and economic feasibility, which provides guidance in the systematic exploration of renewable energy potential, from theoretical potential to economic potential.

In the above research examples, with the spatial analysis and data management function of GIS, how to find a reasonable location for wind farms was considered a key question. Wind speed maps, which indicate wind resources, were used directly as input data in the research. Nevertheless, in some cases, wind resource evaluation is considered the central task because wind characterization in terms of speed, direction and power is the first step in determining the initial feasibility of generating electricity from wind power through a wind farm in a given region (Nedaei, 2012). Numerous studies have been undertaken in different countries, and these studies can be classified according to methods used to conduct them:

The first study category includes research that involves the analysis of wind speed data from meteorological stations, while considering wind turbine characteristics to predict annual energy generation. Hossain (1989) estimated annual wind energy generation in Antarctica, India using Weibull distribution based on wind speed data. Similarly, Ahmed et al. (2006) assessed wind power

potential for coastal areas in Pakistan using available meteorological data. They examined wind speed pattern, extractable wind power, wind energy and associated Weibull parameter and the results indicate which locations offer the greatest wind power potential. Zhou et al. (2006) and Elamouri & Ben Amar (2008) used modified power law and the Weibull distribution model to analyze wind energy potential in the Pearl River Delta region, China and Tunisia respectively. The results include not only wind potential, but also an analysis of seasonal variation. The study of the monthly forecasts of the average wind speed in Portugal and Cadenas et Rivera in the south coast of Oaxaca, Mexico adopted the autoregressive integrated moving average (ARIMA) and artificial neural networks (ANN) methodologies for the treatment of wind time series (Rio et al. 2006; Cadenas, Rivera 2007; Kose et al., 2004). The shortcoming of these studies is that only the wind energy for each specific measurement station is estimated, which does not indicate wind energy potential over a geographical area. This problem can be solved by using the numerical model and GIS methods.

The second category includes studies involving the extrapolation of wind speed over a geographical area with the use of the numerical model. Jackson & Hunt's (1975) theory provided a basis for numerically modelling two-dimensional steady-state turbulent flow over a low hill. According to their theory, the surface Rossby and Reynolds numbers are assumed large enough for the wind profile in most parts of the boundary-layer to be logarithmic. The air flow is separated into inner and outer regions, and the governing momentum equations are linearized using scale analysis and assuming a uniform rough surface and small slope. The inner flow is under the balance of perturbation stress, inertia stress and pressure gradient, while the outer flow is characterized by a pressure gradient driven by irrational flow (Yu et al., 2006).

Application of the theory to wind energy study led to the development of the two most popular microscale-modelling products: WAsP (Mortensen et al., 1993) and MsMicro (Walmsley & Salmon 1989; Yu et al. 2006). The Department of Wind Energy at the Technical University of Denmark introduced WAsP for predicting wind climates, wind resources, wind power productions from wind turbines and wind farms in micro scale. The program includes a complex terrain-flow model, a roughness change model and a model for sheltering obstacles (Yu et al., 2006).

Buflasa et al. (2008) used WAsP modelling to assess wind resources for the Kingdom of Bahrain, while Troen & Petersen (1989) describe the procedure of wind resource assessment using a microscale model. Microscale models can be applied to a horizontal domain of hundreds of square kilometers at a grid spacing of 0.1 km if long-term observation data is available for nearby areas. However, mesoscale effects are ignored in these microscale models (Yu et al. 2006).

Mesoscale models can be used to estimate the wind resource while considering mesoscale phenomena, such as the channeling effect of wind by wide valleys, if large-scale climatological forcing is correctly specified. The Wind Energy Simulation Toolkit (WEST) is a mesoscale model developed by the meteorological service of Canada for use by the wind energy industry. WEST is based on a statistical dynamic downscaling approach that is conducting a statistical analysis of climate data to determine the basic atmospheric states and a dynamic adaptation of each basic state to high-resolution terrain and surface roughness by using mesoscale and microscale models (Yu et al., 2006). Pinard et al. (2005) used the WEST model to simulate wind resource for mountainous terrain in the Yukon.

Another currently widely scientifically accepted mesoscale numerical model is the Weather Research and Forecasting (WRF) Model, presented by the National Center for Atmospheric Research in the United States. This model is a next-generation mesoscale numerical weather prediction system designed to serve both atmospheric research and operational forecasting needs, and it is suitable for a wide range of meteorological applications across scales ranging from meters to thousands of kilometers (WRF, 2014). Storm et al. (2009) investigated wind energy potential over western Texas and southern Kansas using the WRF model. The results indicate that the WRF can capture some of the essential characteristics of observed nocturnal low-level jet and thus offers the prospect of improving the accuracy of wind resource estimates and short term wind energy forecasts.

Other mesoscale models, such as CALMET, have proven to be particularly suitable for complex terrain, as well as large areas and long-term simulations. Furthermore, its use to properly downscale prognostic models for wind resource

assessment purposes has been proven, for example, in combination with Fifth-Generation NCAR/Penn State Mesoscale Model (MM5). Yim et al. (2007) investigated the wind energy potential in Hong Kong, a region with a complex terrain, by coupling the prognostic MM5 mesoscale model with the CALMET diagnostic model to produce high-resolution wind fields. The MM5 model wind field (1.5 km horizontal resolution) output was input into the CALMET diagnostic meteorological model every hour while following an objective analysis procedure using all available observations. The results identified the locations of the highest wind energy potential in Hong Kong down to 100 m resolution.

Thus, the numerical simulation model is used to simulate the surface boundary layer flow in complex terrain to overcome the limitations of simple interpolation or extrapolation of observation data. However, the numerical simulation model requires the support of a super computer because of the heavy simulation workload and the work is time consuming. Under the limited conditions created by the lack of a super computer, it is impossible to investigate wind energy resources over a large area.

The third study category involves the extrapolation of wind speed over a geographical area based on a GIS platform. The evaluation of global wind power conducted by the Department of Civil and Environmental Engineering at Stanford University. This study intended to quantify the world's wind power potential from measured data in surface stations and sounding stations. Wind speed and temperature data from the National Climatic Data Center and Forecast Systems Laboratory for the years 1998-2002 were used to generate maps. To obtain estimates of wind speed at 80 m at all sites (sounding, surface and buoy stations), a revised version of the least square methodology was used. A map of wind speed extrapolated to 80 m indicates the high potential of wind energy (Archer, 2005). Nevertheless, the interpolation or extrapolation of observation data has limitations. One major limitation is that the distribution of measurement stations is uneven, which leads inaccuracy. In regions where few measuring stations are located, inaccuracy can be so significant that it cannot be dismissed.

Similarly, in a study conducted in India by Hossain et al. (2011), the researcher assessed wind energy potential using GIS platform, wind speed measurements

and NCEP/NCAR reanalysis data. This methodology involves computation of wind speeds at boundary layer level through vertical extrapolation of known or measured mean annual wind speed, interpolation of the extrapolated wind speeds to arrive at a mean annual wind field at boundary layer level and computation of wind speed at the hub height of the wind turbine (Hossain et al., 2011). In addition, Sliz-Szkliniarz & Vogt (2011) adopted an interpolation method based on a GIS platform to assess wind energy potential in Kujawsko-Pomorskie Voivodeship, Poland. The results indicate annual wind energy yield and economic potential.

GIS has been used as a tool for performing operations on geographic data to determine the potential for wind energy. It can be used to define the amount of wind energy that could be harnessed as well as whether the land is appropriate for development for both onshore and offshore wind turbines. Moreover, GIS has been used in wind energy research for decision-support systems to evaluate potential locations for wind energy generation, and the spatial analysis function, buffering tool and aggregation function of composite maps in GIS are the most widely used tools in the wind energy field.

2.2 Assessment of solar energy potential

Solar radiation is a key factor in determining the amount of electricity produced by PV system, and primary solar radiation data are measured at a limited number of climatic ground stations (Šúri et al., 2005). Ground-measured solar radiation data are seldom scarcely available for a given site where a solar system is planned, as measurement networks' density is usually far too low (Hammer et al., 2003b). To measure solar radiation over a large region, interpolation techniques, such as spline, inverse distance weighted, kriging interpolation method are used. In addition to obtaining direct measurements from meteorology stations, solar radiation can be calculated using mathematical models, meteorological geostationary satellites and an enabled model in a GIS platform. Several studies have been conducted to estimate the spatial distribution of solar radiation based on mathematical models, satellite data and GIS. (Şenkal & Kuleli, 2009; Gurel & Ergun 2012; Coskun et al., 2011; Janjai et al., 2011;Zarzo & Martí 2011).

From the 20th century, numerous solar radiation mathematical models have been developed in an attempt to estimate solar radiation around the world. Ångström proposed the first theoretical model for model estimating global solar radiation based on sunshine duration. However, Ångström-model estimation of solar radiation is based on the sunshine percentage, which is difficult to interpolate; therefore, the Ångström-model is difficult to use when estimating spatial solar radiation distribution. Katiyar & Pandey (2013) reconsidered this model to make it possible to calculate the monthly average of the daily global radiation on an extraterrestrial horizontal surface (Korachagaon, 2012), while Bristow & Campbell (1984) suggest a relationship between the daily temperature range and daily global solar radiation. Additionally, Allen (1997) estimates mean monthly global solar radiation as a function of extraterrestrial solar radiation, mean monthly maximum temperature and mean monthly minimum.

The Bristow - Campbell model is widely used in ecological science and the geosciences (Luo et al., 2010; Chen et al., 2004; Ball et al., 2004). Thornton & Running (1999) present a reformulation of the Bristow - Campbell model for daily solar radiation using daily observations of radiation, temperature, humidity and precipitation. In contrast, the cloudiness model by Kasten & Czeplak (1980) is based on the observed cloudiness, cloud height, cloud form and so forth, and it depends mainly on the visual records of observers. Because cloud observation data have relatively large uncertainties, cloudiness model has not been widely used (Furlan et al., 2012; Luo et al., 2010). The Ångström sunshine percentage model, Bristow–Campbell model and cloudiness model are empirical models.

The mechanism model, such as meteorological/statistical solar radiation model (METSTAT) by Maxwell (1998), is an alternative type of mathematical model. Mechanism models consider the effects of the main components of air on solar shortwave radiation and simulate solar radiation based on different direct radiation and scattered radiation generation mechanisms (Pan et al., 2013). METSTAT was developed specifically to support the creation of the national solar radiation database for the United States (Maxwell, 1998). The model consists of deterministic algorithms designed to produce accurate monthly means for each element for each hour and statistical algorithms intended to simulate the statistical and stochastic characteristic of multi-year solar radiation data sets.

In recent years, with the development of RS technology, modern algorithms allow the estimation of solar irradiance via satellite measurements, which provides an alternative method of radiation estimation. Qin et al. (2011) estimated monthly-mean daily global solar radiation in the Tibetan Plateau based on Moderate Resolution Imaging Spectro-radiometer (MODIS) monthly averaged land surface temperature and Tropical Rainfall Measuring Mission (TRMM) satellite monthly precipitation dada. Similarly, Janjai et al. (2009) present a model for calculating global solar radiation from geostationary satellite data. This model represents a physical relationship between the earth-atmospheric albedo derived from Geostationary Meteorological Satellite (GMS5) data and the absorption and scattering coefficients of various atmospheric constituents.

One advantage of RS is its ability to collect continuous signals in space and time at the top of the atmosphere (Qin et al., 2011), which makes estimating radiation in remote regions where radiation stations are sparse possible. Geostationary satellites, such as Meteorological Satellite (METEOSAT) provide an opportunity to derive information on solar radiance for a large area at a temporal resolution of up to 30 min and a spatial resolution of up to 2.5 km (Hammer et al., 2003a). Several researchers estimated monthly-mean daily global solar radiation based on remote sensing products (Renne et al., 1999; Qin et al., 2011). However, satellite data are not always free and not typically available for field-scale predictions, and their non-precise historical databases have limitations.

Another group of methods used to estimate solar radiation is based on GIS. Charabi & Gastli (2010) developed solar radiation maps in Oman using a solar radiation tool enabled in ArcGIS, which allows users to map and analyse the effects of the sun over a geographic area for specific periods. It includes area solar radiation and point solar radiation tools, and accounts for atmospheric effects, site latitude and elevation, steepness (slope) and compass direction (aspect), daily and seasonal shifts of the angle of the sun, and effects of shadows cast by surrounding topography (Esri, 2013). Incoming solar radiation originates from the sun, is modified as it travels through the atmosphere, is further modified by topography and surface features, and is intercepted at the earth’s surface as direct, diffuse, and reflected components. The sum of direct, diffuse, and reflected radiation forms global solar radiation. Generally, direct radiation is the principal

component of total radiation, and diffuse radiation is the second largest component. The solar radiation tools in ArcGIS Spatial Analyst do not include reflected radiation in the calculation of total radiation. Therefore, total radiation is calculated as the sum of direct and diffuse radiation. Moreover, the solar radiation tools can perform calculations for point locations or for entire geographic areas (Esri, 2013). This tool is suitable in a small area; in a large area, the calculation process is too time consuming.

R.sun is a solar radiation calculation model implemented in the GRASS GIS open-source environment. It is widely used in the calculation of solar radiance due to its open-source design and the accuracy of the simulation (Šúri et al., 2005; Hofierka & Kaňuk, 2009; Nguyen & Pearce; 2010). This model is based on a comprehensive methodology for spatially and temporally distributed computation of solar irradiation and irradiance developed by Šúri and Hofierka (2004), and the methodology follows the research conducted for the European Solar Radiation Atlas. The integration of r.sun with the open-source environment of GRASS GIS provides another GIS tool for direct input and output data processing directly within a single computing environment (Šúri & Hofierka 2004).

At present, various data sets offering solar radiation and other climatic data, such as the European solar radiation Atlas, are available. Information on solar radiation and related parameters also is available on various website. The market development of solar energy not only depends on solar resource but also is strongly affected by policy, technological development, and whether solar energy products are economic. It is necessary to integrate all these influencing factors to analyse the potential of solar energy as a source for producing electricity and to plan the exploitation of solar energy in a given area (Sun et al., 2013).

2.3 Assessment of bioenergy potential

Voivontas et al. (2001) conducted pioneering research in the analysis of biomass resources based on the GIS method and national statistical data. They used Crete, the largest Greek island, as a case study and evaluated biomass resource by separately assessing theoretical biomass potential, available biomass potential, technological biomass potential and economic biomass. In this study, theoretical biomass potential is viewed as the total annual production of

agricultural, forestry and other residues in a region. The potential represents the total quantity of agriculture residues generated in a region and is considered the upper boundary of the bioenergy that actually can be derived from cultivated crops in the area. The theoretical biomass potential from agricultural residues in a specific region is a function of the cultivated area and the biomass production yield of each crop, while the available biomass potential is defined as the biomass that can be technically and economically harvested and used for energy purposes (Voivontas, 2001). The technological biomass potential for a particular biomass source and a specific energy form is defined as the energy that can be produced and is restricted by the characteristics of the selected energy production technology (Voivontas, 2001).

A wide array of technologies makes energy production from biomass possible. The most popular are direct firing for steam production, integrated gasification combined cycle, and co-firing with fossil fuels (US Department of Energy, 1997). The technology selected to exploit the biomass from crop residues depends on specific energy needs and the efficiency of the energy production process. The first step in the assessment of biomass energy potential is the estimation of biomass amount.

Methods of biomass estimation are classified into three groups based on the different methodologies, namely field measurement, RS technology and GIS method.

The first category is estimation of biomass based on filed measurement. Traditional techniques based on field measurement are the most accurate ways for collecting biomass data. A sufficient number of field measurements are a prerequisite for developing biomass estimation models and for evaluating the above ground biomass (AGB) estimation results (Lu, 2006).Thus, Klinge et al. (1975) analyzed the AGB of a central Amazonian rain forest using destructive sampling based on sample trees, while Overman et al. (1994) conducted a study near Araracuara in Colombia to determine AGB by means of regression analysis. Dry weight, total height and specific wood density were measured on 54 harvested trees chosen in a selected random manner. In addition, Gillespie et al. (1990) developed an exponential model for converting volume of residues to

biomass. However, these approaches are often time consuming, labour intensive and difficult to implement, especially in remote areas; and they cannot provide the spatial distribution of biomass in large areas.

The second category is estimation of biomass based on RS, which are divided into four groups based on the scales of data - spatial resolution data, medium spatial resolution data, coarse spatial resolution data and radar data.

Tiwari & Singh (1984) used black-and-white aerial photographs and non-destructive field sampling to map forest biomass in the Kumaun Himalaya in India, while Thenkabail et al. (2004) used multi-data IKONOS images to develop biomass models and to calculate the carbon stock levels of West African oil palms. These two studies were based on fine spatial-resolution data. The drawback of this technique is the lack of shortwave infrared images, which often are important for AGB estimation. Moreover, obtaining high-resolution images is significantly more expensive and the implementation of data analysis is far more time consuming than when using medium spatial-resolution images.

The Medium spatial-resolution ranges from 10 to 100 m, and includes Landsat Thematic Mapper (TM) and Enhanced Thematic Mapper (ETM+) data. Lu & Batistella (2005) used TM data to explore relationships between TM image textures and aboveground biomass in Rondonia in the Brazilian Amazon. Zheng et al. (2004) coupled aboveground biomass values, calculated from field measurements of tree diameter at breast height, with various vegetation indices derived from Landsat 7 ETM+ data through multiple regression analysis to produce an initial biomass map. In practice, it is difficult to identify which texture measures, window sizes, and image bands are suitable for a specific research topic, and the lack of guidelines on how to select an appropriate texture further complicates the process (Liu, 2012a).

Coarse spatial resolution is often greater than 100 m and includes National Oceanic and Atmospheric Administration (NOAA) Advanced Very High Resolution Radiometer (AVHRR), SPOT VEGETATION and MODIS, which frequently are used on national, continental and global scales. Baccini et al. (2004) used MODIS data in combination with precipitation, temperature and elevation

information for mapping AGB in national forest lands in California in the United States.

In many areas, frequent cloud cover limits the acquisition of high-quality remotely-sensed data. Thus, radar systems offer a feasible method of acquiring remotely sensed data within a given time because the systems can collect earth feature data irrespective of weather or light conditions. Radar backscatter in the P and L bands is highly correlated with major forest parameters, such as tree age, tree height, basal area, and AGB (Lu, 2006). Synthetic aperture radar (SAR) L-band has proven to be particularly valuable for AGB estimation (Sun et al., 2002). However, several constraints limit the use of radar data in biomass estimation: data are captured through airborne sensors, which is an expensive, and the data analysis involved in pre-processing, the removal of noise, and image processing require specialist software and advanced skills and knowledge (Lu, 2006).

Nevertheless, RS data has advantages in repetitive data collection: it is digital format allows the rapid processing of large quantities of data (Lu, 2006). Shi et al. (2008) conducted a case study using RS and GIS to evaluate the biomass potential, feasibility of establishing new biomass power plants and the optimization of the locations of plants in Guangdong, China. The researchers estimated the available biomass potential using MODIS/Terra data based on RS and GIS. Furthermore, the biomass was connected to the biomass power plants. The feasibility of establishing new biomass power plants was assessed with the aid of a network analysis function in GIS.

When combined with ancillary data, such as slope, soil, precipitation and statistical data, GIS offers an additional method for biomass estimation and the assessment of bioenergy potential.

Brown & Gaston (1995) used the GIS method to produce geographically referenced, spatial distributions of potential and actual AGB density of all forest types in tropical Africa. Similarly, Zhuang et al. (2011) used ancillary data and GIS techniques to assess marginal land resources and bio-fuel potential in China. The multi-factor analysis method allowed them to identify marginal lands for bioenergy development, but the researchers focused on the siting of a bioenergy plant and land use, and not on the utilization of residues from farmland and

forests. The results indicated that 10% of this marginal land was utilized fully for growing energy plants; 13.39 million tons of bio-fuel would be produced. GIS further allows spatial analysis for site selection of biomass power plants. Shi et al. (2008) used network analysis in GIS to select optimal biomass energy plants in Guangdong province, China.

Graham et al. (1996) designed a GIS model for analyzing the geographic variation in potential bioenergy feedstock supplies and optimal locations for siting bioenergy facilities. This model is designed for examining individual American states but could readily be adapted to any geographic region. It combines soil quality, climate, land use and road network information with transportation, economic and environmental models to predict both where energy crops would be grown and the marginal cost of supplying biomass from energy crops to specific locations (Graham et al., 1996).

GIS-based methods using ancillary data requires high-quality ancillary data, the existence of indirect relationships between AGB and ancillary data and information regarding the comprehensive effects of environmental conditions on AGB accumulation (Lu, 2006). Moreover, research on bioenergy involves ABG biomass estimation, bioenergy potential based on energy plants, bioenergy potential from residues of farmland and forests, and the economic analysis of biomass power generation schemes under renewable energy initiatives based on economic analysis methods, for example, net present value analysis.

In addition to the analysis methods mentioned above, several other analysis technique exits in the field of biomass energy, including economic analysis methods. Moon et al. (2011) conducted an economic analysis of biomass power generation in South Korea for two technologies, namely direct combustion with a steam turbine and gasification with a syngas engine. In view of the present domestic biomass infrastructure of Korea, a small and distributed power generation system ranging from 0.5 to 5 MW was considered and it was found that gasification with a syngas engine becomes more economically feasible as plant size decreases. Wu et al. (2002) conducted an economic analysis of biomass gasification and power generation in China. In this study, experimental data from 1MW scale circulating fluidized bed biomass gasification and power

generation (BGPG) plants were analyzed. It was found that the unit capital cost of BGPG is only 60-70% of that of a coal power station and its operation cost is much lower than that of a conventional power plant (Wu et al., 2002).

2.4 Multi-criteria decision making method

Multi-criteria decision making (MCDM) methodology is a branch of operation research models and a well-known method of decision making. These methods can manage both quantitative and qualitative criteria and can be used to analyze conflict in criteria and decision makers (Pohekar & Ramachandran, 2004). MCDM can be divided into two categories, namely multi-objective decision making (MODM) and multi-attribute decision making (MADM). In MODM, the decision-making problem is characterized by the existence of multiple and competitive objectives that should be optimized against a set of feasible and available constraints; in contrast, in MADM, a set of alternatives is evaluated against a set of criteria (Pohekar & Ramachandran, 2004). MCDM is helpful solving the complex interactions for decision making in renewable energy systems. Compared to the single-criterion approach, the advantage of MCDM methods is employing multiple-criteria or attributes to obtain an integrated decision-making result.

MCDM includes several different methods, the most important of which involve the analytic hierarchy process (AHP), the preference ranking organization method for enrichment evaluation (PROMETHEE), elimination and choice translating reality (ELECTRE) and multi-attribute utility theory (MAUT) (Abu Taha, 2013). MAUT is the most common MCDM method used in energy planning literature, followed by AHP, PROMETHEE, ELECTRE, and decision-support systems (DSS) (Pohekar & Ramachandran, 2004). A brief summary of the most well-known MCDM methods follows.

- MAUT: One of the most popular MCDM methods in decision making, the theory considers the decision maker’s preferences in the form of the utility function, which is defined over a set of attributes where the utility of each attribute/criterion does not have to be linear (Wang et al., 2010).
- AHP: A MADM method first introduced by Saaty (Saaty, 1980), AHP is a type of weighted sum method. In AHP, the problem is constructed as a

hierarchy by breaking down the decision from the top to the bottom. The goal is at the first level, criteria and sub-criteria are in the middle levels and alternatives are at the bottom layer of the hierarchy. The input of experts and decision makers are considered as pair-wise comparison, and the best alternative can be selected according to the highest rank between alternatives (Abu Taha, 2013).

- Analytic network process (ANP): The ANP methodology is a general form of the AHP; Saaty (1996) introduced both. Although AHP is easy to use and apply, its unidirectional relationship characteristics cannot manage the complexity of many problems. ANP deals with the problem as a network of complex relationships between alternatives and criteria where all the elements can be connected. Cheng & Li (2005) provide an empirical example to illustrate the use of ANP.
- PROMETHEE: This method is characterized by ease of use and decreased complexity. It uses the outranking principle to rank the alternatives and performs a pair-wise comparison of alternatives to rank them with respect to a number of criteria. The family of PROMETHE includes PROMETHEE I & II (Oberschmidt et al., 2010).
- ELECTRE: This method is capable of managing discrete criteria that are both quantitative and qualitative in nature and provides complete ordering of the alternatives. The analysis is focused on the dominance relationship between alternatives and is based on the outranking relations and exploitation notions of concordance. The outranking method uses pair-wise comparison between alternatives (Wang et al., 2009). The family of ELECTRE includes ELECTRE I, II, III and IV.

Abu Taha (2013) has notes that MCDM methods include four main stages: (1) structuring the decision process, alternative selection and criteria formulation; (2) displaying trade-offs among criteria and determining criteria weights; (3) applying value judgments concerning acceptable trade-offs and evaluation; and (4) final evaluation and decision making.

The application of MCDA in energy-related matters includes energy planning and power plant allocation (Akash et al., 1999; Madlener et al., 2009), energy

resource allocation (Ramanathan & Ganesch, 1993), energy policy (Greening & Bernow, 2004) and energy management (Ben Salah et al., 2008). Developing evaluation criteria and methods is a prerequisite for selecting the best alternative, identifying energy supply systems, informing decision makers of the integrated performance of the alternatives, and monitoring effects on the social environment.

Weights are assigned to the criteria to indicate their relative importance and are determined by the variance degrees of criteria, the independency of criteria and the subjective preferences of the decision makers. The methods used to assign weights include equal weights and rank-order weights. However, the equal-weights method has been criticized because it ignores relative importance among criteria. Rank-order weighting methods are classified into three categories: the subjective weighting method, objective weighting method and combination weighting method. Criteria weights determined by the subjective weighting method depend only on the preference of decision-makers and not on the quantitative measured data of energy projects. Conversely, objective weights are obtained using mathematical methods based on the analysis of the initial data. Subjective weighting methods explain the evaluation clearly, while objective methods are relatively weak. Additionally, the judgments of decision makers sometimes depend on their knowledge or information. Thus, errors in assigning criteria weights are unavoidable to some extent. An integrated method could overcome these shortcomings and could be the most appropriate technique for determining criteria weights (Wang et al., 2009).

Pair wise comparison and AHP are the most commonly used methods in sustainable energy decision making. In the pair wise comparison method, participants are presented a worksheet and are asked to compare the importance of two criteria at a time, each time answering the question, ‘‘Which one of these two criteria is more important, and how much more important?’’ (Wang et al., 2009). Relative importance is scored using various scales; a scale of 0 (equal importance) to 3 (absolutely more important) is usually adopted. The results are consolidated by adding the scores obtained by each criterion when preferred to criteria with which it is compared.

The classic MCDA methods generally assume that all criteria and their respective weights are expressed in clear values and, thus, that the rating and ranking of the alternatives can be carried out without any problem (Wang et al., 2009). Nevertheless, in a real-world decision situation, the application of the classic multi-criteria evaluation methods may face serious practical constraints from the criteria, perhaps because of imprecision or vagueness inherent in the information. Due to the availability and uncertainty of information and the vagueness of human feeling and recognition, such as classifying agreement as ‘equally’, ‘moderately’, ‘strongly’, ‘very strongly’, ‘extremely’ and a ‘significant degree’, it is difficult for decision makers to assign exact numerical values to the criteria, make precise evaluation and convey their feelings about and recognition of objects (Wang et al., 2009). Hence, most of the selection parameters cannot be provided precisely and the evaluation data of the alternative suppliers’ suitability for various subjective criteria and the weights of the criteria are usually expressed in linguistic terms by the decision makers. Furthermore, it is also recognized that human judgment on qualitative criteria is always subjective and therefore imprecise.

The fuzzy set theory introduced by Zadeh (1965) can solve this problem and play an important role in the decision situation. The combination of MCDM methods and fuzzy set theory has been applied in renewable energy cases. Mamlook et al. (2001) used fuzzy set methodology to perform the comparison between different solar power systems for various applications to determine the order in which systems should be prioritized for use in Jordan.

3 Study area and renewable energy development

3.1 Study area

The study area of this research—Hebei Province; Beijing, the capital of China and Tianjin, one of four municipalities in China—lie in northern China (Figure 3.1). The area covers 217,141 km^2, of which 73,237 km^2 is agricultural land and 54,800 km^2 is forest, and there is abundant biomass residue resource in the study area. It has a continental monsoon climate, with temperatures of -14 to -2 ^oC in January and 20 to 27 ^oC in July, and annual precipitation of 400 to 800mm, occurring mostly in summer.

The population of the study area was 95 million in 2013, and population density is illustrated in Figure 3.2. In the same year, the region's gross domestic product (GDP) reached USD 882.3 billion, accounting for 11% of the national GDP (China Statistics Bureau, 2013). The spatial distribution of GDP can be seen in Figure 3.3. Economic growth and a large population have led to enormous energy consumption in the area (Figure 3.4).

Most central and southern parts of the study area lie within the North China Plain. The western part is raised into the Taihang Mountains, while the Yanshan Mountains are located in the north-eastern part. The northern part is adjacent to the Inner Mongolia Plateau. The highest peak is Mount Xiaowutai in north-western Hebei. Wind conditions during the year are characterized chiefly by the same mechanisms, including south-east trade winds during summer and autumn, and north-west trade winds during winter and spring. The abundant biomass resources, economic growth and large population in the study area attract research regarding the assessment of biomass potential and site selection for biomass potential.

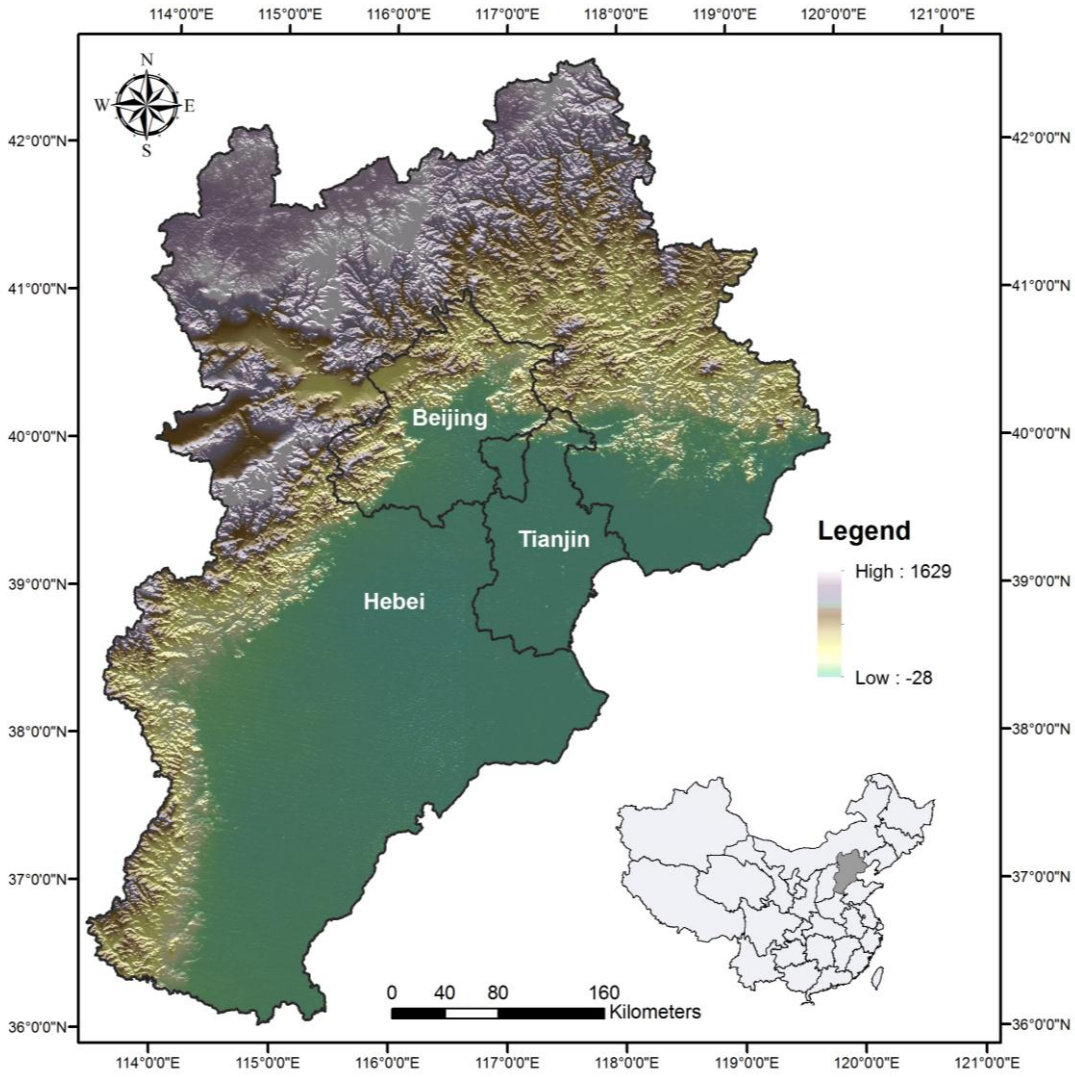

Figure 3.1 The geographical position and elevation (m) of study area

Source: Own illustration, elevation data from International Scientific Data Service Platform (http://www.cnic.cn/zcfw/sjfw/gjkxsjjx/)

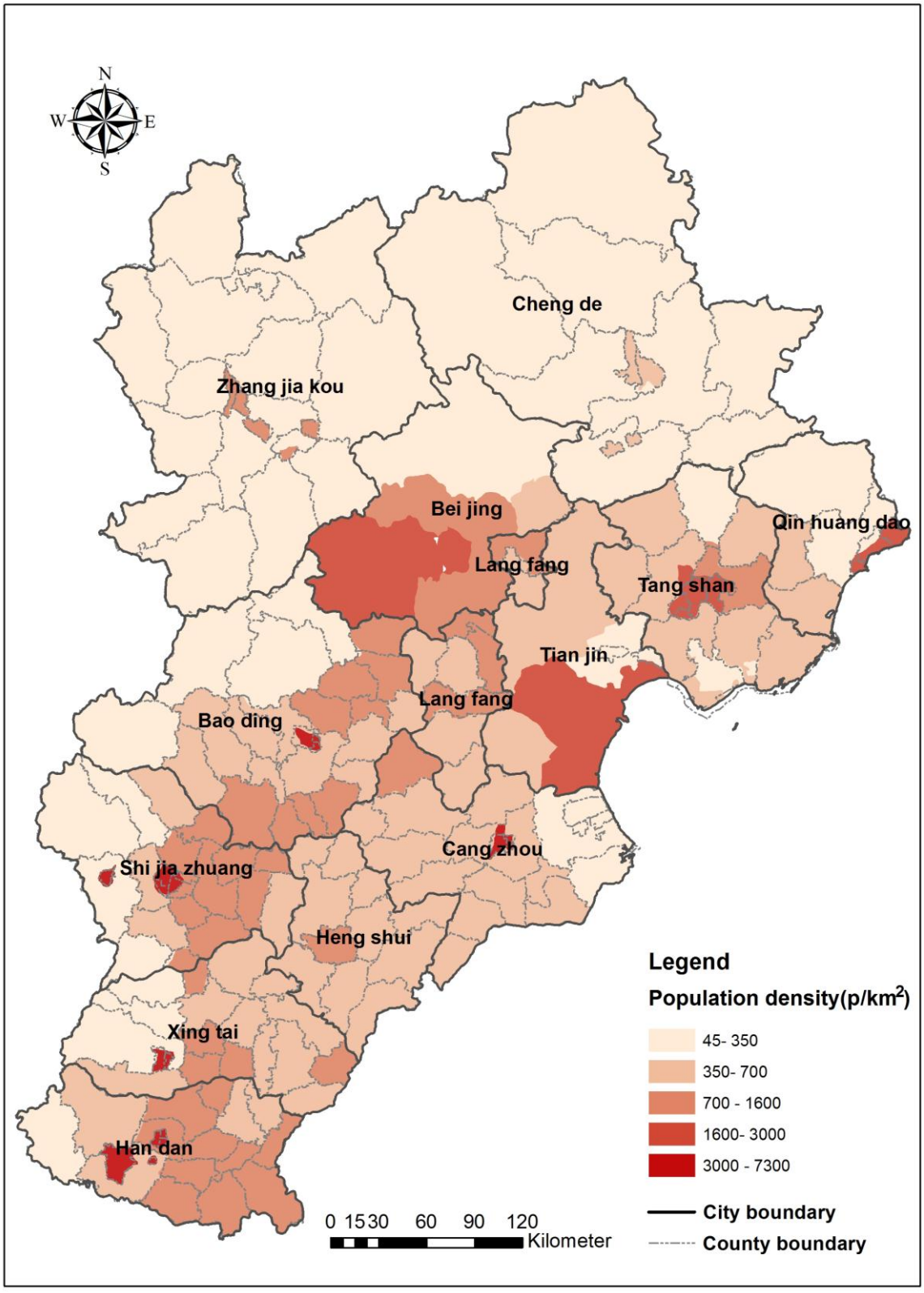

Figure 3.2 Population density in the study area in the year of 2013

Source: Own illustration, population data is based on statistic year book from 2014

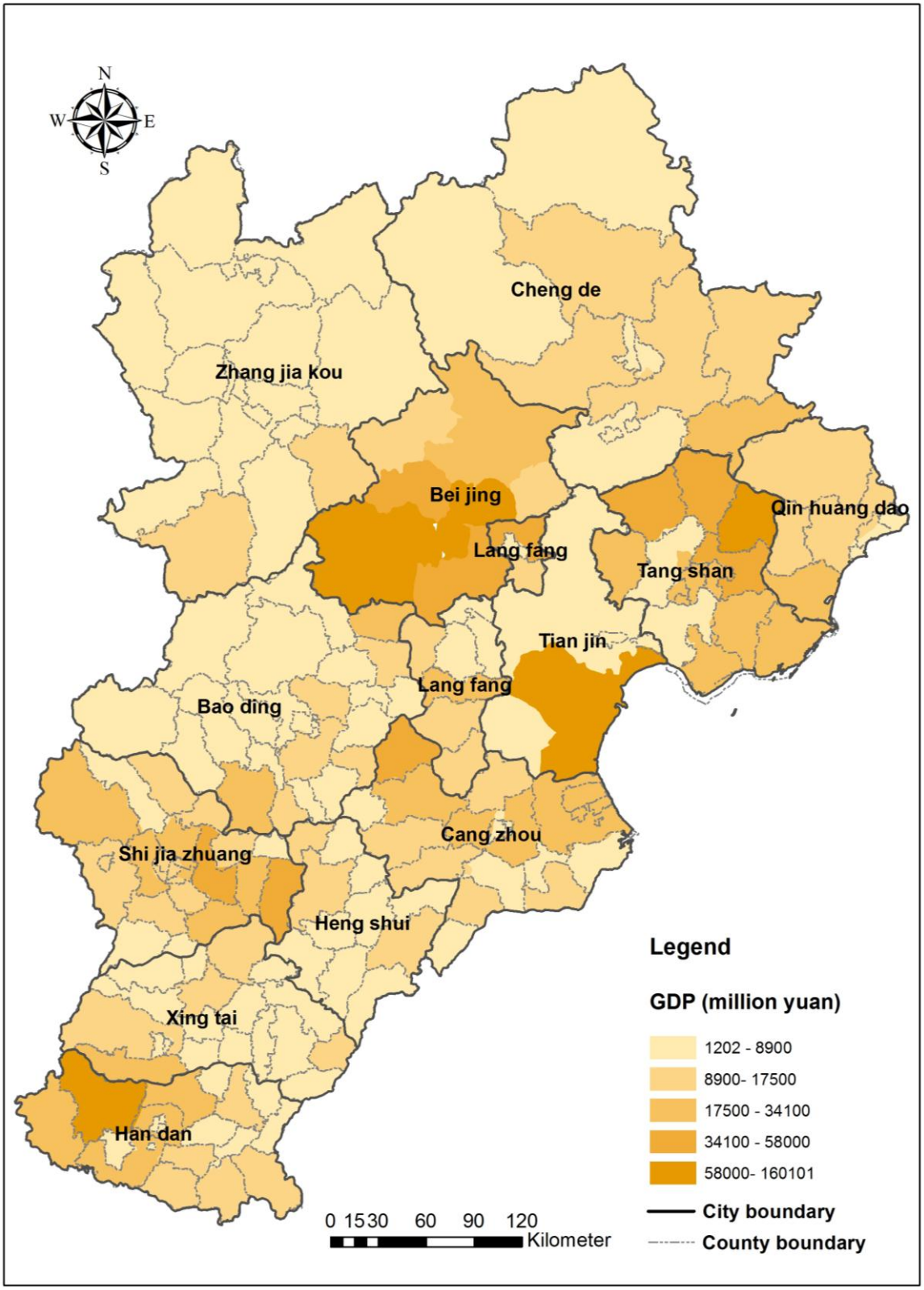

Figure 3.3 GDP in the study area in the year of 2013

Source: Own illustration, population data is based on statistic year book from 2014

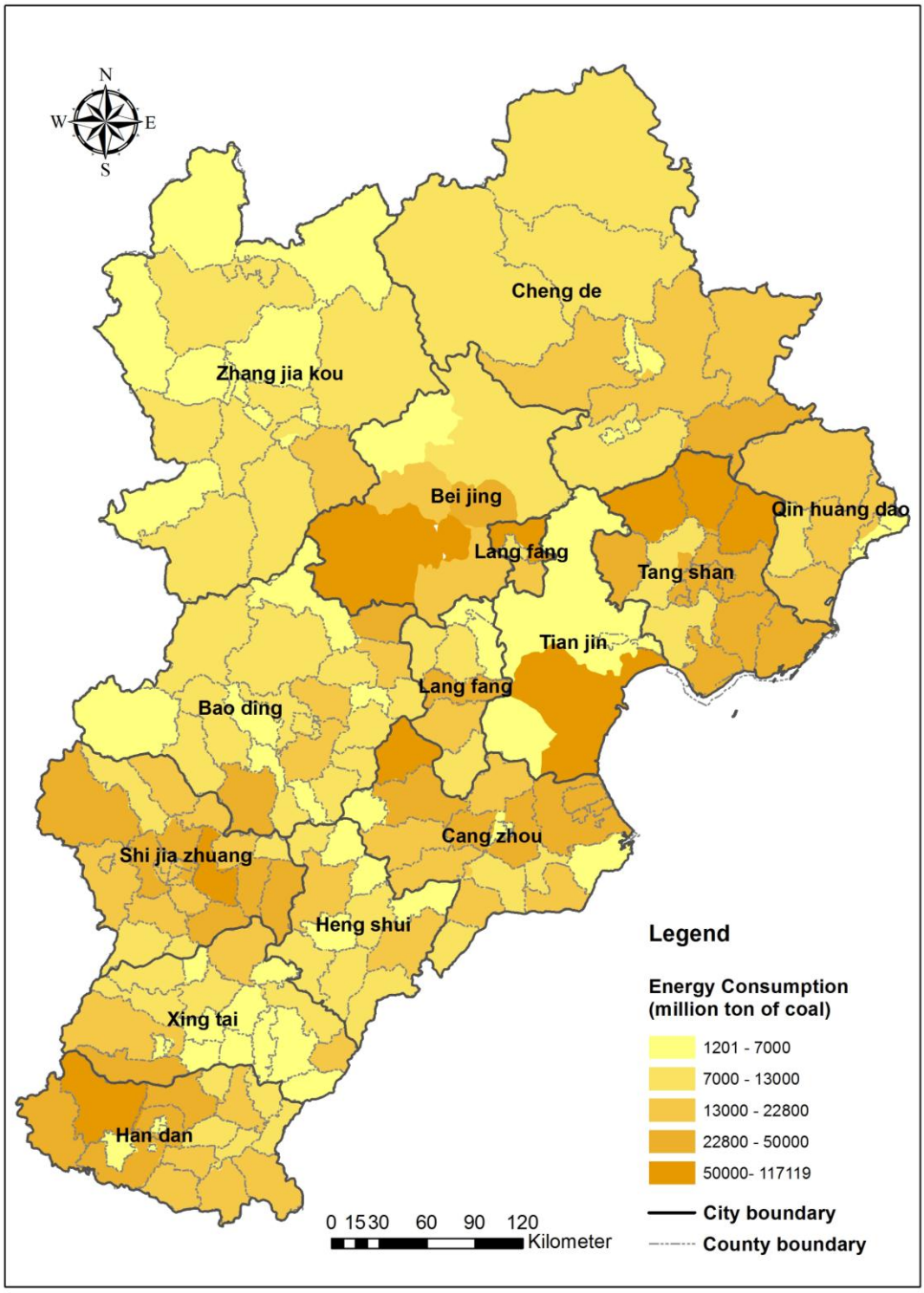

Figure 3.4 Energy consumption in the study area in 2013

Source: Own illustration, population data is based on statistic year book from 2014

3.2 Renewable energy development and energy policies in the study area

Hebei Province ranked the second behind Inner Mongolia on installed wind power capacity in China at the end of 2013; the cumulative installed wind capacity was 8.59 GW. With the installed wind power capacity in Beijing and Tianjin, total cumulative installed wind power capacity in the study areas was 8.96 GW, and the total installed capacity in China was 92 GW (China Renewable Energy Statistic Year-book, 2013). With the substantial growth in the last 10 years (Figure 3.5), these areas play an important role in the future of wind-generated power. By the end of 2015, installed wind power capacity in these areas is planned to reach 11GW, based on the 12th national five-year plan.

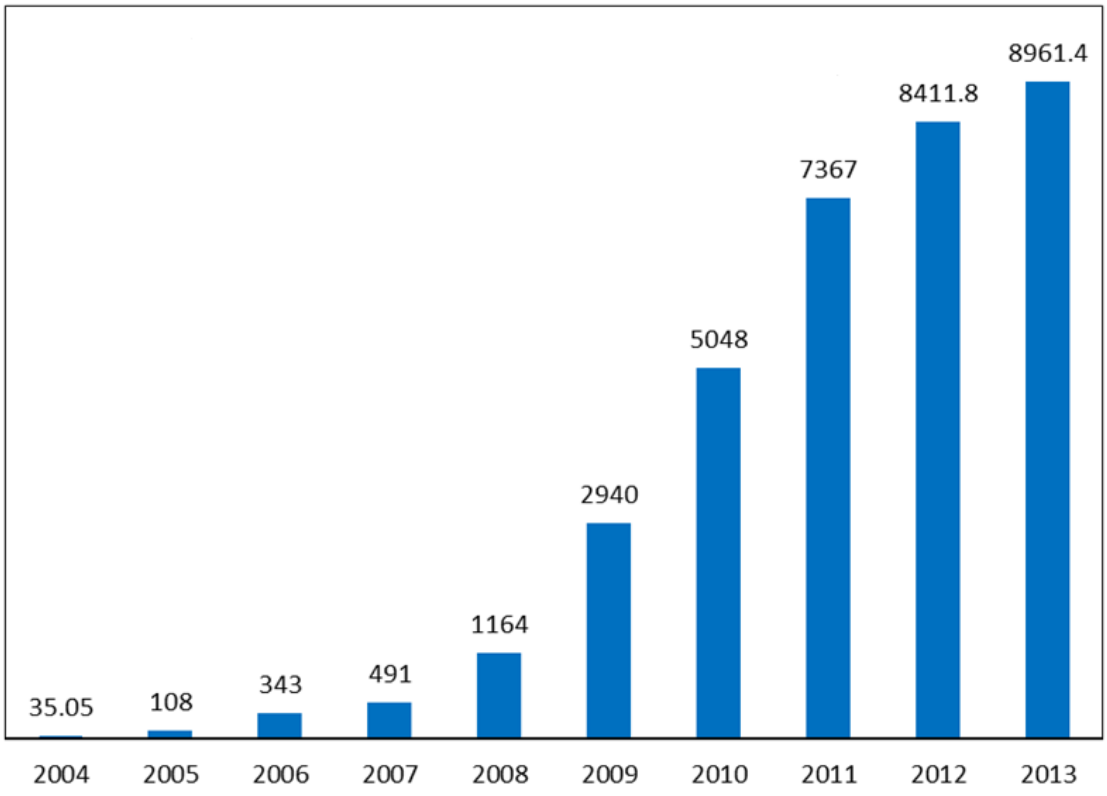

Figure 3.5 Growth of the cumulative installed wind power capacity (MW) in study area (2004-2013)

Source: Own illustration, based on China renewable energy statistic yearbook from 2014

The Renewable Energy Law, published in 2006, states that the gap between the costs of electricity generated from renewable energy and conventional energy sources should be subsidized by the Renewable Energy Development Fund (Zhang et al., 2014). The National Development and Reform Commission

(NDRC), the country's economic planning agency, identified four categories of onshore wind projects in 2009 based on the locations of wind farms. Areas with better wind resources had lower feed-in-tariffs, while those with lower outputs were able to access more tariffs that were more generous. The four wind feed-in-tariff (FIT) levels ranged from 0.51 to 0.61 ¥/kWh (1¥=$0.16 at time of writing) nationwide. Under this scheme, grid operators are forced to offer a premium for wind-generated power over coal power. This represents a significant premium on the average rate of 0.41 ¥/kWh paid to coal-fired electricity generators. Two different FIT exist in this study (see Figure 3.6): northern parts of study area, the two cities of Zhangjiakou and Chengde, have lower FIT than other regions due to their superior wind resources.

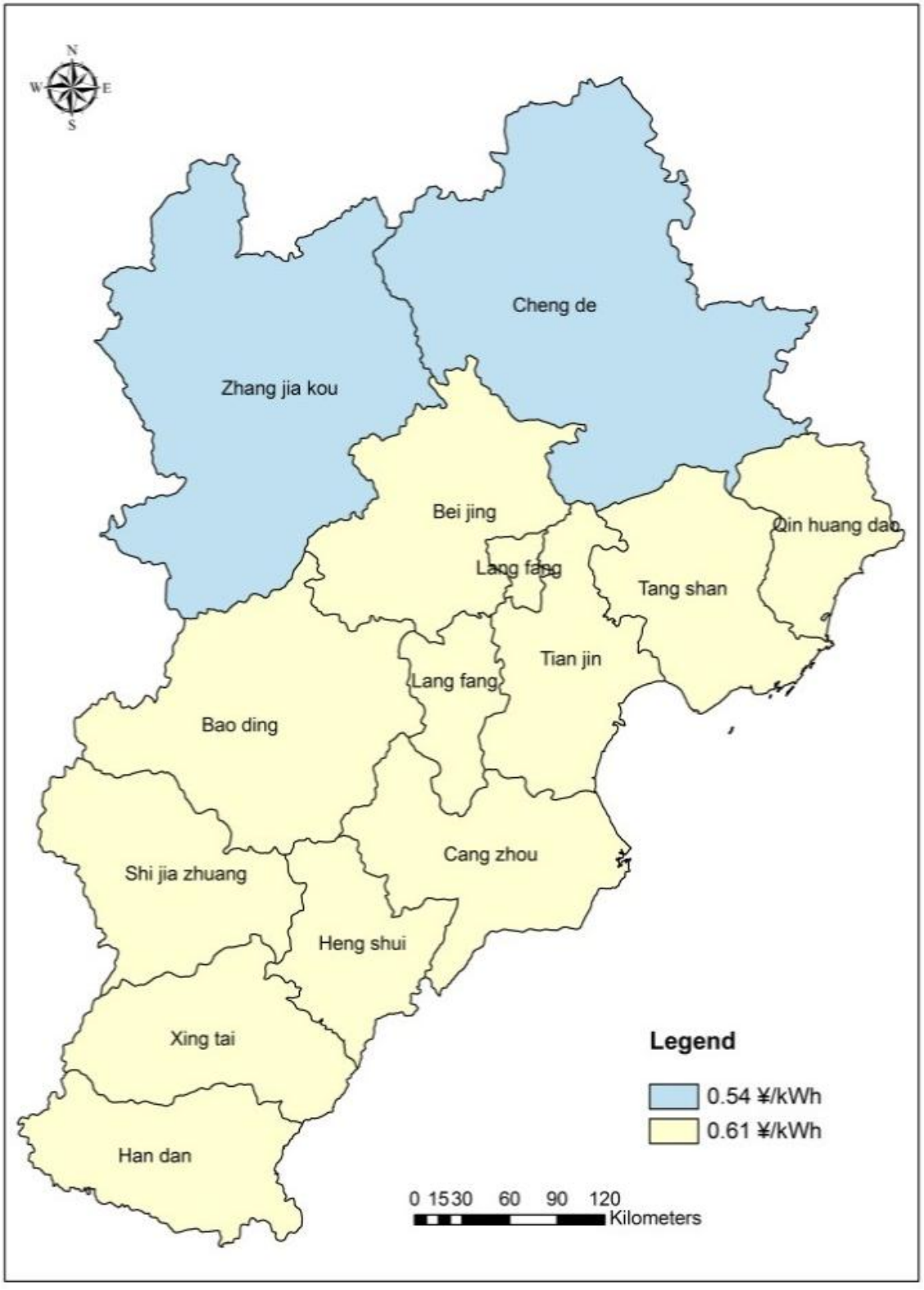

Figure 3.6 Two level of feed-in-tariffs for onshore wind power in China

Source: Own illustration, based on the publish report from NDRC

Because of this FIT, a rapid increase in wind installations has taken place since 2006. In addition, other forms of financial support from the national and provincial

governments are essential incentives for the dramatic growth of wind power installation in China. To promote wind power, the State Tax Bureau has instituted a preferential discount of 50% on value added tax (VAT) on wind power; thus, VAT has been discounted to 8.5%. Similarly, in Hebei Province, the VAT on wind power has been reduced to 6%. Preferential policies further allow for an initial two-year income tax exemption, followed by three years at 50% of the normal rate (hence, 12.5% at the current rate), and the next 15 years at a rate of 15%.

Compared to the cumulative installed wind capacity, the cumulative installed PV capacity in this region is significantly lower, with only 680 MW in 2013. The high cost of PV has historically restricted China's PV market growth. For many years, China's PV power market concentrated only on off-grid electrification projects in rural areas. Moreover, large-scale PV development in China is related closely to the government's incentive policies, such as the Golden Sun Demonstration Program (2009) and the national feed-in-tariff scheme (2011). The Golden Sun Demonstration Program has supported the development of more than 500 MW of solar PV projects in two to three years, and the program provides 50% of the total costs for on-grid projects. However, it requires the system size to be larger than 300 kW (Zhang and He, 2013). According to the regulations of the feed-in-tariff policy, projects which completed construction and achieved commercial operation before 31 December 2011 receive a tariff of 1.15 ¥/kWh; projects that did not complete construction before 31 December 2011receive a tariff of 1 ¥/kWh, which equals 0.16 $/kWh at the current exchange rate (Zhang and He, 2013).

In China, a total amount of 480 million tons of oil equivalent from biomass is available annually, of which approximately 76% is usable for electricity generation. Crop residue accounts for 50% of the total biomass resources; however, crop residue is dispersive and greatly influenced by seasons, and hence costs of transportation and storage are two important factors that determine the technical route, generating capacity, and location of power stations (Wu et al., 2010).

Biomass power generation includes three types of technologies: power is generated through biomass gasification, biomass direct combustion and co-firing. The Law of Renewable Energy, published in 2005 and implemented from 2006, has set the purchase price of electricity from biomass power generation at

0.25 ¥ higher than that of electricity from coal-fired power plants (NDRC,2005). Due to this incentive-based renewable energy policy, 39 biomass power projects with installed capacities totalling 1284 MW obtained construction licenses from local governments by the end of 2006. Most of these projects employ biomass direct combustion technology introduced by Danish company BWE. The first two power stations, with the capacities of 2∗12 MW and 25 MW were established in the Hebei and Shandong Provinces.

By the end of 2013, based on information contained in the author's incomplete statistical study, 12 biomass plant projects had been constructed or were under construction in the study area. The total installed capacity exceeds 300 MW, and installed capacity for each project ranges from 12 MW to 30 MW, with an average installed capacity size of 24 MW. All the projects use biomass direct combustion technology and combine power and heat production.

Energy policies for biomass generation include electricity price subsidies, a VAT refund (defined uniformly by the Ministry of Finance) and an income tax reduction. In some areas, such as industrial parks, reduction of income tax is a method used to attract investment, for example, by offering exemption from income tax for the first three years and a 50% reduction for the next two years. The electricity price subsidiary increases the price to 0.75 ¥/kWh, which equates to the benchmark price plus a subsidiary price equal to 0.75 ¥/kWh. In addition to these, different provinces might have other supportive policies for biomass power generation, especially soft policies, such as lower rental of land or energy-saving reward.

3.3 Data

Data is the fundamental and essential element for GIS analysis. The data used in this thesis include data derived from remote sensing, raster and vector data in GIS, meteorological data from meteorological stations and other ancillary data. The categories and data sources are listed in Table 3.1.

Table 3.1 Data and data source

Data Category	Data	Source
Data derived from remote sensing	Land cover data	United States Geological Survey(USGS)
	NPP data	United States Geological Survey(USGS)
GIS data	Elevation data	International Scientific Data Service Plat form
	Natural reserve data	Digitalization based on published map
	Road network data	AutoNavi Holdings Limited
	Airport data	Digitalization based on Google Earth
	Existed coal power plants distribution data	Compiled based on related data
Meteorology data	Wind speed data	China meteorological data sharing service system
	Temperature data	China meteorological data sharing service system
Ancillary data	Population data	Statistic yearbook from the year of 2014
	Crop production data	Statistic yearbook from the year of 2013

Annual land cover type in the global region is provided by the US Geology Survey (USGS), while the MODIS Land Cover Type product contains five classification schemes that describe land cover properties derived from observations spanning a year's input of Terra- and Aqua-MODIS data. The primary land cover scheme identifies 17 land cover classes defined by the International Geosphere Biosphere Programme, which includes 11 natural vegetation classes, 3 developed and mosaicked land classes, and three non-vegetated land classes (USGS, 2014). Land cover type with 500m spatial resolution in 2010 was adopted in this study.

Net primary productivity (NPP) defines the rate at which all plants in an ecosystem produce net useful chemical energy. In other words, NPP is equal to the difference between the rate at which plants in an ecosystem produce useful chemical energy (or GPP), and the rate at which they expend some of that energy for respiration (USGS, 2014).

The Version-55 of the NPP product produced by the Numerical Terra Dynamic Simulation Group /University of Montana corrects the problem with cloud-contaminated MODIS LAI-FPAR inputs to the MOD17 algorithm. Version-55 Terra/MODIS NPP products are validated to stage 3; this means that their accuracy was assessed and uncertainties in the product were established via independent measurements made in a systematic and statistically robust way that represents global conditions. These data are deemed ready for use in science applications (USGS, 2014). In this study, NPP with 1,000 m spatial resolution in 2010 was downloaded.

Meteorological data from meteorological stations were adopted from China's meteorological data sharing service system, built and managed by the Climatic Data Center of China Meteorological Administration. The wind speed and temperature data were obtained from this sharing system. Overall, 47 meteorological stations are distributed in the study area and its surroundings. As some meteorological stations only have a 21 years' data source (1989-2009), 21 years data were used and information from the three stations with 6 to 15 years' data was excluded.

The International Scientific Data Service Platform, built and maintained by Chinese Academy of Science, provided digital elevation data for this study. Original elevation data with 30 m spatial resolution was acquired from the Shuttle Radar Topography Mission (SRTM). The SRTM obtained elevation data on a near-global scale to generate the most complete high-resolution digital topographic database worldwide.

The author digitalised the natural reserve data based on the published map, AutoNavi Holdings Limited Company provided road network data, and the author digitalised the airport data based on Google Earth. Existing power plants have been compiled by geographic locations. Other ancillary data, such as population data and crop production data were obtained from the China Statistic Yearbook (2013).

4 Methodology

The GIS-based methodology in this study is presented separately according to the different topics, namely the assessment of wind energy potential, solar energy potential and biomass energy potential. The methodology for the assessment of wind and solar energy potential includes the analysis of theoretical potential, the definition of geographic restrictions for power plants, the analysis of technical and economic potential, and land use suitability analysis for power plants. In the section addressing biomass, methods of estimation of usable biomass potential, the definition of geographic restrictions for power plants, an economic analysis based on specific biomass power plants and site selection for biomass power plants are explained. The research framework is shown in Figure 4.1.

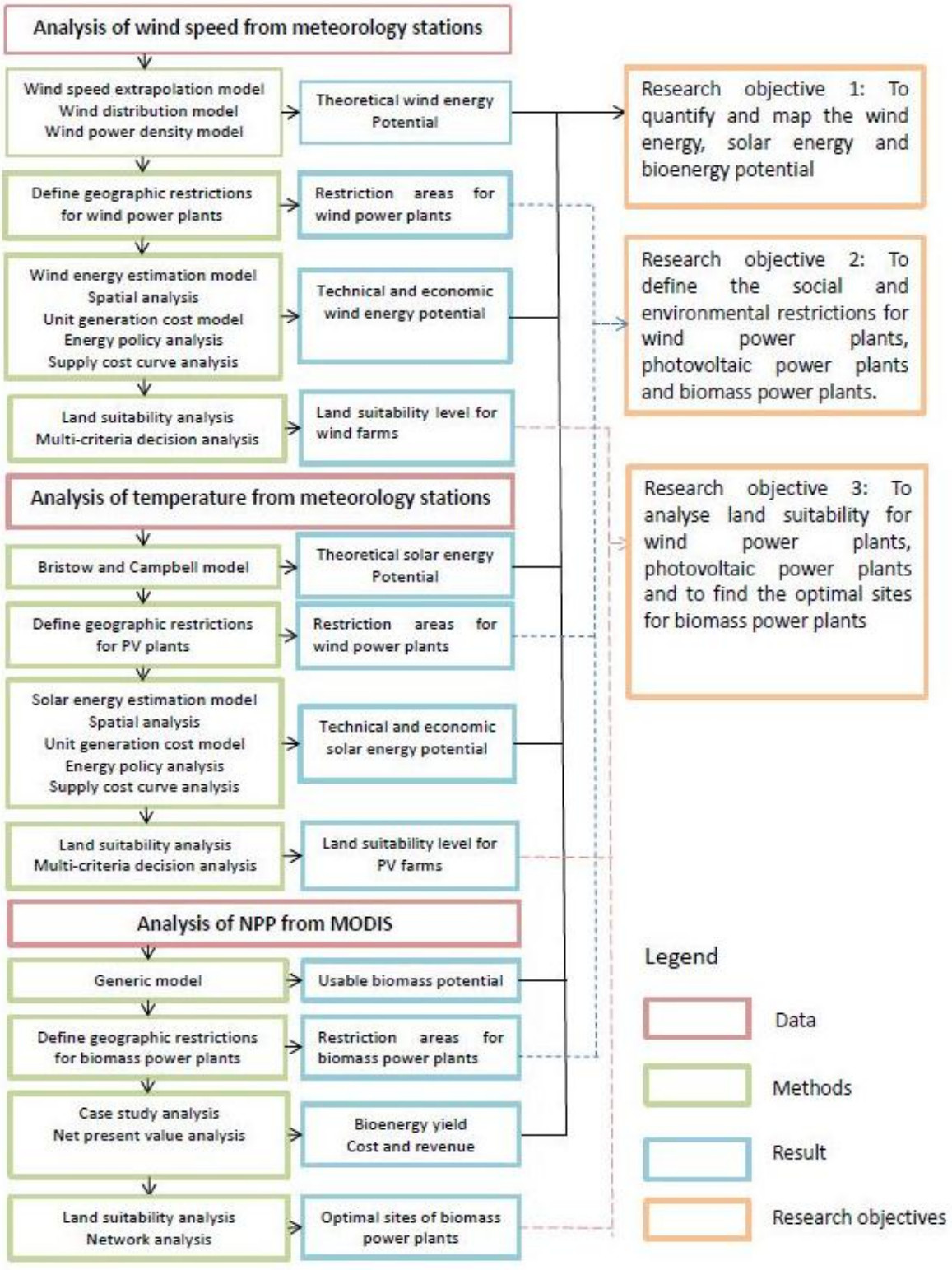

Figure 4.1 Research framework

4.1 Assessment of wind energy potential

The assessment of wind energy potential assessment is based on the wind speed data from meteorological station and using theoretical calculation method on the GIS platform. The methodology includes wind speed height extrapolation model,

wind interpolation model, wind speed distribution model, wind power density model, wind energy production calculation formula, and cost-and-revenue comparison analysis. Wind power density is the indicator used to express theoretical wind power potential, and the assessment of technical wind power potential integrates the wind speed condition, available area for wind power plants and technical characteristics of wind turbines. Annual wind energy generation expresses the technical wind power potential, while the unit generation cost of wind energy combines the cost and revenue of wind power. The economic wind energy potential is calculated based on the unit generation cost and wind energy policy. The workflow for the assessment of wind energy potential is shown in Figure 4.2.

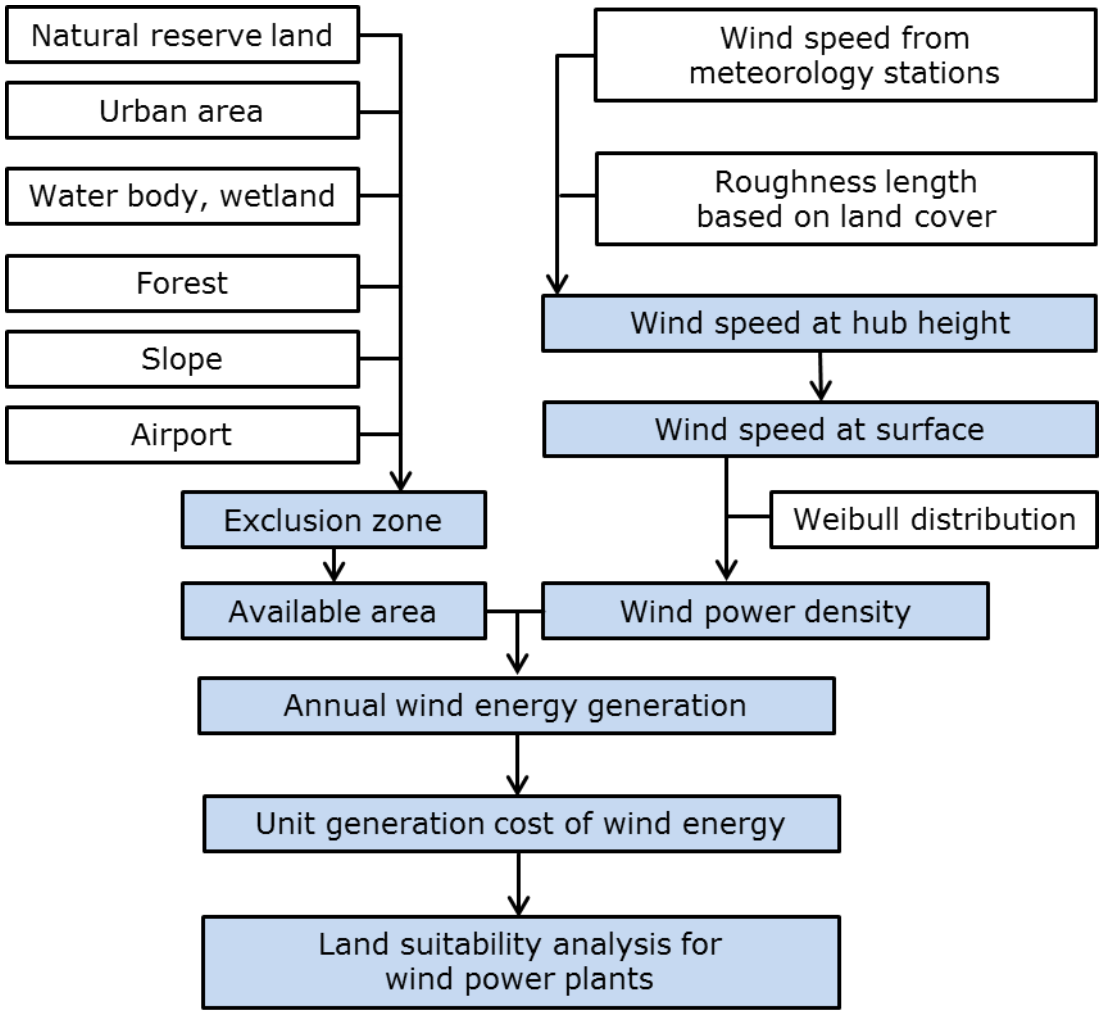

Figure 4.2 Overview of approach to assessing wind energy potential

4.1.1 Analysis of theoretical wind power potential

Wind speed largely determines theoretical wind power potential, and the records of wind speed from meteorological station provide essential data to evaluate theoretical wind power potential. However, at meteorology station, wind speed is measured at 10 m above the ground, and the height of wind turbines is different from that of meteorological stations and varies according to wind turbine type. Thus, a wind speed height extrapolation model is used to calculate wind speed at a given height. Wind speeds measured at a given height can be extrapolated to another height within the boundary layer (wind turbine hub height) using the modified power law or 1/7th power law (Mikhail, 1985). The power law equation is a simple but useful model of the vertical wind profile, which first was proposed by Hellmann (1914). According to the revision by Simiu & Scanlan (1996), the general form of this equation is given by the relationship

$$\frac{V_2}{V_1} = \left(\frac{Z_2}{Z_1}\right)^{\alpha_m},$$

where V_2 is the average wind speed at hub height Z_2, α_m is the modified power law exponent, and V_1 is the average wind speed measured at the measurement height Z_1. Early work by Von Karman showed that under certain conditions α_m equals 1/7, but in the general case, α_m is a highly variable quantity. Moreover, Sisterson & Frenzen (1978) measured wind profile exponents that change from 1/7 during the day to 1/2 at night over the same terrain. In this case, two factors should be considered to calculate α_m, namely the nature of the terrain in terms of surface roughness and the wind speed. Thus, to calculate the power law exponent, Hossain et al. (2011) adopted the formula

$$\alpha_m = a_m + b \ln V_1,$$

where,

$$a_m = \frac{1}{\ln\left(\frac{Z_g}{Z_o}\right)} + \frac{0.088}{\left[1 - 0.008 \ln\frac{Z_1}{10}\right]},$$

$$b = -\frac{0.008}{1 - 0.008 \ln\frac{Z_1}{10}},$$

$$Z_g = (Z_1 * Z_2)^{1/2},$$

and Z_0 is the surface roughness length, which has a close relationship with landscape type. Table 4.1 shows roughness class and roughness length (Hossain et al., 2011).

Table 4.1 Landscape type and roughness class

Rough-ness class	Surface Roughness Length (m)	Landscape Type
0	0.0002	Water surface
0.5	0.0024	Completely open terrain with a smooth surface, e.g. concrete runway in airports, mowed grass .etc
1	0.03	Open agriculture area without fence and hedgerows and very scattered buildings; only softly rounded hills
1.5	0.055	Agricultural land with some houses and 8 m tall sheltering hedgerows with a distance of approximately. 1250m
2	0.1	Agricultural land with some houses and 8 m tall sheltering hedgerows with a distance of approximately.500m
2.5	0.2	Agricultural land with many houses, shrubs and plants, or 8m tall sheltering hedgerows with a distance of approximately.250m
3	0.4	Villages, small towns, agricultural land with many or tall sheltering hedgerows, forests and very rough and uneven terrain
3.5	0.8	Larger cities with tall buildings
4	1.6	Very large cities with tall buildings and skyscrapers

Source: Hossain et al., 2011

The wind speed from meteorological stations is the point data; it cannot cover the entire area. To provide the continuous surface wind speed, which covers the whole study area, the wind speed interpolation model has been adopted. Previous results confirm that kriging methods produce the most accurate results when compared to deterministic techniques (Sliz-Szkliniarz & Vogt, 2011). Using kriging methods, the point wind-speed data was interpolated to the surface.

Weibull wind speed distribution is a mathematical idealization of the distribution of wind speed over time (Odo et al., 2012) The function shows the probability of the wind speed in a 1 m/s interval centred on a particular speed (V), taking both seasonal and annual variations into account. It is a two-parameter function characterized by a dimensionless shape (K) parameter and scale (C) parameter (in unit of speed) (Odo et al., 2012).

Weibull's law is the model used most frequently to describe the distribution of wind speed. This distribution also is used in other sectors, such as the automotive sector, for the analysis of survival data. Takle & Brown (1978) give the probability density function (PDF) of wind speed as

$$f\ (V) = \left(\frac{K}{C}\right)\left(\frac{V}{C}\right)^{K-1} \exp\left(-\frac{V}{C}\right)^{K}$$

where

f (V) is the probability density function of wind speed,

V is wind speed (m/s),

C is the Weibull scale parameter (m/s), and

K is the dimensionless Weibull shape parameter.

Then, the cumulative distribution function F (V) is written as follows:

$$F(V) = 1 - \exp\left(-\frac{V}{C}\right)^{K}$$

The value of K determines whether the Weibull distribution is similar to other kinds of statistical distribution (K = 1.0: exponential, K = 2.0: Rayleigh, K = 3.5: Normal).

K=2.0, or Rayleigh distribution typically is used for the calculation. In this study, K and C are estimated using mean wind speed and the standard deviation of wind speed by the formula from Wang et al. (2012),

$$K = 0.9846(\frac{\sigma}{\mu})^{-1.0944}$$

where K is the dimensionless Weibull shape parameter,

μ is mean wind speed and

σ is the standardized deviation of wind speed.

K has different values at different heights; it increases as height increases to 70 m but decreases above 70 m. Justus created the formula (Justus et al., 1978)

$$K = K_1 \frac{1 - 0.088\ln(\frac{Z_1}{10})}{1 - 0.088\ln(\frac{Z}{10})}$$

where

K_1 is the dimensionless Weibull shape parameter at Z_1 height.

The average wind speed $\bar{V}$ can be expressed as a function of the scale parameter “C” and the shape parameter “K”, by the relationship (Wang et al., 2012):

$$C = \sigma / Gamma(1 + K^{-1})$$

where Gamma denotes the Gamma function

The power of the wind that flows at speed (V) through a blade sweep area (A) is expressed as the cube of its velocity and is given by

$$P(V) = \frac{1}{2}\rho A V^3$$

Where ρ is air density.

The wind power density (D) of a site based on a Weibull probability density function is expressed by Chang et al. (2003) as:

$$D = \frac{P}{\mathrm{A}} = \int_0^{\infty} P(V) f(V) dV = \frac{1}{2} \rho \mathrm{C}^3 \mathrm{Gamma}\left(\frac{K+3}{K}\right)$$

4.1.2 Analysis of geographical wind power potential

The first reduction of the theoretical potential in this study is the restriction of available land for wind turbines: certain land is excluded because of planning or physical constraints. Unfeasible land includes land with specific functions (such as a nature reserve), land where wind turbines would interfere with current use (airports, built-up areas and wetland) and land where it is physically impossible to install turbines (water bodies, porous ground and slopes greater than 10%) (Haaren & Fthenakis, 2011).In addition, aspects such as visual intrusion, noise pollution, ecological effects, and physical constraints influence wind farm placement.

The visual intrusion of wind turbines is a debatable issue. Although some people see wind turbine farms as the obliteration of nature, others welcome the clean power from wind farms and like the structures in their area (Haaren & Fthenakis, 2011). The findings of Grady's (2002) survey in North Carolina in the United States support this view. Of the respondents 58% (n=400) did not see wind turbines as a problem or could not think of a problem with developing a wind industry in the state. Of the people who had a problem, the majority (44%) considered visual "pollution" their major issue with wind power. Kaldellis (2005) has shown that public attitudes towards wind power are more positive in areas with wind farms than in areas where people have not previously experienced the phenomenon, and the study's conclusions indicate that public acceptance increases with information and experience levels. The placement of turbines in the visual periphery of urban areas would benefit the public opinion of wind power and stimulate the placement of more wind turbines in the area (Haaren & Fthenakis, 2011).

Noise is a quantifiable issue and numerous guidelines and regulations can be found on this issue. Serwan & Baban (2001) note that wind project developers

keep a distance of 500 m from single dwellings to keep sound levels at an appropriate level. Noise propagation is described by the logarithmic relationship of sound power level at the source (L_w) and sound pressure level at a location (L_p), both measured in dB. Haaren & Fthenakis (2011) offer a simple relationship between L_p and distance to turbine

$$L_p = L_w - 10log_{10}(2\pi R^2) - \alpha R$$

where

$$R^2 = H^2 + X^2$$

and H is the tower height, X is the observer's distance to the tower, and α is the atmospheric absorption of 1000 Hz sound and corresponds to 0.005 dB/m. With the Vestas V82 (selected wind turbine type, detail follow in the next section), which has a sound power level of 101-103 dB at the hub and a tower height of 78 m, the approximate decrease of sound pressure level over distance depicted in Figure 4.3 can be expected. Based on the regulations related to noise level published by the Chinese government, noise in residential and commercial areas should be between 40 and 55 dB. In light of these results, a 500 m buffer zone from an urban area is sufficient to lessen the noise and visual intrusion.

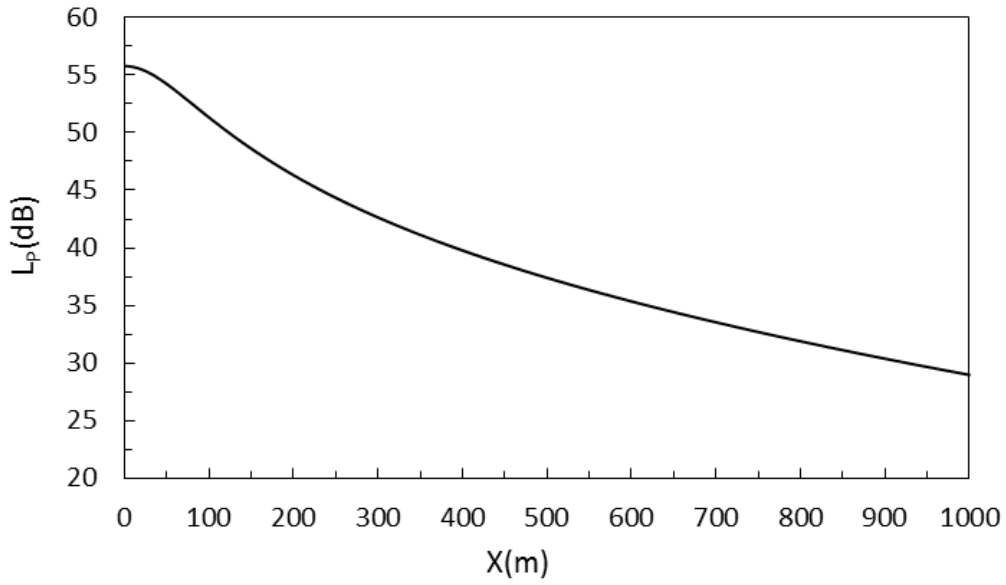

Figure 4.3 Approximation of the sound pressure level as a function of distance

Furthermore, wind turbines have negative effects on ecology, which can be categorized into three groups: creating collision hazards for birds and bats, the

destruction of wildlife habitat and the destruction of vegetation. A study conducted by Miller (2008) showed that 18 wind turbine farms that contain 1,569 turbines were reportedly the cause of 0.04 – 10 bird mortalities per turbine per year and 0.07 – 64 bat mortalities per turbine per year. Although researchers use different bias corrections, which complicates comparison, the averages indicate what can be expected: 2.4 birds and 12.2 bats per turbine per year.

However, the strategic placement of turbines outside ecologically sensitive and dense population areas can reduce their ecological impact. To prevent the disturbance of animals in their habitats, wind turbines should be placed a safe distance away from breeding grounds, specifically wetlands and wildlife refuge forests. Wetlands are protected for their hydrologic characteristics (for example, the collection of runoff water). In this study, wetlands and forests with woody plants and buffered areas around them are considered unfeasible sites for these reasons. Although strict regulations do not exist on distances, Serwan & Baban (2001) suggest a 500 m buffer between wind farms and wetlands based on literature and a questionnaire investigation, and a 1,500 to 2,000 m distance between wind farms and airports.

Finally, physical constraints for slope were set at 10% based on a survey conducted by Serwan & Baban (2001). Constructing turbines on a slope greater than 10% is difficult due to the limited access of the cranes needed to lift heavy turbine components. Criteria for excluded areas were developed as the following table shows:

Table 4.2 Criteria of restriction area for wind farms

Feature	Recommendation for buffer zones
Natural reserve	Buffer zones around natural reserve:500m
Forest	Buffer zones around woody land: 500m
Airports	Buffer zones around airports: 2500m
Slope	Slope greater than 10% is not allowed
Urban area	Buffer zones around urban area: 500m
Water body	Buffer zones around water body: 500m
Wetland	Buffer zones around water body: 500m

Source: Own illustration, based on the mentioned literature above

4.1.3 Analysis of technical wind power potential

Once the excluded area for wind power plants has been defined, the size of the eligible area is clear. The next challenge is to estimate annual wind energy generation, namely technical wind power potential. The wind energy harvest is determined by wind speed, its frequency distribution and the characteristics of wind turbines. A wind power density map with 1 km spatial resolution calculated from theoretical potential analysis is used to calculate annual wind generation, and the available area for wind power plants is divided into 1 km grid to match wind power density resolution.

The Vestas 82 (V82 1.65 MW) wind turbine produced by Vestas company was chosen as an example. Vestas has gained a market-leading position with more than 60 GW of installed wind turbines, comprising close to 19% of total global capacity (Vestas, 2014). The V82 is an extremely competitive turbine in areas with low and medium wind speed. It is optimised for sites with an average wind speed of 6 m/s at hub height, while a breeze of as little as 3.5 m/s is all that is needed to start production. The technical parameters of the V82 are shown in Table 4.3.

Table 4.3 Technical parameters of V82 wind turbine

Hub height	Rated power	Rotor diameter	Swept area	Cut-in speed	Cut-off speed
80 m	1650 KW	82 m	5281 m2	3.5 m/s	25 m/s

The annual wind energy ($\boldsymbol{E_i}$) in grid i can be extracted by wind turbines is defined by the equation

$$E_i = D * A * C_p * n * h_e$$

where

D is wind power density, calculated in wind power density model, and

A is the swept area of the wind turbine.

C_p represents the percentage of power which can be extracted from the wind, depending on the available wind energy and the operating characteristics of the wind energy extraction device. However, wind turbine cannot use 100% of this power due to the Berz limit. The wind power available according to the previous equation can be rewritten by adding a coefficient, C_p, which defines the maximum efficiency of the Betz limit (0.593) (Lima & Filho, 2012).

The number of turbine in the given grid is represented by n, calculated as

$$n = \frac{A_i}{(5 * 10 * \varphi^2)}$$

where

A_i is the size of grid i, in this case, is 1 $km^{2,}$ and

φ is the rotor diameter of the wind turbine(82 m).

The symbol $\boldsymbol{h_e}$ represents the effective hours for which the wind turbine works. A wind turbine cannot work when the wind speed is beyond the range between the cut-in and cut-off speeds. Effective hours were calculated based on the following formula (Jiang et al., 2010)

$$\frac{h_e}{h_o} = \exp\left(-\left(\frac{V_{cut\ in}}{C}\right)^K\right) - \exp\left(-\left(\frac{V_{cut\ off}}{C}\right)^K\right),$$

where

h_o is 365*24, 8760 hours,

$V_{cut\ in}$ is cut-in speed, 3.5 m/s for Vestas 82,

$V_{cut\ off}$ is cut-off speed, 25 m/s in this case,

C is the Weibull scale parameter (m/s), and

K is the dimensionless Weibull shape parameter**.**

In 2011, more than 1500 GWh of wind power in China was not integrated, accounting for more than 12% of total wind generation. Therefore, annual wind energy production was adjusted by multiplying by 0.88 in this case. For a typical

onshore wind farm, adjusted parameters of 0.95, 0.98 and 0.97 array, air foil soiling and icing loss rates, and the miscellaneous loss rate were selected to adjust annual wind energy production (Zhang et al., 2014). Adjusted annual energy production is the index of technical wind energy potential.

4.1.4 Analysis of economic wind power potential

The above sections addressed the physical wind speed and geographical constraints for wind power plants and the technical aspects of wind energy. Additional aspects that influence the growth of wind energy utilization are market and policy factors that play significant roles in the promoting the development of renewable energy projects (Madlener & Stagl, 2005). These factors include electricity tariffs, subsidies and administrative project-related policy.

He et al. (2013) indicate that for onshore wind energy, the costs of generators still account for around 75 – 85% of the total investment expenses. Wind turbine cost accounts for approximately 80% of investment cost according to the data from existing projects. The expenditure related to the auxiliary and road infrastructure as well as to grid connection may amount to up to 15% of the total cost. Of this share, the majority is the cost of connecting to existing transmission lines; this represents the 6 to 8% of the investment cost. Annual operation costs include debt service costs, insurance, property tax and lease of land, and expenditure on maintenance, and amount to 3% of the initial capital cost. Additional expenses vary from project to project depending on site-specific conditions.

In China, the total amount earned by the producers of wind energy is composed of the market price of electricity and the government subsidy. The average annual cost per kilowatt-hour of electricity generated by a wind turbine was derived from the sum of total annual investment costs, operating costs and the turbine's annual energy yield. The unit cost of energy was calculated using the formula

$$PC_i = \frac{C_{o\&m} + L}{E_i}$$

$$L = I \frac{r(1+r)^n}{(1+r)^n - 1}$$

where

PC_i is the cost of 1 kWh of electricity generated in a grid cell;

$C_{o\&m}$ is the operation and maintenance costs, and is assumed to be a constant rate(0.03 of investment) over the life time Cost (Hoogwijk, 2004);

E_i is the annual energy yield in a grid;

L is the annual loan payment and it is assumed that the total investment is obtained from loans;

I is the initial investment cost, where turbine cost takes 80% of the investment (Hoogwijk, 2004);

r is the interest rate (5%); and

n is the life time of the system (25 years).

The average cost of wind energy investment per kW is estimated to be around $1,000 to $1,200, reaching up to $1,600 in extreme cases (Sliz-Szkliniarz & Vogt 2011). In this study, the cost of a wind turbine is $1,200 per kW and the rated power of the Vestas 82 1.65 MW is 1650 kW.

The supply-cost curve of renewable energy sources is an essential tool for synthesising and analysing large-scale energy policy scenarios, both in the short and long terms (Izquierdo et al., 2010). It often is used in global, regional or country analyses of energy-policy scenarios. Similarly, supply cost usually is employed as an essential tool in the analysis of economic potential. In this study, geospatial supply cost is introduced to estimate economic potential in different situations. Using the calculation model described above, the spatial distribution of wind energy generation and unit generation cost are available. The x axis is the aggregate supply, or the amount of wind energy production, while the y axis represents the average unit generation cost.

Moreover, it is assumed that wind turbine installation begins in the area with the lowest unit generation cost before wind projects gradually move to areas with higher unit generation cost gradually. Hence, average unit generation cost increases with the increase of wind energy supply. Economic potential is defined as the amount of wind energy supply at the point of intersect where average unit

generation cost equals the sum of market price and subsidy. The proposed relationship between aggregate supply and average unit generation cost is shown in Figure 4.4. Although a linear relationship is selected as a simple example to show the method, in reality, it probably would not be a linear relationship.

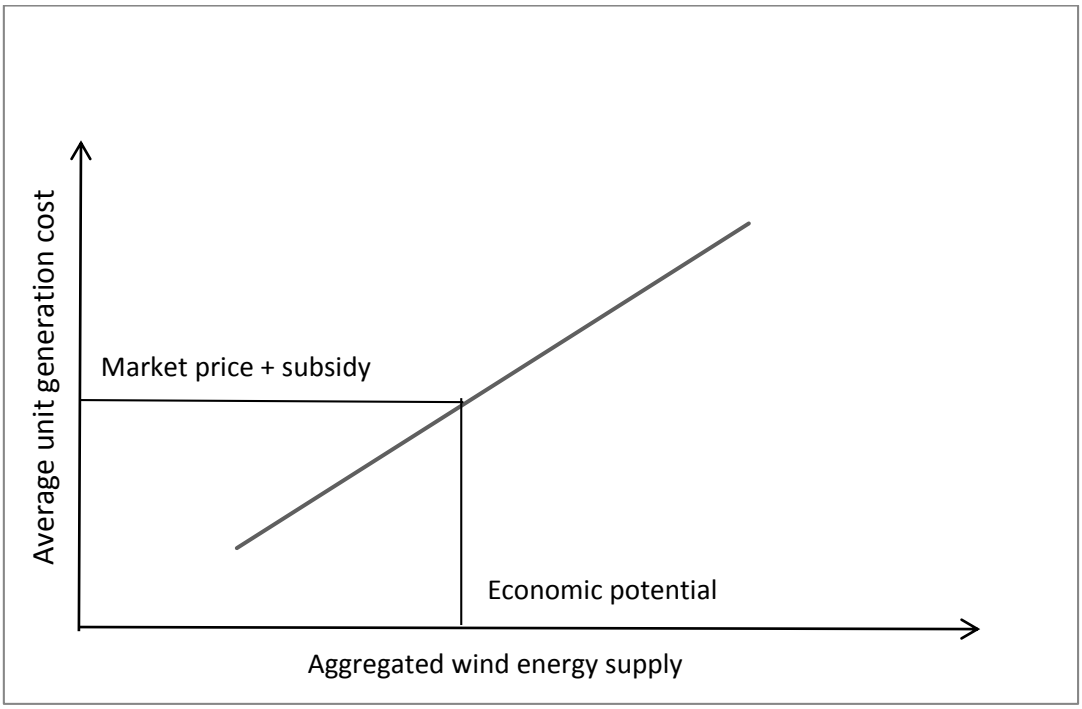

Figure 4.4 Proposed relationship between aggregated wind energy supply and average unit generation cost

4.1.5 Land suitability analysis for wind power plants based on multi-criteria method

After wind energy potential is assessed, the final step is to site the wind power plants. In this phase, a land suitability analysis for wind power plants is conducted to find the most suitable areas. Mendoza (1997) defines land use suitability as a generic term associating a combination of factors and their effects with respect to potential land uses. The generic model of land suitability can be formulated as:

$$S = f(i_1, i_{2,\dots} i_n)$$

where S is the suitability measure, and $i_1, i_{2,\dots} i_n$ are the indicators affecting the suitability of the land. Suitability analysis involves an appropriate approach to

combining these indicators, and AHP often has been used for land suitability analysis. This mathematical method, developed in decision analysis determines weight for each criterion and forms part of multi-attribute decision analysis. AHP is used to site wind farms because of its advantages summarized by Thinh & Vogel (2007) as follows:

- It provides a structured approach to measuring the suitability by breaking the problem into hierarchical units and levels.
- The AHP relies less on the completeness of the data set and more on expert judgements or observations about the different indicators.
- This method is more transparent and thus easily accepted, especially when the suitability analyses serve as a basis of land allocation.
- The approach permits the participation of both experts and stakeholders in the process

Wind potential is considered the most influential criterion in determining the suitability of land for wind farms. In addition, wind farm sites ideally should be close to roads and the existing power grid system. In this study, unit generation cost is considered the most important criterion because it defines the feasibility of wind electricity production and integrates the technical wind energy potential and cost. Moreover, several geographic criteria should be considered. An area with a mild slope is more suitable for a wind farm than a steep area, as construction is significantly easier and costs lower where the ground is flat. Finally, economic factors including distance to roads, urban areas and transmission lines, viewed as the least important criteria, should be considered.

The weight of each criterion was derived through AHP by directly comparing the importance of one criterion to that of another. Saaty (1980) employed an underlying scale with values from 1 to 9 (Table 4.4) using pairwise comparison of criteria to offer a ratio scale. For each pair of criteria, the decision maker is required to respond to a pairwise comparison question asking the person to compare the relative importance of the two. Responses are gathered in verbal form and subsequently codified on a nine-point intensity scale (Table 4.4) (Bennui, 2007). After the development of the pairwise comparison matrix A= (aij) (i,j=1(1)n) (Table 4.5), criterion weights were computed as follows (Thinh & Vogel, 2007):

1) Calculate the sum of the values in each column of the matrix a_{ij}.
2) Divide each element in the matrix by its total column (the resulting matrix bij (i,j=1(1)n) is the normalised pairwise comparison matrix (Table 4.6)
3) Compute the average of the elements in each row of the normalised matrix; these averages are used as the relative weights wi(i=1(1)n) of the criteria (Table 4.7).

Table 4.4 Scale for pairwise comparison

Intensity of importance	Definition
1	Equal importance
2	Equal to moderate importance
3	Moderate importance
4	Moderate plus
5	Strong importance
6	Strong plus
7	Very strong importance
8	Very, very strong importance
9	Extreme importance

Source: Saaty,2006

Table 4.5 Comparison matrix

Criteria	Unit generation	Slope	Distance to roads	Distance to urban	Distance to transmission
Unit generation cost	1	3	5	5	5
Slope	1/3	1	3	3	3
Distance to roads	1/5	1/3	1	1	1
Distance to urban areas	1/5	1/3	1	1	1
Distance to transmission lines	1/5	1/3	1	1	1
Total	1.93	5	11	11	11

Table 4.6 Normalised pairwise comparison matrix

Criteria	Unit generation	Slope	Distance to roads	Distance to urban	Distance to transmission
Unit generation	0.516	0.758	0.467	0.467	0.467
Slope	0.172	0.152	0.333	0.333	0.333
Distance to roads	0.104	0.03	0.067	0.067	0.067
Distance to urban areas	0.104	0.03	0.067	0.067	0.067
Distance to transmission lines	0.104	0.03	0.067	0.067	0.067

Table 4.7 Weights of criteria

Criteria	Unit generation cost	Slope	Distance to roads	Distance to urban	Distance to transmission
Weights	0.535	0.264	0.067	0.067	0.067

The next step is to investigate whether the comparisons are consistent. For controlling the consistency of the estimated weight values, the consistency ratio (CR) is calculated as follows:

First, calculate the eigenvector and the maximum eigen-value for each matrix.

Then, calculate an approximation to the consistency index (CI) using the equation

$$CI = \frac{\lambda_{max} - n}{n - 1}$$

where

λ_{max} is the eigenvalue of the pairwise comparison matrix and

n is the number of criteria.

Finally, to check the consistency of the pairwise comparison matrix, the consistency judgement must be checked for the appropriate value of n by CR:

$$CR = \frac{CI}{RI}$$

RI is the random consistency index, and the RI values for different numbers of n are shown in Table 4.8. If CR is smaller than or equal to 0.10, the degree of consistency is satisfactory (Saaty 1980). The CR value in this study is smaller than 0.1 for each criterion.

Table 4.8 RI table values

n	1	2	3	4	5	6	7	8	9	10
RI	0	0	0.58	0.90	1.12	1.24	1.32	1.41	1.45	1.49

Source: Saaty 1980

Each criterion is normalized on a scale of 1 to 9, where 1 is the lowest value, and 9 is the highest (Table 4.9). The land suitability value is expressed as follows:

$$\boldsymbol{S = \sum_{i=1}^{n} v_i * w_i}$$

where

i is indicator,

n is the number of indicators,

v_i is the normalized value of indicator i, and

w_i is the weight of indicator i.

Table 4.9 Score of indicators

Criteria	Indicators	value
Unit generation cost	0.07 - 0.3 $/KWh	9
	0.3 - 0.6 $/KWh	7
	0.6 - 0.9 $/KWh	5
	0.9 - 1.2 $/KWh	3
	>1.2 $/KWh	1
Distance to road	<2 km	9
	2 km - 5 km	7
	5 km - 10 km	5
	10 km - 20 km	3
	>20 km	1
Distance to transmission	<5 km	9
	5 km - 10 km	7
	10 km - 15 km	5
	15 - 20 km	3
	>20 km	1
Distance to urban area	<5 km	9
	5 km - 10 km	7
	10 km - 15 km	5
	15 km - 20 km	3
	>20 km	1
Slope	<1%	9
	1% - 2.5%	7
	2.5% - 5%	5
	5% - 10%	3
	10% - 15%	1
	>15%	Restricted area

4.2 Assessment of solar energy potential

The assessment of solar energy potential includes simulating solar radiation, defining the excluded areas for PV power plants, estimating solar energy production considering PV technology and calculating unit generation cost. The temperature data from meteorological stations in the Bristow and Campbell model is used to simulate solar radiation. The assessment of technical solar power potential considers solar radiation resources, the available area for solar power plants, the energy efficiency of the PV module and the unit generation cost of solar energy which combines the costs and revenues of solar energy. The

economic solar energy potential is calculated based on the unit generation cost and solar energy policy. The workflow of the assessment of solar energy potential is shown in Figure 4.5.

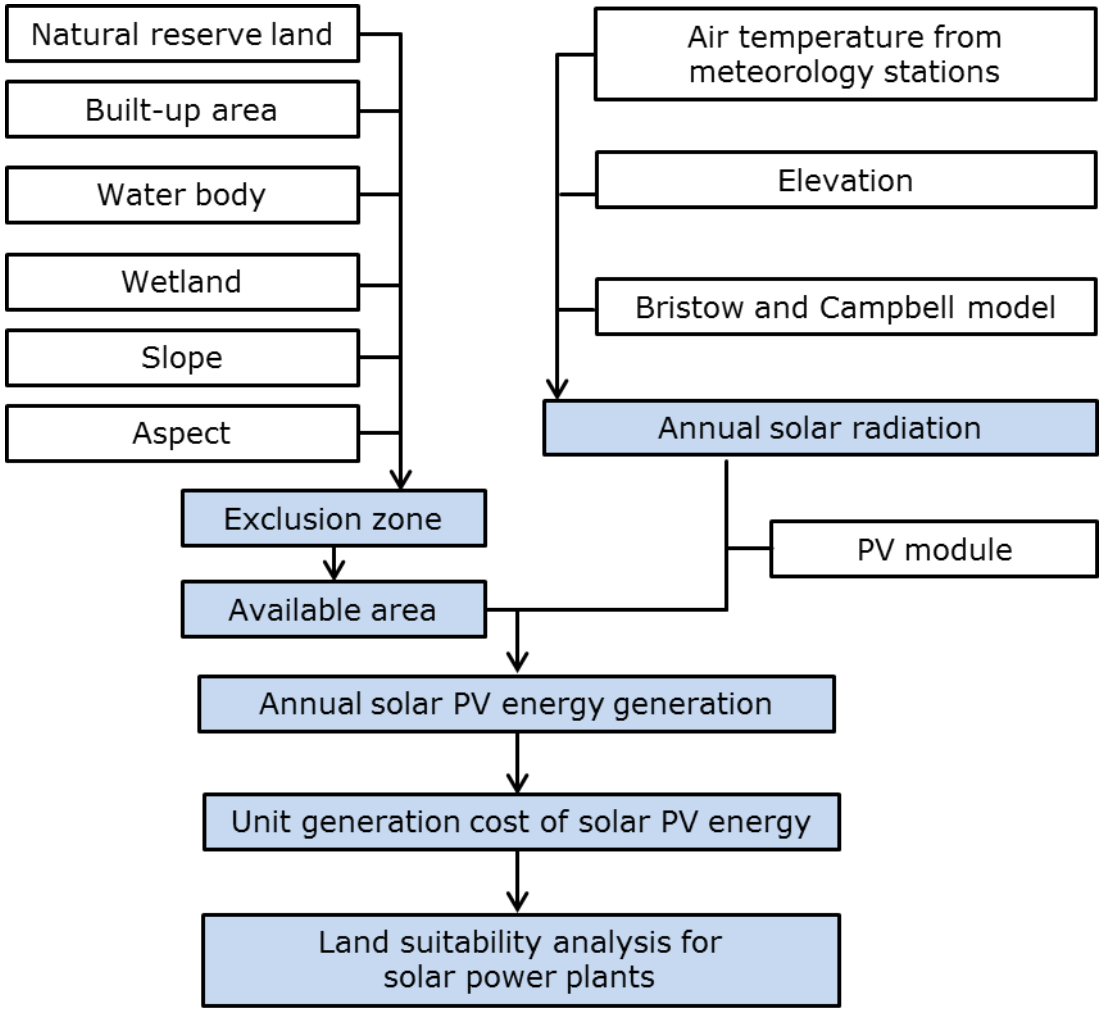

Figure 4.5 Overview of approach to assessing solar energy potential

4.2.1 Theoretical solar radiation potential simulation

Solar radiation resources directly affect the theoretical solar energy potential. Incoming solar radiation originates from the sun, is modified as it travels through the atmosphere, is further modified by topography and surface features, and is intercepted at the earth's surface as direct, diffuse and reflected components. Direct radiation is the principal component of total radiation (Charabi & Gastli, 2010). The sum of the direct, diffuse and the reflected radiation forms global solar radiation. Bristow and Campbell proposed a method for estimating the daily global solar radiation from daily maximum and minimum air temperature

measurements; this method requires less input data. The range of daily temperature extremes ΔT was calculated as follows:

$$\Delta T(J) = T_{max}(J) - (T_{min}(J) + T_{min}(J+1))/2$$

where

T_{max} is the daily maximum temperature (˚C);

T_{min} is the daily minimum temperature (˚C);

J is the day number.

The mean of the two minimum temperatures that occur on either side of the daily maximum value was used to help reduce the effect of large-scale hot or cold air masses that may move through the study area. A warm air mass moving through the area of interest on day J could increase $T_{max}(J)$ above the value possible for incoming radiation alone. By not incorporating$T_{min}(J+1)$, the resultant ΔT would imply a greater radiation load than actually occurred. The opposite situation occurs in the case of a cold air mass, and underestimation of incoming radiation would result from these conditions (Bristow & Campbell 1984).

The total transmittance for the day includes both the direct and diffuse components occurring on a horizontal surface, and T_t is the daily total transmission coefficient. It is computed as

$$T_t = \frac{daily\ measured\ irradiance}{daily\ extraterrestrial\ insolation}$$

Daily total extraterrestrial insolation (Q_o) occurring on a horizontal surface in (J/m^2) was computed using the equation (Gillespie et al., 1990):

$$Q_0 = 86400 S_0 \left({}^{d_{mean}}/_{d}\right)^2 (h_s sin\varphi sin\delta + cos\varphi cos\delta sinh_s)/\pi$$

where

S_0 is the solar constant(1360w/m^2),

d_{mean} is the mean value of the distance from sun to earth,

d is the distance from the sun to the earth; $\left({}^{d_{mean}}/_{d}\right)^{2}$ never differs by more than 3.5% and was therefore taken as unity (Gillespie et al., 1990),

h_s is the half daylength ($cosh_s = -tan\varphi tan\delta$),

φ is the latitude of the location of interest, and

δ is the solar declination ($\delta = 0.409 * \sin((\frac{2\pi J}{365}) - 1.39)$).

The equation used to describe T_t as a function of ΔT according to the Bristow-Campbell model is expressed as follows:

$$T_t = A[1 - \exp(-B\Delta T^C)]$$

where A, B, and C are empiric coefficients. Although these coefficients are determined empirically, they display the physics involved in a relationship. A represents the maximum clear sky of the study area and it varies with elevation and the pollution content of the air. B and C determine how soon maximum T_t is achieved as ΔT increases. They display the partitioning of energy that is characteristic of the region and differ, for example, from humid to arid environments (Bristow & Campbell, 1984). Kreith & Kreider (1978) describe the atmospheric transmittance for beam radiation by the empirical relationship given in the equation:

$$A = 0.56 * (e^{-0.56M} + e^{-0.095M})$$

where A is the clear sky atmospheric transmittance and M is the air mass ratio. The constants account for the radiation attenuation by the different factors discussed above. Because scattering is wavelength dependent, the coefficients represent an average scattering over all wavelengths. This relationship gives the atmospheric transmittance for clear skies to within a 3% accuracy.

The air mass ratio is the relative mass of air through which solar radiation must pass to reach the surface of the earth and is defined by the ratio of the actual path length mass to the mass when the sun is directly overhead. The two main factors affecting the air mass ratio are the direction of the path and the local

altitude. The paths direction is described in terms of its zenith angle, H, which is the angle between the path and the zenith position directly overhead. The ratio M is defined in the following equation where p is the local pressure; Mo and Po are the corresponding air mass and pressure at sea level.

$$M = (p/p_0)\, M_o$$

The formula above is valid only for zenith angles less than 70°. When the zenith angle is greater than 70°, the secant approximation underestimates solar energy because atmospheric refraction and the curvature of the earth have not been accounted for. Keith and Kreider suggest using the following equation to calculate the value of air mass ratio:

$$M_o = (1229 + (614sinH)^2)^{0.5} - 614sinH$$

$$\frac{p}{p_o} = (1 - 0.0065 * h/288)^{5.256}$$

where h is the height above sea level and

H is zenith angle

The value of B and C were adopted from the research work of Liu & Pan (2012). B and C in this study area are 0.019 and 1.876.

Annual global solar radiation can be calculated as the sum of daily global solar radiation. However, using this technique leads to an overly heavy workload. Thus, a linear interpolation method was introduced. Every 15th day of each month was chosen to be the monthly mean day (the 15th, 46th, 74th, 105th, 135th 166th, 196th, 227th, 258th, 288th, 319th and 349th day in the year). After calculating the global solar radiation of the monthly mean day, linear interpolation methods were used to calculate the daily global solar radiation. The linear interpolation formula is expressed as follows:

$$X_i = X_1 - \frac{DOM_i - DOM_1}{(DOM_2 - DOM_1) * (X_1 - X_2)}$$

where

X_i is the global solar radiation of day i, X_1 and X_2 are the global solar radiation of monthly mean day, DOM_1 and DOM_2 are the day numbers of the monthly mean day and DOM_i is the day number of i. The annual global solar radiation is the sum of X_i.

4.2.2 Analysis of geographical solar PV potential

Not all theoretical solar energy potential can be utilized due to geographic restrictions. The definition of unfeasible land is similar to that of the exclusion area for wind power plants. Therefore, the exclusion area for solar power plants includes land where PV modules would interfere with current land use, such as built-up areas, wetlands and land where it is physically impossible to install PV modules, such as bodies of water and steep areas.

Large-scale PV farms require flat terrain or fairly steep slope. Slope is a measure of the steepness of the surface. Although steep slopes can be utilized for home installations, flatter surfaces are desirable for large-scale solar farms (Arnette & Zobel, 2011). Furthermore, aspect is the direction in which a slope faces. Aspects of southern exposure are more desirable than slopes facing other directions for harnessing solar power because the study area is in the northern hemisphere. Based on previous research, an area with a slope of less than 2.5% is acceptable with any aspect for solar power plants (Arán Carrión et al., 2008). Southern exposure is not required in flat areas as the solar panels can be titled to the south with no effect on potential. In addition, Arnette & Zobel (2011) consider areas with slopes of 2.5% to 15% and a south-facing aspect as suitable for PV modules. Any location with a slope greater than 15%, regardless of the exposure, is considered unfeasible for solar farm development.

The next criterion applied in determining whether land is feasible for solar farms is based on land use restrictions. Any area restricted due to conservation, such as natural reserve, wetland and bodies of water, is excluded. PV systems have been recognized as a technology that has virtually no environmental impact, as they are clean and silent. Thus, there is no need to consider the use of a buffer for natural reserves or urban areas. Buffer analysis is used when siting wind farms mainly due to visibility, noise and the effect on wildlife associated with wind turbines, but buffers have not been used in previous solar farm siting research.

Unlike wind farms, which can be placed on agricultural land without substantially decreasing the amount of productive land, PV modules require that the majority of the land be utilized solely for PV installation. From this standpoint, solar farm sites should avoid built-up areas and productive agriculture land.

In summary, excluded areas for PV farms include any area with a slope greater than 15%, areas with a slope of 2.5% to 15% that don't have a south-facing aspect, nature reserves, built-up areas, wetlands and bodies of water. As the information regarding productive agricultural land in the study area is vague, fertile agricultural land is not considered.

4.2.3 Analysis of technical solar PV potential

The area of suitable land for PV farms becomes evident after the excluded area has been defined. The next task is to estimate annual solar energy generation, namely the technical solar energy potential. The solar energy harvest is determined by solar radiation and solar energy technologies. The branch of solar energy includes different types of concentrated solar power (CSP) technologies, such as parabolic trough, power tower, parabolic dish and concentrated photovoltaic systems (CPS).

Parabolic trough systems comprise rows of trough-shaped mirrors that direct solar insolation to a receiver tube along the focal axis of each trough (Stoddard et al., 2006). The focused radiation raises the temperature of heat-transfer oil, which is used to generate steam. The steam is used to power a steam turbine-generator to produce electricity. Power tower systems consist of a field of thousands of sun-tracking mirrors that direct insolation to a receiver at the top of a tall tower. A molten salt heat-transfer fluid is heated in the receiver and is piped to a ground based steam generator. The steam drives a steam turbine-generator to produce electricity (Stoddard et al., 2006).

Parabolic dish systems use a dish shaped arrangement of mirror facets to focus energy onto a receiver at the focal point of the collector. A working fluid such as hydrogen is heated in the receiver, and drives a turbine or stirling engine. Most current dish applications use sterling engine technology because of its high efficiency. The PV cells generate direct current electricity, which is converted to alternating current using a solid-state inverter (Stoddard et al., 2006).

Among the large-scale solar power systems, parabolic trough systems and power tower systems have been proven best suited for large-scale plants of 50 MW or larger. Trough and tower plants, with their large central turbine generators and balance of plant equipment, can take advantage of economies of scale for cost reduction, as cost per kW decreases with increased size. Additionally, these plants use thermal storage or hybrid fossil systems to achieve greater operating flexibility and dispatchability, accounting for situations in which sufficient solar insolation is unavailable (Tao & Rayegan, 2011).

Large-scale flat panel PV array systems for utility power production are also widely used because they are easy to scale up or down. When tied into electric grids, they provide flexible, variable power generation options. However, their costs are much higher in comparison to those of parabolic trough systems. Dish and CPS are modular in nature, and a single unit could produce power in the range of 10 kW to 35 kW. They could be used for either distributed or remote generation applications, or in large arrays of several hundred or thousand units for a utility scale application. Moreover, they have the potential advantage of mass production of individual units (Tao & Rayegan, 2011), and the implementation of PV plants is significantly faster than other technologies, which affords greater flexibility to cope easily with the development of the grid system (Charabi & Gastli, 2011).

Concentrating photovoltaic plants provide power by focusing solar radiation onto photovoltaic modules, which convert the radiation directly to electricity. Three main parameters determine PV production energy: solar radiation of the local area and the size and performance ratio of PV systems. PV production energy is calculated as:

$$E_i = G_i * A * A_f * \eta * pr$$

where,

E_i is electric power generation potential per year (GWh/year);

G_i is annual solar radiation received per unit horizontal area (GWh/km^2/year);

A is the calculated total area of suitable land (km^2);

A_f is the area factor indicating what fraction of the calculated areas can be covered by solar panels, assumed to be 10% (Gastli & Charabi, 2010); and

η is the efficiency with which the solar system converts sunlight into electricity.

Conversion efficiency varies with PV cells. Based on the current report from the Fraunhofer Institution, the highest conversion efficiency is between 36 and 41.1% using high-efficiency tandem cells. The efficiency of mainly c-Si cells is between 20 and 24%, and the conversion efficiency of simple c-Si cells is 14 to18%. With thin film cell technology, efficiency is only 6 to 11%. Considering the technologies used in existing PV projects, efficiency falls between 11 and 15%. Thus, based on existing research conducted by Hoogwijk (2004) and Stoddard (2006), η is taken as 14.3% in this study.

pr, is 0.75, performance ratio or PV system, taking energy loss in storage and connection into the electricity grid into account.

4.2.4 Analysis of economic solar PV potential

To show the spatial distribution of PV generation costs and draw the geospatial supply curve, unit PV electricity costs in the study area was calculated. The total production cost of solar PV energy comprises initial investment cost as well as operation and maintenance costs. The total initial investment cost is the sum of PV system costs and construction costs, and the annual operation and maintenance costs are considered constant and defined as a fraction (3%) of investment cost (Hoogwijk, 2004). The transmission cost has been neglected. N is the life-time of the system, which is 25 years (Sun et al., 2013). The nominal discount rate is taken as 5%, and it is assumed that the total investment of PV plants is obtained completely from loans.

The average annual cost per kilowatt-hour of electricity generated in a grid cell was derived from the sum of total annual investment and operating costs and the annual energy yield. The unit cost of energy was calculated using the formulae:

$$PC_i = \frac{C_{o\&m} + L}{E_i}$$

$$L = I \frac{r(1+r)^n}{(1+r)^n - 1}$$

where

PC_i is the cost of 1 kWh of electricity generated in a grid cell;

$C_{o\&m}$ is the operation and maintenance costs, and is assumed to be a constant rate (0.03 of investment) over the life time;

E_i is the annual energy yield in a grid;

L is the annual loan payment;

I is the initial investment cost. Based on the current market report, PV module cost in this study is considered as 1.2 $/w. Capacity of PV per square kilometer is assumed as 41.13 MW (Gastli & Charabi, 2010);

r is the interest rate;

n is the life time of the system.

The method used to calculate the economic potential of solar energy is similar to that used in the section related to the assessment of wind energy potential. It is also assumed that PV module installation begins in the area with lowest unit generation cost before solar energy projects gradually move to areas with higher unit generation costs. Economic potential is defined as the amount of solar energy supply at the point of intersection where average unit generation cost equals the sum of market price and subsidy.

4.2.5 Land suitability analysis for PV plants based on the multi-criteria method

Arán Carrión et al. (2008) note that when allocating land for solar farms, the number of sun hours, irradiance, temperature, and aspect must be considered to maximize potential. Geographic variables such as land cover or vegetation that increase shade, access to highways for maintenance and repair, population density, and the location of substations play a role, as do factors such as solar radiation, slope and aspect, which maximize temperature. Large-scale PV farms require flat terrain or relatively steep slope facing south, with less than a 5% graded slope. Moreover, Charabi & Gastli (2011) suggest that proximity to roads can avoid additional cost of infrastructure construction and consequential

damage to the environment. PV farms are particularly suitable where the connection to the existing electric grid is effortless, and establishing farms in proximity to the existing grid and load poles reduce significant transmission losses. As multiple factors influence the suitability of an area or the establishment of a solar farm, the multi-criteria method is appropriate for land suitability analysis. The methodology is identical to that used in land suitability analysis for wind power plants.

Solar radiation is considered the most influential criterion in determining the suitability of land for solar farms. The sites of PV farms should avoid mountain summits and steep slopes, as the complex terrain makes the installation of PV modules and the construction of other infrastructure difficult. PV module installation requires a large area, unlike wind turbines, and land cover type is an important indicator. Barren land is considered the most desirable; forest and farmland are less suitable. Ideally, solar farm sites should be close to roads, the existing power grid system and urban areas. Energy demand in urban areas is significantly higher than in rural areas, and locating solar farms near urban areas reduces loss during energy transmission. The costs of constructing transmission lines also decreased.

In this study, unit generation cost is considered the most important criterion because it defines the feasibility of solar energy production and integrates the technical solar energy potential and cost. Geographic criteria are next: an area with a mild slope is more eligible for a PV farm than a steep area is, and barren land is given high priority, while forest and farmland are considered a poor choice. Economic factors, distance to roads, urban area and transmission lines are the least important. The weight of each criterion was derived using the AHP method, by directly comparing the importance of one criterion to another; the comparison matrix is shown in Table 4.10.

Table 4.10 Comparison matrix of criteria for solar farm

Criteria	Unit generation cost	Slope	Landcover	Distance to road	Distance to urban area	Distance to transmission line
Unit generation cost	1	3	3	5	5	5
Slope	1/3	1	1	3	3	3
Landcover	1/3	1	1	3	3	3
Distance to roads	1/5	1/3	1/3	1	1	1
Distance to urban area	1/5	1/3	1/3	1	1	1
Distance to transmission lines	1/5	1/3	1/3	1	1	1
Total	2.26	6	6	14	14	14

Table 4.11 shows the normalised pairwise comparison matrix of criteria for solar farms. Finally, the weights of criteria are displayed in Table 4.12.

Table 4.11 Normalised pairwise comparison matrix of criteria for solar farm

Criteria	Unit generation cost	Slope	Landcover	Distance to road	Distance to urban area	Distance to Transmission line
Unit generation cost	0.442	0.5	0.5	0.357	0.357	0.357
Slope	0.147	0.167	0.167	0.215	0.215	0.215
Landcover	0.147	0.167	0.167	0.215	0.215	0.215
Distance to roads	0.088	0.055	0.055	0.071	0.071	0.071
Distance to urban area	0.088	0.055	0.055	0.071	0.071	0.071
Distance to transmission lines	0.088	0.055	0.055	0.071	0.071	0.071

Table 4.12 Weights of criteria for solar farm

Criteria	Unit generation cost	Slope	Landcover	Distance to road	Distance to urban area	Distance to Transmission line
Weights	0.418	0.188	0.188	0.0685	0.0685	0.0685

The next step is to investigate whether the comparisons are consistent. For controlling the consistency of the estimated weight values, CR is calculated using the formula detailed in section 4.1.5. If CR is less than or equal to 0.10, the degree of consistency is satisfactory (Saaty, 1980). The CR value of each criterion for solar farms is smaller than 0.1.

Once the weights are assigned, the criteria or indicators are ordered according to their degree of importance and normalized on a scale of 1 to 9, where 1 is the lowest value and 9 is the highest, as Table 4.13 shows.

Table 4.13 Scores of indicators for solar farm

Unit generation cost	0.164 - 0.178 $/KWh	9
	0.178 - 0.187 $/KWh	7
	0.187 - 0.194 $/KWh	5
	0.194 - 0.205 $/KWh	3
	0.205 - 0.229 $/KWh	1
Slope	<1%	9
	1% - 2.5%	7
	2.5% - 5%	5
	5% - 10%	3
	10% - 15%	1
	>15%	Restricted area
Landcover type	Built-up area, water body and wetland, natural reserve	Restricted area
	Forest	1
	Farmland	3
	Scrub	5
	Grassland	7
	Barren land	9
Distance to road	<2 km	9
	2 km - 5 km	7
	5 km - 10 km	5
	10 km - 20 km	3
	>20 km	1
Distance to transmission line	<5 km	9
	5 km -10 km	7
	10 km - 15 km	5
	15 - 20 km	3
	>20 km	1
Distance to urban area	<5 km	9
	5 km - 10 km	7
	10 km - 15 km	5
	15 km - 20 km	3
	>20 km	1

4.3 Biomass energy potential assessment

Biopower, or biomass power, is the use of biomass to generate electricity. Biopower system technologies include direct-firing, cofiring, gasification,

pyrolysis, and anaerobic digestion. Most biopower plants use direct-fired systems that burn biomass directly to produce steam. Co-firing refers to mixing biomass with fossil fuels in conventional power plants. Coal-fired power plants can use cofiring systems to significantly reduce emissions, especially sulphur dioxide emissions. Gasification systems use high temperatures and an oxygen-starved environment to convert biomass into synthesis gas, a mixture of hydrogen and carbon monoxide. The synthesis gas, or syngas, then can be chemically converted into other fuels or products, burned in a conventional boiler or used instead of natural gas in a gas turbine. Gas turbines are much like jet engines, only they turn electric generators instead of propelling jets. Highly efficient to begin with, they can be made to operate in a combined cycle in which their exhaust gases are used to boil water for steam, a second round of power generation, for even higher efficiency (National Renewable Energy Laboratory, 2013).

The assessment of biomass energy potential in this study includes the assessment of usable biomass potential from agricultural and forestry residues, the economic analysis of biomass power plants based on case studies, and site selection for biomass power plants. Usable biomass is derived from NPP data. Biomass energy is different from wind and solar energy. One obvious difference is that biomass needs to be transported from farmland or forests to biomass power plants, which makes it impossible to assess the spatial distribution of the technical potential of biomass energy. In addition, the energy production from biomass must be evaluated based on specific biomass power plants, which accounts for the introduction of case studies in this section. Biomass energy production, cost and revenue are analyzed in the case studies. As the biomass needs to be transported from collection points to biomass power plants, transport cost accounts for a large percentage of total cost. The selection of optimal sites is based on network analysis to reduce transport cost. The workflow of the assessment of biomass energy potential is shown in Figure 4.6.

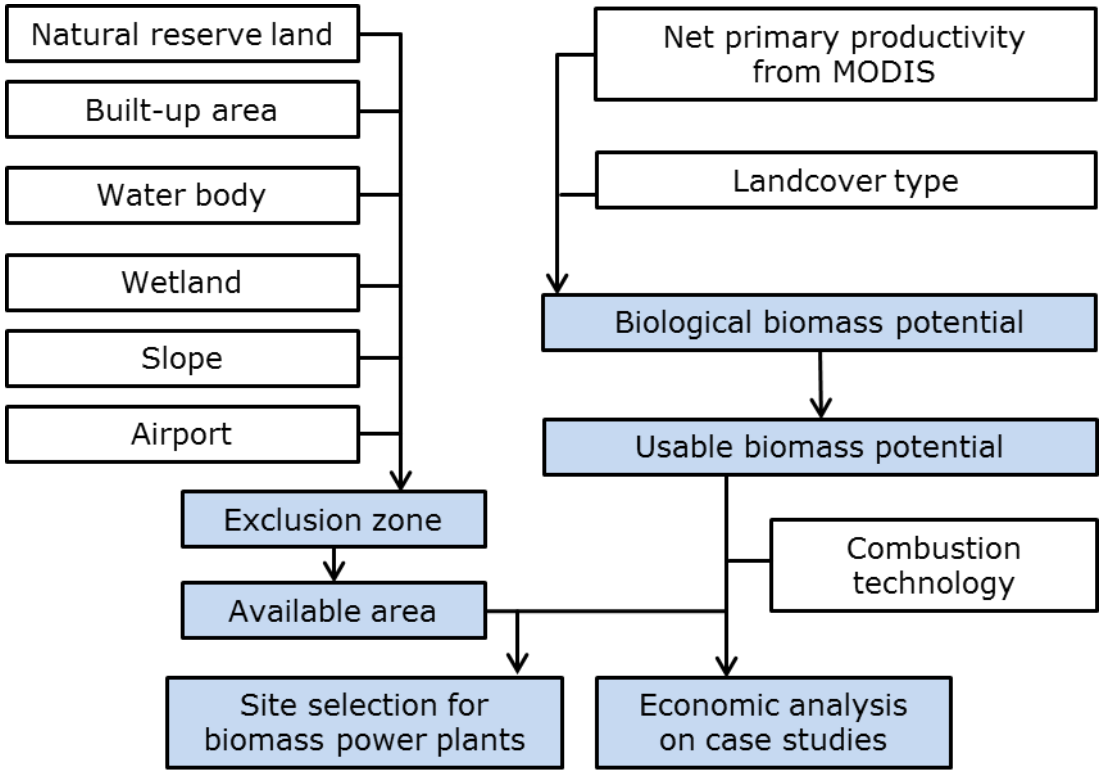

Figure 4.6 Overview of approach to assess biomass energy potential

4.3.1 Estimation of usable biomass power potential

The assessment of usable biomass power potential begins from biological biomass potential, which is the quantity of total residues from crops and forestry and is derived from the annual NPP. NPP is defined as the net flux of carbon from the atmosphere into green plants per unit time. In other words NPP is equal to the difference between the rate at which plants in an ecosystem produce useful chemical energy (or GPP), and the rate at which they expend some of that energy for respiration. NPP is a fundamental ecological variable, not only because it measures the energy input to the biosphere and terrestrial carbon dioxide assimilation, but also because of its significance in indicating the condition of the land surface area and status of a wide range of ecological processes. The MODIS product (MOD17A3) provides annual global NPP at 1 km resolution. The University of Montana produced Version-55 of the NPP product (USGS, 2014).

NPP includes both above-ground and below-ground production and is measured as the amount of carbon per unit area (gC/m^2). Only the above-ground biomass is used for energy production, so conversion is needed to obtain the above-ground NPP value from the overall value. The following equation is used to

convert NPP from MODIS/Terra data to biologically available biomass based on the research of (Shi et al., 2008).

$$B = NPP * \alpha/\beta$$

B is biologically biomass;

α is the proportion of above ground biomass in the total biomass;

β is carbon concentration in dry biomass; and

for crops and grass, α is 0.8 and β is 0.45, while for forest and other woody vegetation, α is 0.5 and β is 0.5 (Shi et al., 2008).

Not all biologically available biomass can be used for energy production due to restrictions, such as soil carbon maintenance, papermaking and other economic purposes. Usable biomass is introduced to express the part of biologically available biomass that can be used for energy production and is calculated based on the equation

$$U = B * r * (1 - e - l)$$

where

U is usable biomass;

B is biologically biomass;

R is the fraction of B that is not primary yield. For crops, only the residues (such as straw and stems) are used for energy production. For fast-growing grass or trees that are dedicated to energy production, r can be equal or close to 1 (Liao et al., 2004).

e is the fraction of excluding the biomass used for economic purpose other than energy production, such as forage and papermaking.

l presents the loss during the whole process, for example, the loss occurring during the harvest.

As the land cover data in the land use dataset does not exactly match the crop and forest classes due to the two different classification systems, adjustment is

required. Specifically, cropland as one class of land cover includes varieties of crop types. Bi et al. (2009) provide ratio values of different crop types in China, including wheat, corn, soybeans, sugarcane, green beans, cotton, peanuts and rape. Using residual/production ratio (r) and production of each crop, the composite ratio for cropland in a specific administrative region is calculated using the formula:

$$R = \sum_{i=1}^{n} r_i p_i \Big/ \sum_{i=1}^{n} p_i(1 + r_i)$$

where

R is the composite ratio for cropland;

r_i is residue/production ratio, derived from the 'ratio of grass to grain' data (Bi, et al., 2009); r for different wood types is derived from the 'the estimated coefficient of forest residue in China' in the research of Liao et al.(2004);

p_i is the production of crop i in 2010, recorded from the China Statistic Yearbook (2014);

n is the number of crops.

The rate for 'forest' in the land use data is calculated in the same way, as forest is also a composite type that includes economic forests, timber forests, sparse forests, production forests, firewood forests and fast-growing forests (Shi et al., 2008). The production data for each type of forest from the China Statistic Yearbook (2014) is available only for provincial regions. Table 4.14 shows the composite residue/production ratio for cropland and forest.

Table 4.14 Composite residue/production ratio for cropland and forest

Region		Composite ratio for cropland	Composite ratio for forest
Beijing		0.472415801	0.1691
Tianjin		0.498991045	0.2710
Hebei Province	Shijiazhuang	0.491261316	0.3267
	Tangshan	0.475428581	
	Qinhuangdao	0.472356799	
	Handan	0.493186946	
	Xingtai	0.49517735	
	Baoding	0.484521497	
	Zhangjiakou	0.509070714	
	Chengde	0.499377042	
	Cangzhou	0.487101238	
	Langfang	0.47779864	
	Hengshui	0.491461368	

For shrubbery and grass and other fast growing vegetables, r is considered 1; for savanna land cover type, 0.5 is used in this study according to the MOA/DOE report (Dai et al., 1998). The report states that in China the percentage of crop residue returned to or left in the field is approximately 15%. However, according to the field survey conducted by Shi, et al.(2008), this percentage can be as high as 70%. As insufficient information is available to make a more accurate estimation, 50% is has been chosen as the percentage of residue that returns to the soil.

Based on the MOA/DOE report, 2.3% of the total available straw and stalk is used as industrial material for papermaking, and approximately 24% is utilized as forage; hence, the percentage of economic use is 26.3%. Loss for the entire process is assumed to be 5%. Table 4.15 shows the parameter values of different land cover types for calculating usable biomass.

Table 4.15 Parameter values of different land cover types for calculating usable biomass

Land cover type	α	β	r	e_1(return to soil)	e_2 (economic use)	loss
Forest	0.5	0.5	composite ratio	0.5	0	0.05
Cropland	0.8	0.45	composite ratio	0.5	0.263	0.05
Shrubbery	0.5	0.5	1	0.5	0	0.05
Savanna	0.5	0.5	0.5	0.5	0	0.05
Grassland	0.8	0.45	1	0.5	0.263	0.05
Other	0	1	0	0	0	0.05

4.3.2 Economic analysis of biomass power plants

Biomass fuels are burned directly to produce steam, which drives a turbine that turns a generator that converts the power into electricity. In some biomass applications, the turbine exhaust steam from the power plant also is used for manufacturing processes or to heat buildings. Such combined heat and power systems greatly increase overall energy efficiency. The systems usually operate 24 hours per day and 7 days per week, with several weeks of downtime per year for maintenance and repairs (Tomberlin & Mosey, 2013). The amount of energy generated by a biopower system depends on several factors, such as the type of biomass, the technology used and other economic factors. In this study, combined heat power (CHP) technology has been selected because of its high overall energy efficiency. CHP is technically the concurrent generation of multiple

forms of energy in a single system (Tomberlin & Mosey, 2013). CHP systems include reciprocating engines, combustion or gas turbines, steam turbines, micro turbines, and fuel cells. While generating electric power, the thermal energy from the system can be used to produce steam, hot water, or chilled water for process cooling (Tomberlin & Mosey, 2013).

Biomass power plants are different from wind power plants and solar PV plants, because biomass has to be collected from farmland, forests or other places and transported to biomass power plants (Liu, 2012a). Unlike the free wind resource and solar radiation, biomass has to be bought from farmers. Furthermore, the installed cost of biomass power generation systems is estimated based on several key factors, including the equipment arrangement, plant size, and geographical factors. These costs include permitting, engineering, equipment, construction, commissioning, and all soft costs such as development fees and the costs for financing. The economics of a biopower system depend on incentives, plant costs, labour costs, biomass resource costs and the sales rate for electricity and thermal energy. Operational costs are a major component and economy of scale is critical concerning operating costs. While larger plants are more efficient, cost per kilowatt is also lower due to labour costs. For example, a 20 MW biopower facility may have only a few more employees than a 10 MW facility (National Renewable Energy Laboratory, 2013).

Table 4.16 shows related data for biomass power plants on different scales derived from practical projects in China. According to the case studies from Liu (2012b), in the study area the necessary investment is 10,000 yuan per 1kW installed capacity. This number includes the purchase and installation costs for the biomass combustion boiler and other facilities and the initial investment for ancillary infrastructure, thus it can be considered total investment cost. Annual operation and maintenance costs are assumed to be 3% of investment cost based on the empirical data.

The field studies from Liu (2012b) offers some guidance on fuel consumption. Biomass power plants with 12 MV installed capacity consume 140 thousand tons of biomass residues per year. Other biomass residue consumption for different scales of biomass power plants are described in Table 4.16. Fuel cost for

biomass power plant is 300 ¥/t, which includes collection costs and transportation cost from the farms to biomass power plants.

Heat values for residues from different crops vary, and 15 MJ/kg is used to calculate heat value. The results of a study undertaken by Thek (2004) show that the average efficiency for electricity from the heat value of biomass is 16.9%, and average efficiency for heat is 71 %. In this study, these values are used to estimate electricity and heat production. The annual production of electricity and heat are estimated based on the formulae:

$$E_b = F * hv * e_p$$

$$H_b = F * hv * e_h$$

where

E_b is the annual production of electricity from biomass residue;

H_b is the annual production of heat from biomass residue;

F is the consumed biomass fuel;

hv is the heat value;

e_p is the transfer efficiency from heat value of fuel to electricity production;

e_h is the transfer efficiency from heat value of fuel to heat production.

Including the government subsidy, the price of electricity produced from biomass is 0.75 ¥/kWh, while the benchmark of electricity produced from coal is 0.45 ¥/kWh. The heat price is 45 ¥/GJ from biomass power plants in the study area. To simplify the calculation process, all investment costs are assumed to be paid from loans, and the interest rate is 5% annually. The annual loan is calculated based on the formula

$$L = I \frac{r(1+r)^n}{(1+r)^n - 1}$$

where

L is the annual loan payment;

I is the initial investment cost;

r is the interest rate;

n is the lifetime of biomass power plants, taken as 15 years.

Table 4.16 The basis of economic analysis for biomass power plants

Installed capacity (MW)	12	15	24	30
Total investment cost (million yuan)	120	150	240	300
O&M cost (million yuan)	3.6	4.5	7.2	9
Annual fuel Consumption (t)	140,000	163,443	280,000	300,000
Annual fuel Cost (thousand yuan)	42,000	49,032.9	84,000	90,000
Heat value from fuel (million MJ)	2100	2452	4200	4500
Production of electricity (MWh)	99,167	115,772	198,333	212,500
Production of heat (GJ)	1,470,000	1,716,151	2,940,000	31,50,000
Heat (MWh)	408.	477	817	875
Electricity price sales revenue (thousand yuan)	74,375	86,829	148,750	159,375
Heat price sales revenue (thousand yuan)	66,150	77,226	132,300	141,750
Loan payment (million yuan)	11.56	14.45	23.12	28.90

In reality, the production of electricity and heat cannot be constant due to the decline of facility performance. The decline ratio identified by Moon et al. (2011) is utilized in this study. Revenue, costs and net profile for two case studies, with

annual CHP of 12 MW and 30 MV were calculated as a result of economic analysis.

4.3.3 Site selection for biomass power plants

Environmental and social constrains must be considered when planning a site for a biomass power plant. Factors that affect restrictions on location include pollution, bad smells, and the existence of protected areas and citizens' reactions (Ma et al. 2005). Based on studies by Voivontas (2001) and Perpiñá et al. (2009), the constraints in Table 4.17 can be applied to site biomass power plants.

Table 4.17 Environmental and social constraints to apply for sitting bioenergy plants

Feature	Recommendation for buffer zones
Wetlands and lakes	Buffer zones around wetlands and lakes:100m
Protected areas	Buffer zones around protected areas: 500m
Airports	Buffer zones around airports: 500m
Slope	Slope greater than 15% is not allowed
Residential area	Buffer zones around residential area: 500m

Source: Own illustration, based on the mentioned literature above

Once the excluded areas for biomass power plants are defined, research focuses on the selection of optimal sites. The techniques used to optimize the locations for plants include location-allocation modelling and supply area modelling. Location-allocation modeling optimizes plant locations based on all usable biomass in the area, even if some biomass locations are beyond the reasonable transportation distance to the plant locations. This modelling is suitable when the planner intends to send all usable biomass to the plant location (Shi et al., 2008). Ranta (2005) used this modelling to find optimal power plant locations for utilizing logging residue in Finland. In supply or service area modeling, power plants are located sites surrounded by high local biomass density as only the biomass near the plants is useful; distant biomass is useless because of high transport costs. Thus, supply area modeling is appropriate when there is a threshold for transportation costs. The first approach is to set the size of the power plant and

expand the supply area of a candidate site until the biomass in the supply area meets the scale of the plant. The costs for transporting the biomass in the supply area to the plant are calculated to evaluate whether a plant at a specific location is profitable. Zhan et al. (2005) adopted this approach to evaluate pricing strategies for a potential switchgrass to ethanol conversion facility in Alabama. The second approach directly sets a transportation cost threshold and finds sites whose supply areas contain sufficient biomass. Voivontas (2001) used this approach to site biomass power plants.

In this study,a combination of location-allocation modelling and supply area modelling is used because it is rational to set limits on transportation costs in a large study area. Transportation costs in this study are measured by distance, and 100 km has been chosen as the transportation cost threshold. This threshold stems from a technical report from the National Renewable Energy Laboratory (Montague et al., 2002). The location-allocation method in network analysis enabled in ArcGIS has been used to find optimal sites for biomass power plants. This is a powerful tool for developing a spatial decision support system for private or public facilities planning. The principle behind it is that biomass power plants should be located at locations surrounded by sufficient biomass while transportation costs should be minimized. As the name suggests, location-allocation is a two-fold problem that simultaneously sites facilities and allocates demand points to the facilities. In this study, biomass power plants are facilities and biomass supply sites are demand points in location allocation analysis. The goal of location allocation is to site the facilities in a way that supplies the demand points most efficiently.

Location-allocation analysis enabled in ArcGIS layer offers seven problem types to site facilities and allocation demand points, namely minimizing impedance, maximizing coverage, maximizing capacitated coverage; minimizing facilities, maximizing attendance, maximizing market share and target market share. The siting of biomass power plants forms part of the minimizing impedance problem because it can reduce overall transportation costs. Because the spatial resolution of usable biomass distribution geodata is 1 km^2 and considering the efficiency of location-allocation analysis, each 5 km^2 is considered a point. Each centroid of a 5 km^2 grid contains the usable biomass (t), as the example in Figure 4.7 shows.

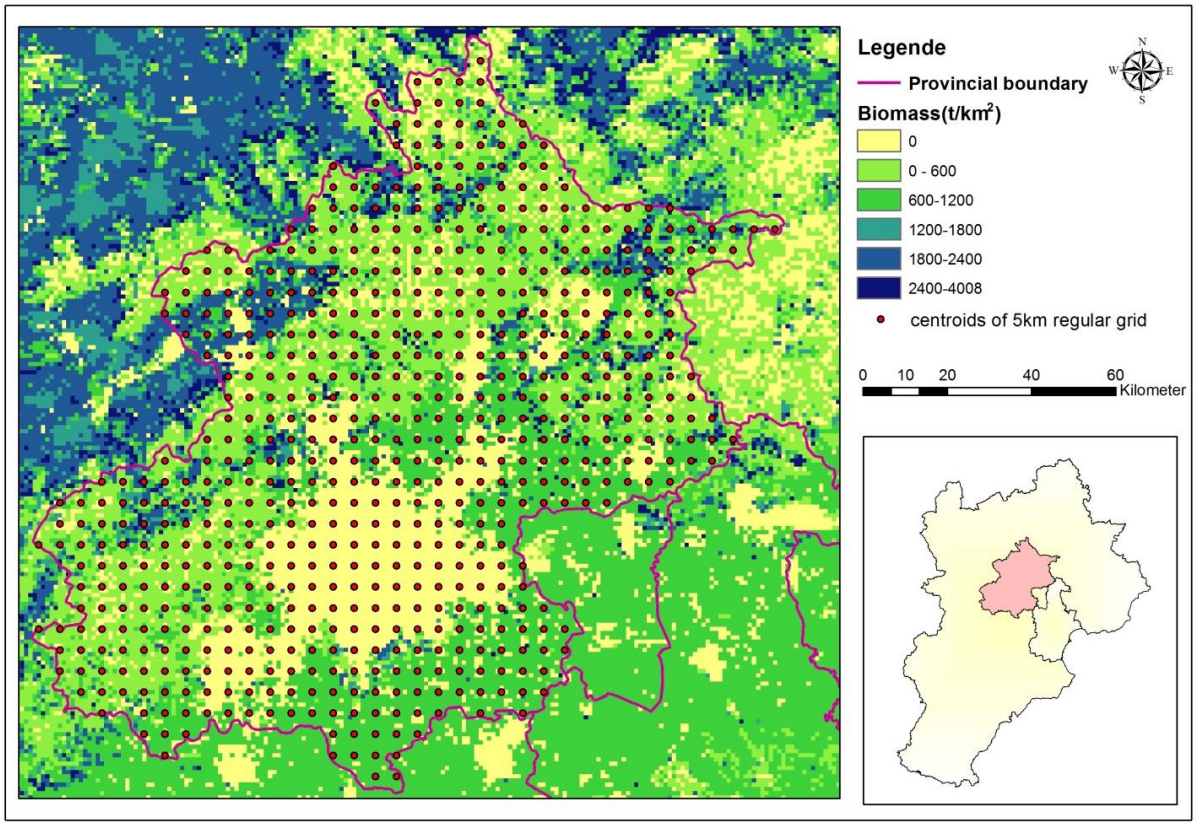

Figure 4.7 Centroids of 5 km grid, each one contains usable biomass

The entire territory contains:

- 8,873 biomass retrieving points; and
- 7,182 potential sites of biomass power plants — 691 points have been eliminated due to environmental and social constraints.

The most important work required to implement location - allocation analysis is to build a road network. General attributes of the road network include

- road type, which provides the information of the road hierarchy, such as highway, national road or provincial road;
- length, which refers to the road stretch length of the routes; and
- one way, which refers to the travel direction. In this case, traffic is allowed to travel in both directions.

After the road network is built, location-allocation analysis can be implemented by loading facilities and demand points. The important aspect of demand points in location-allocation analysis is usable biomass. This setting of weight

guarantees that the points with sufficient usable biomass are more important than those with less usable biomass are. The top 10 sites are selected during this process. Considering the population density and existing coal and biomass power plants, only 4 sites have been selected as the final optimal biomass power plant locations. Each optimal site has an individual supply area providing biomass. The distribution of optimal sites and statistical results appear in the results and discussion section.

5 Results and discussion

The section contains the results of the assessment of wind, solar and biomass energy potential. All results are derived from the methodology described in Chapter 4. Based on the results and current situation of renewable energy development, suggestions for future development are provided.

5.1 Wind energy

5.1.1 Theoretical wind power potential

Figure 5.1 illustrates the annual wind speed at the height of 80 m and wind power density are presented and they were calculated based on the formula in the section 4.1.1. Wind speed differs in value over the region from 2.6 to 6.0 m/s. Wind power density, which indicates theoretical wind power potential, varies from 4.5 to 210 w/m^2.

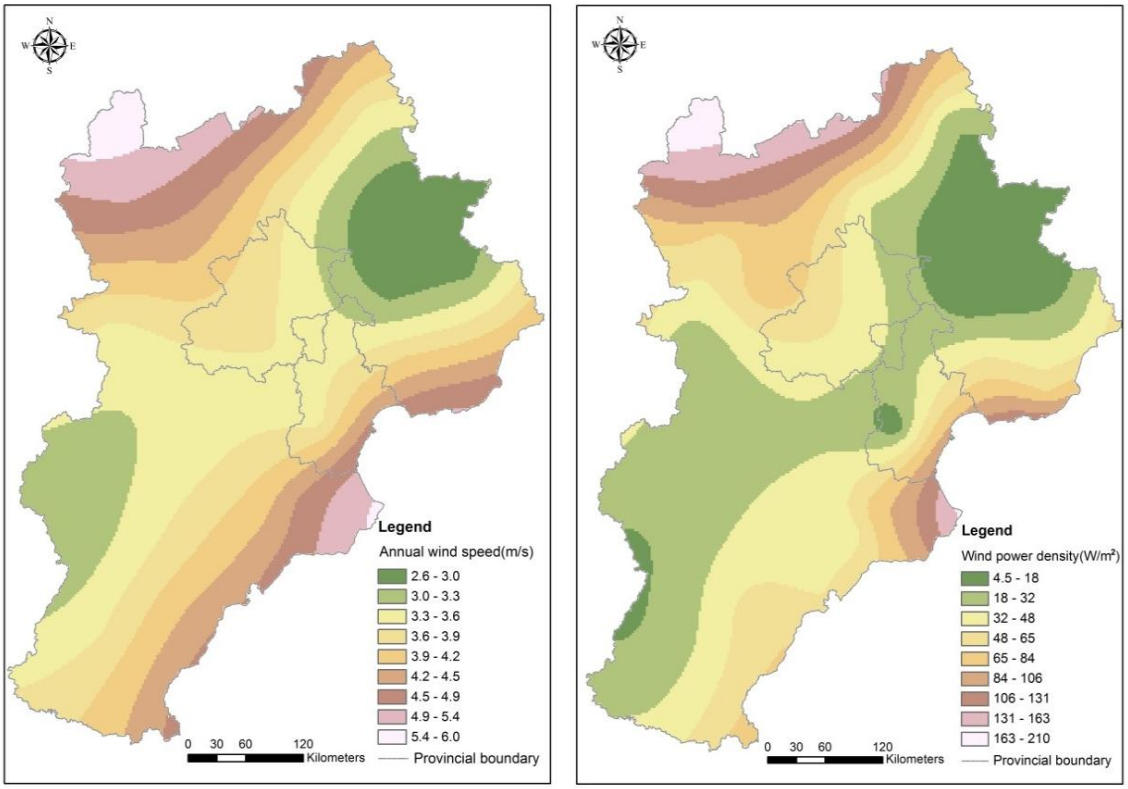

Figure 5.1 Spatial distribution of annual mean wind speed and wind power density

The highest wind speed is located in the north-western part of the study area, on the Bashang Plateau next to the southern edge of the Mongolian Plateau. In winter, the Asian continental cold high pressure passes through this area from the north-west to the south-east, and the Wind speed on the Bashang Plateau is

higher than in areas because of this. The eastern side of the study area, near the Bohai Sea, also experience high wind speed. The lowest wind speeds occur in the north-eastern part, in the Yanshan Basin, and the second lowest wind speeds occur in the south-western part, in the Taihang Mountains, as the Taihang Mountains block the cold high pressure system in winter. Thus, terrain and wind regime largely determine the spatial distribution of wind speed in the study area. The distribution of wind power density depends on wind speed, and the north-western area (the Bashang Plateau) and eastern area near the sea are endowed with excellent wind energy resources.

5.1.2 Geographic wind power potential

Wind power plants cannot be built in restricted areas. Based on the criteria in this study, restricted areas are shown in Figure 5.2. The restricted section of the study area covers 80,189 km^2, which accounts for 36.9% of the total area.

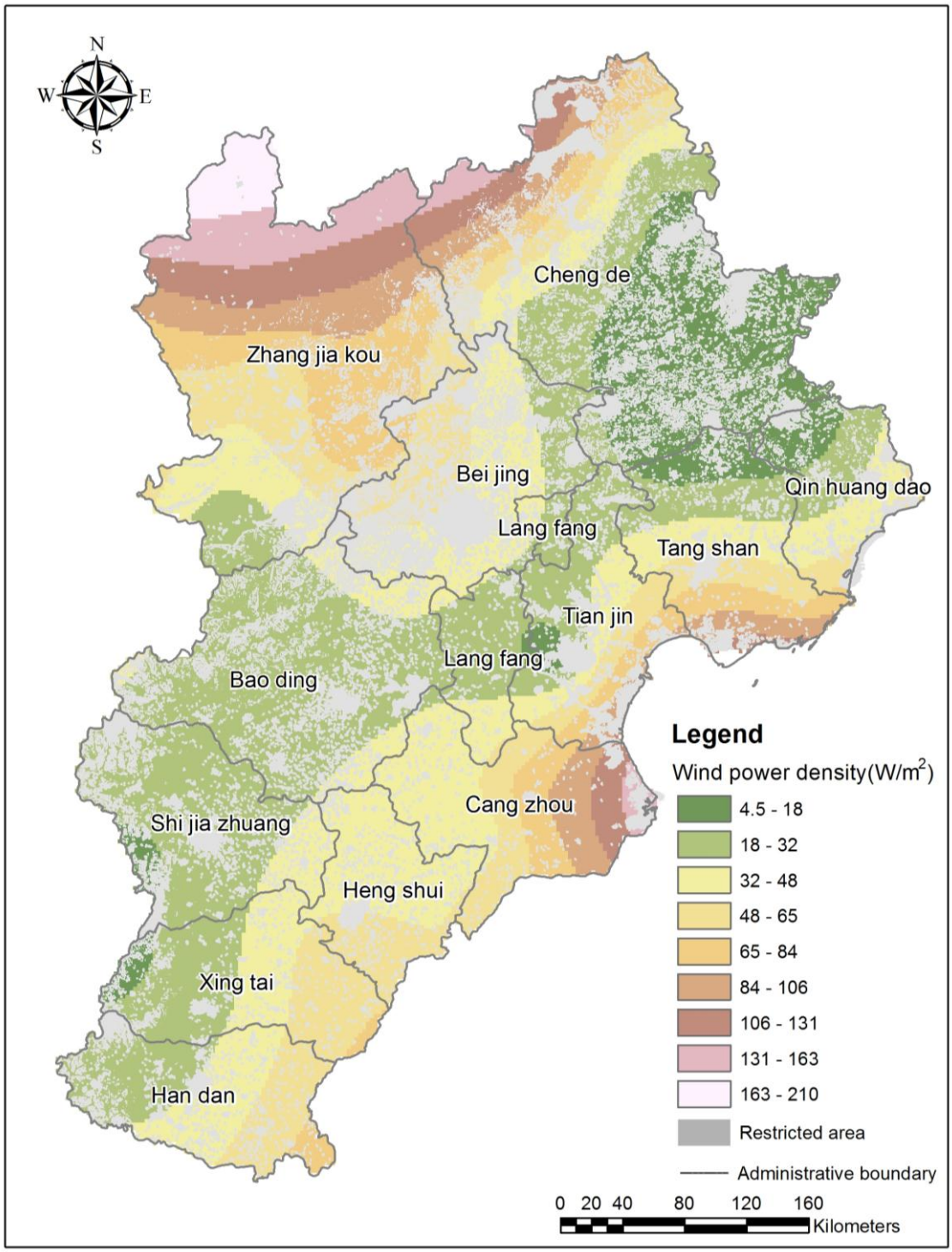

Figure 5.2 Spatial distribution of wind power density and restricted area

5.1.3 Technical wind power potential

Annual wind power production in a given region is closely to wind speed, the conversion efficiency of wind turbines and the suitability of the area and was calculated based on the formulae in the section 4.1.3. The spatial variation of technical potential is similar to theoretical wind power potential. The north-

western region next to the Mongolian Plateau and the eastern section near the Bohai Sea have abundant technical wind power potential. The zonal statistics function in ArcGIS was used to summarize electricity production within the administrative boundary of 12 cities (see Table 5.1). Zhangjiakou, located in the northwestern region, is ranked first with 125 TWh/year technical potential and 4.05 GWh/year/km^2 technical potential density, which is the annual energy yield divided by the area available for wind farms. The regional potential is estimated to be 307 TWh/year; in 2012, total electricity consumption in study area exceeded 467.47 TWh. The consumption far exceeds the total technical wind potential.

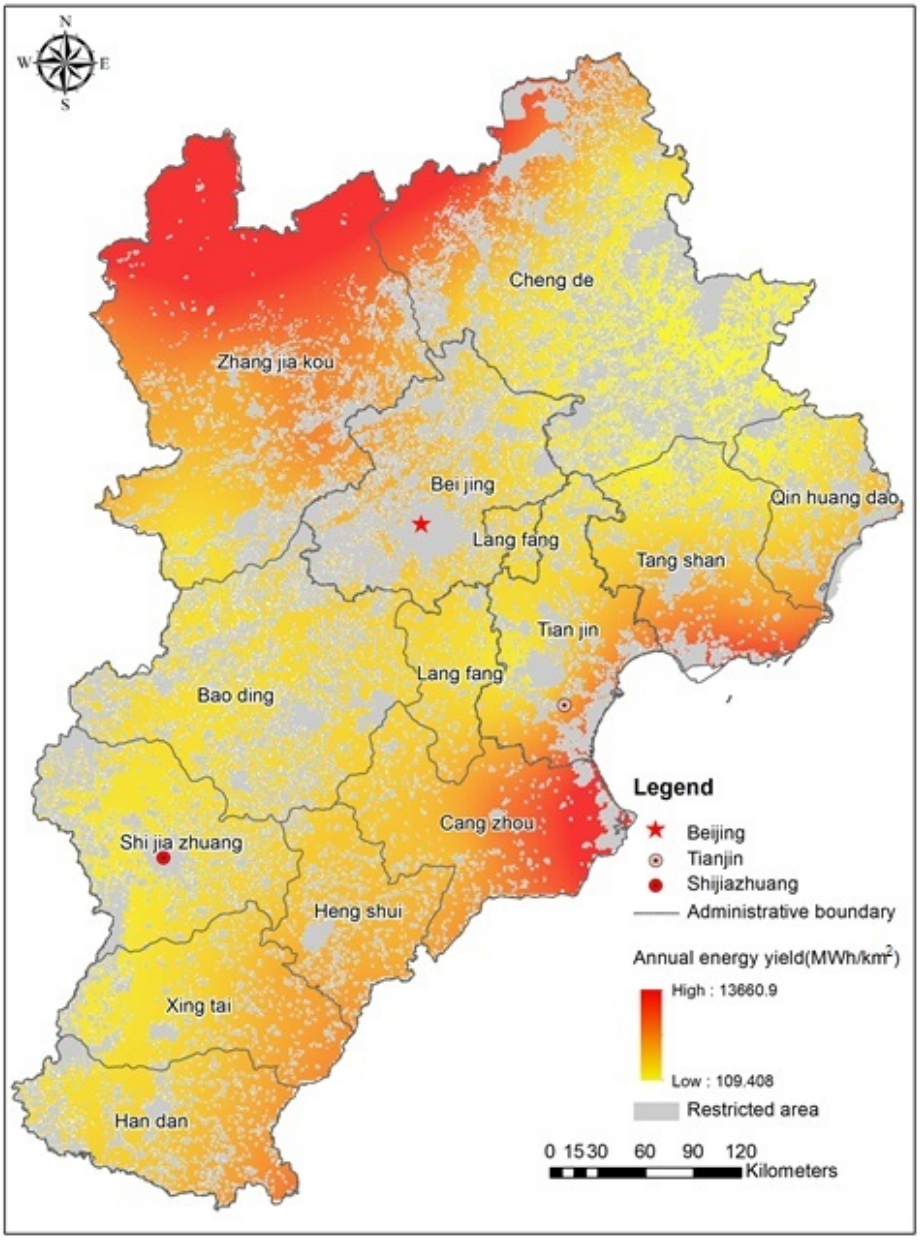

Figure 5.3 Spatial distribution of technical wind energy potential

Table 5.1 Technical potential of wind energy in different cities

Cities	Technical potential(TWh/year)	Available area for wind power plants (km^2)	Technical potential density(GWh/year/km^2)
Zhangjiakou	124.99	30840	4.05
Chengde	36.48	23359	1.56
Cangzhou	36.42	12133	3.00
Tangshan	17.30	9609	1.80
Xingtai	14.41	10118	1.42
Handan	13.64	8488	1.61
Hengshui	12.43	6754	1.84
Tianjin	12.39	7846	1.58
Baoding	11.80	13146	0.89
Beijing	9.71	7050	1.37
Shijiazhuang	6.47	8673	0.74
Qinhuangdao	5.83	5188	1.12
Langfang	5.54	5270	1.05

5.1.4 Economic wind power potential

According to the cost model described in the section 4.1.4, the unit generation cost ranges from 0.07 $/kWh to more than 1 $/kWh under present price level (see Figure 5.4 Spatial distribution of unit generation cost for wind energy). Using wind energy is more economically feasible in region with lower costs, and the north-western plateau and eastern side near the sea offers lower generation cost. At present, the average tariff in this study area is around 0.069 $/kWh, but Unit generation cost is higher than the average tariff. The incentive policies are critical to promoting the further development of wind energy; hence, the national and provincial administrations have published policies to promote its development. One is the feed-in-tariff policy for onshore wind power, which has been available since 2009. This policy defines four wind feed-in-tariff levels based on the estimated regional wind resources, ranging from 0.08 to 0.1 $/kWh. The north-western part of the study area falls under the 0.09$/kWh level.

Figure 5.5 shows the wind supply curve in the study area. Under the current feed-in-tariff for this study area (0.09 $/kWh), it is estimated that the economic wind power potential is 34 TWh/year and the economic wind installed capacity is 32 GW.

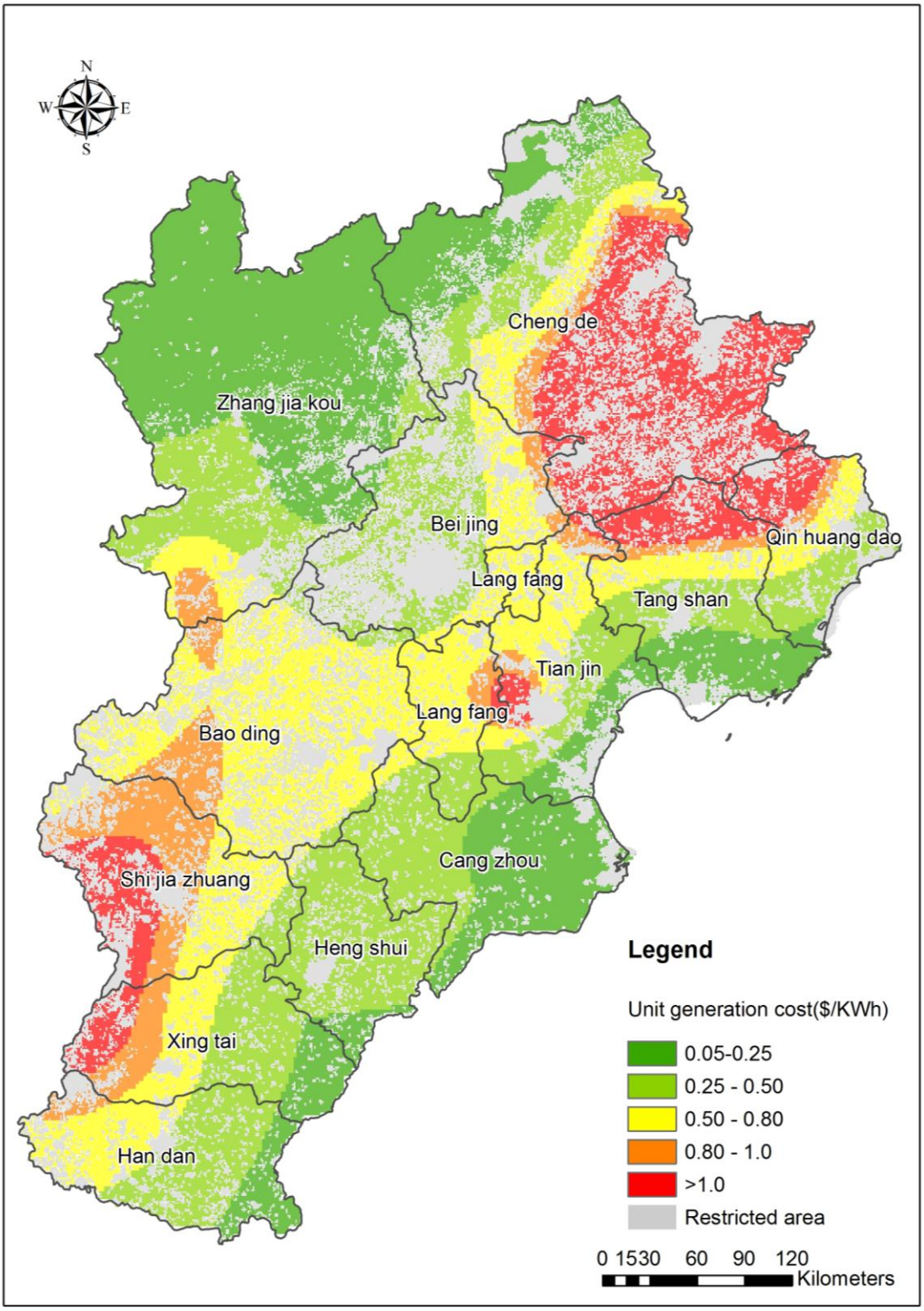

Figure 5.4 Spatial distribution of unit generation cost for wind energy

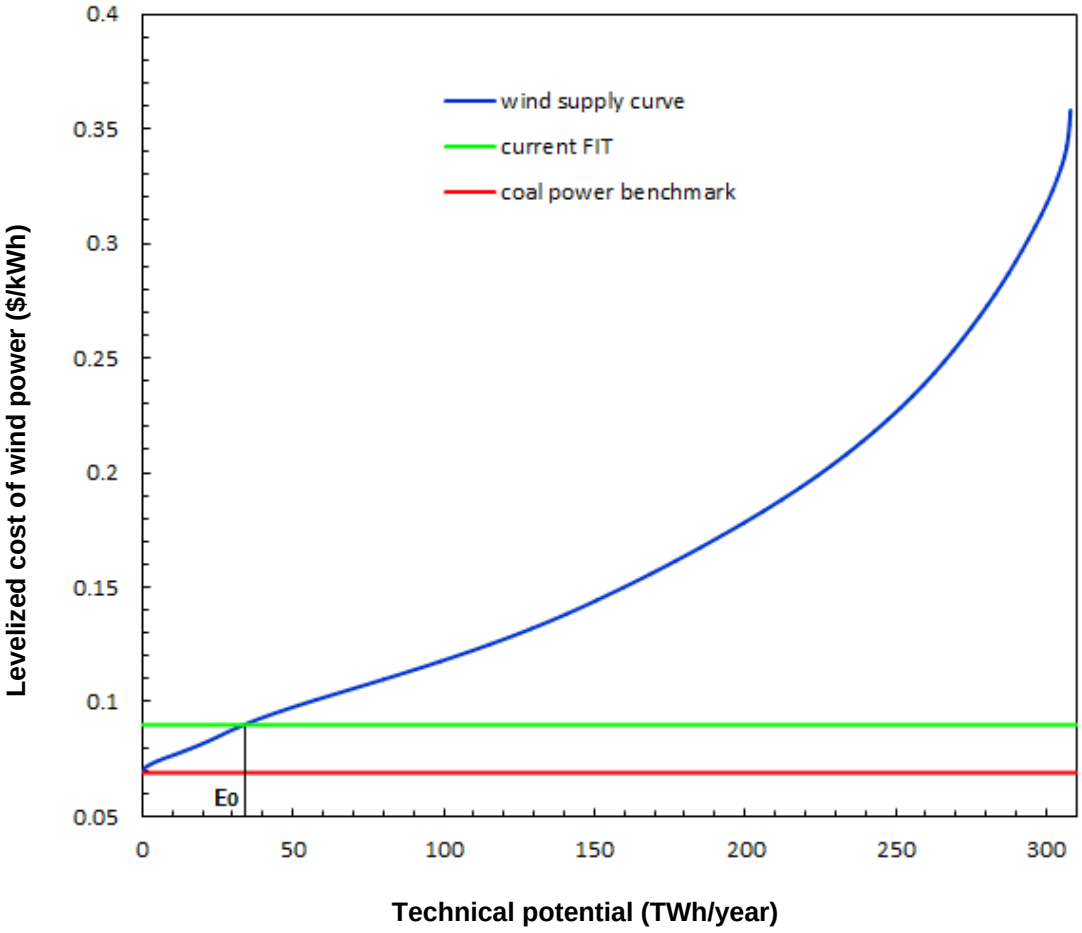

Figure 5.5 Supply cost curve of wind power

The lowest level of wind generation cost is 0.05 $/kWh, which is slightly lower than the average electricity price from coal-fire power generation (0.069 $/kWh). The cost of wind turbines accounts for almost 80% of investment costs. Fortunately, the price of a wind turbine has decreased tremendously in the past decade, and this decrease could lead to a significant reduction in the corresponding levelized cost. To examine the uncertainty of wind cost developments in the future, two scenarios of 15% and 30% capital cost reduction were analyzed, and the results are shown in Figure 5.6. With 15% reduction of investment cost, the economic potential E_1 in Figure 5.6 under the current feed-in-tariff increases to 70 TWh/year, and with a 30% reduction, the economic potential increases to 122 TWh/year.

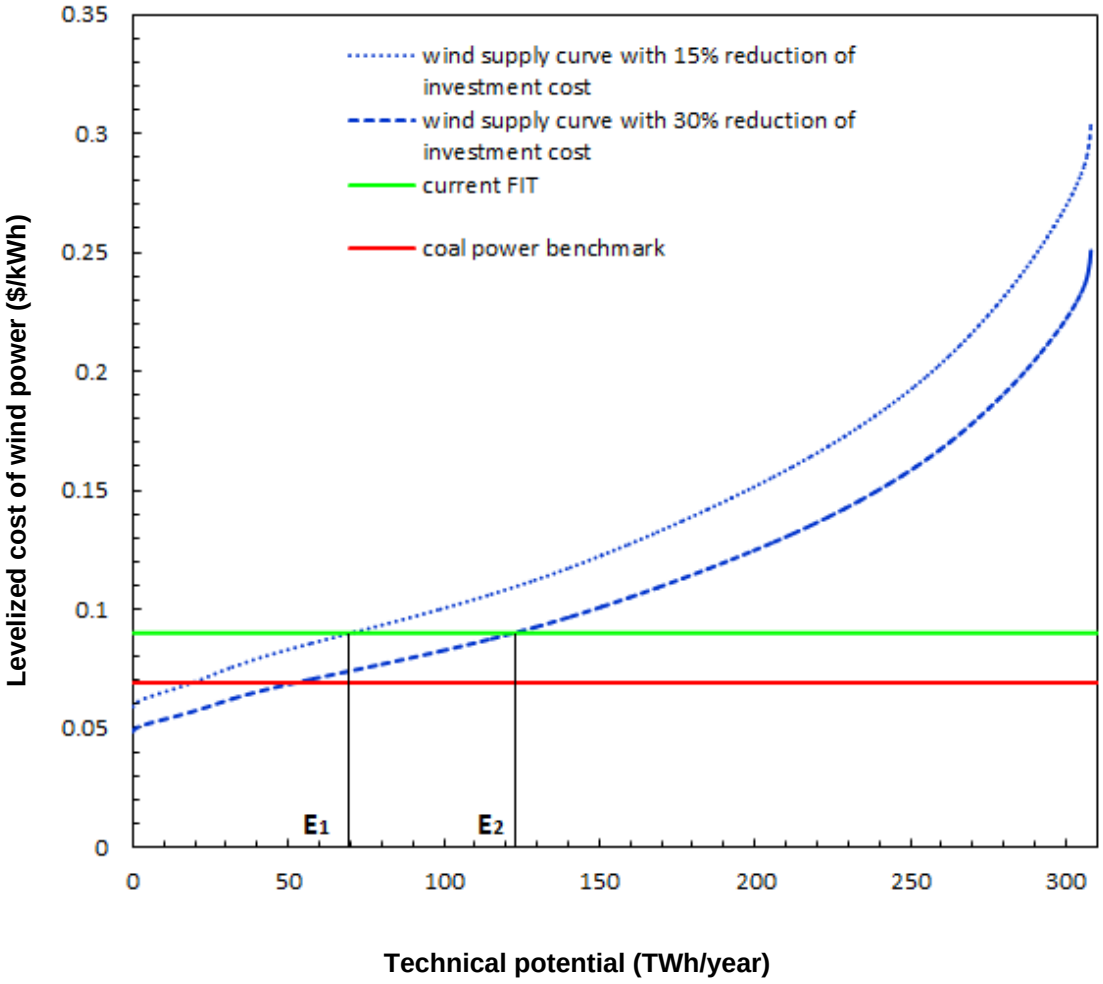

Figure 5.6 Supply cost curve of wind power with reduction of investment cost

5.1.5 Sensitivity analysis

Uncertainty leads to the imprecision of results, and sensitivity analysis is used to address this uncertainty and quantify the effects of each input on modelling results.

In the formula used to calculate annual wind energy production in the analysis of technical wind power potential, maximum efficiency of the Betz limit (C_p) is a key input for estimation of technical wind energy production. The value of 0.593 is the maximum efficiency, but in reality, the efficiency of a wind turbine cannot reach this value. The value ranges from 0.3 to 0.5 based on the current technical report. Efficiency ratios of wind turbines of 0.3, 0.35, 0.4, 0.45, 0.5, 0.55 and 0.593 have been selected to show the variation in technical potential. The relationship is linear (Figure 5.7). If the efficiency increases 1%, total technical potential increase by 5 TWh/year.

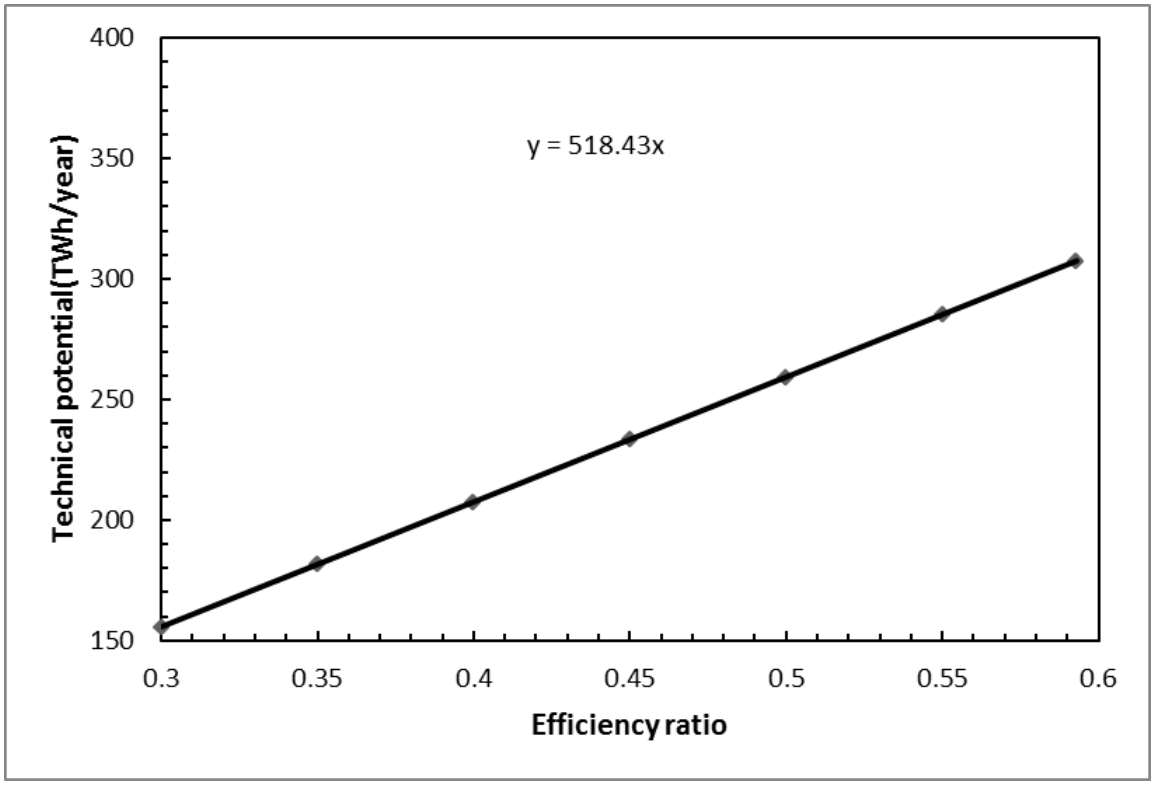

Figure 5.7 Sensitivity of total technical potential to the efficiency ratio of wind turbine

5.1.6 Land suitability level of wind power plants

Figure 5.8 shows the land suitability level of wind power plants based on the multi-criteria method. An area with a score higher than 8 is classified as having very high suitability level, which in this study are the north-eastern part of study area, the Bashang Plateau, and the eastern side near to the sea. These regions cover 21,543 km^2, if all the space available for wind farms is used to install wind turbines. The maximum installed capacity in this very suitable area for wind farm could be 103 GW and maximum technical potential is 85.52 TWh/year.

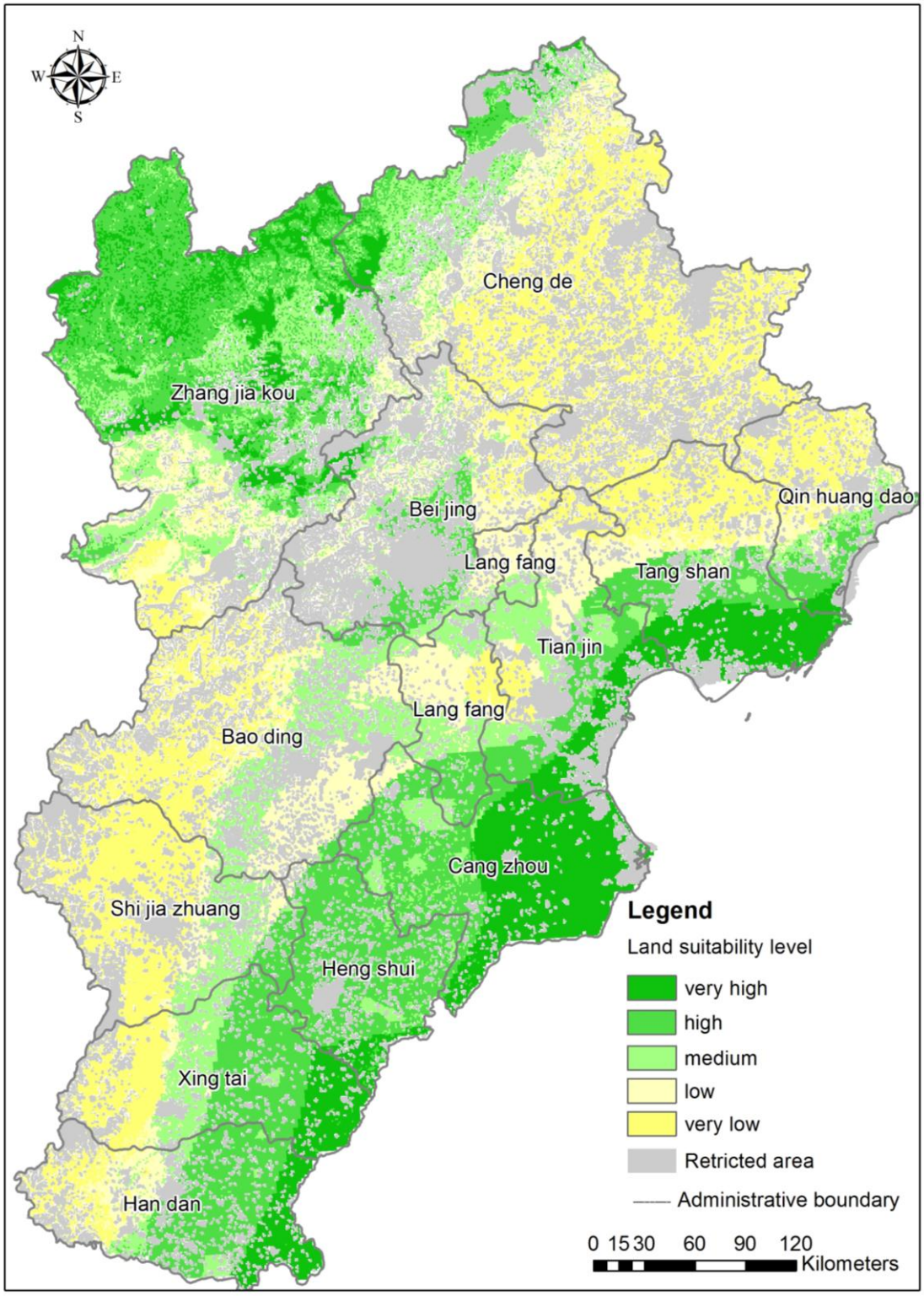

Figure 5.8 Land suitability level of wind power plants

5.2 Solar energy

5.2.1 Theoretical solar radiation resource

Latitude, continent, terrain and local climatic variations determine solar energy resource (Šúri et al., 2007). The spatial variation of annual global solar radiation on the horizon in the study area, calculated based on the formula in section 4.2.1, is shown in Figure 5.9. Annual solar radiation differs in value over the region from 1406 kWh/m^2 to 1960 kWh/m^2. The northern mountain area is endowed with excellent solar energy resources. Terrain largely determines the spatial distribution of solar radiation in this study area, and seasonal variability of the solar energy plays a crucial role for planning power grid management. Figure 5.10 shows the seasonal variability of monthly average solar radiation in the study area. The highest value of monthly average solar radiation is obtained during the summer (June) and lowest value is obtained during winter (January), as the study area is located in the northern hemisphere.

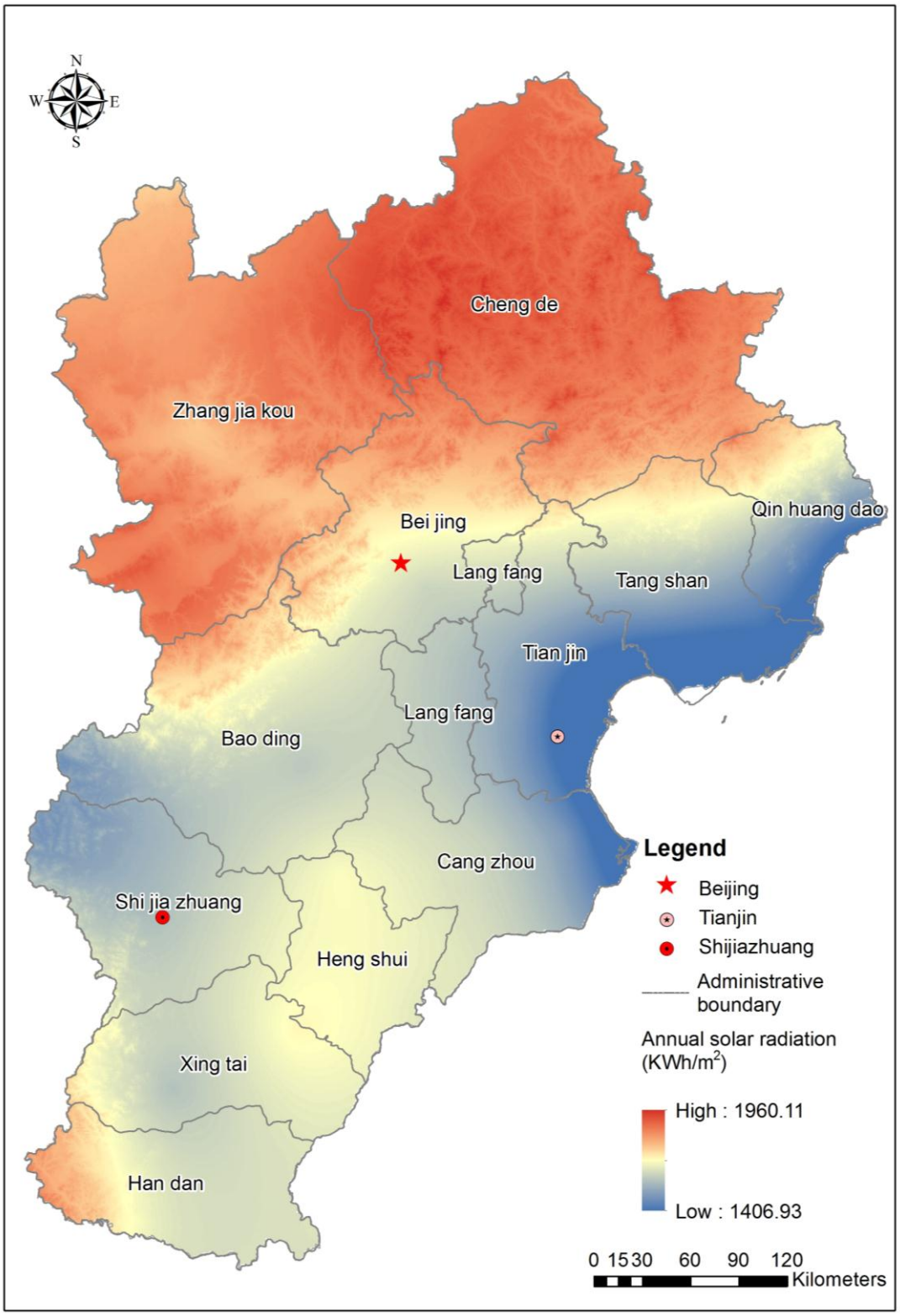

Figure 5.9 Spatial distribution of annual solar radiation

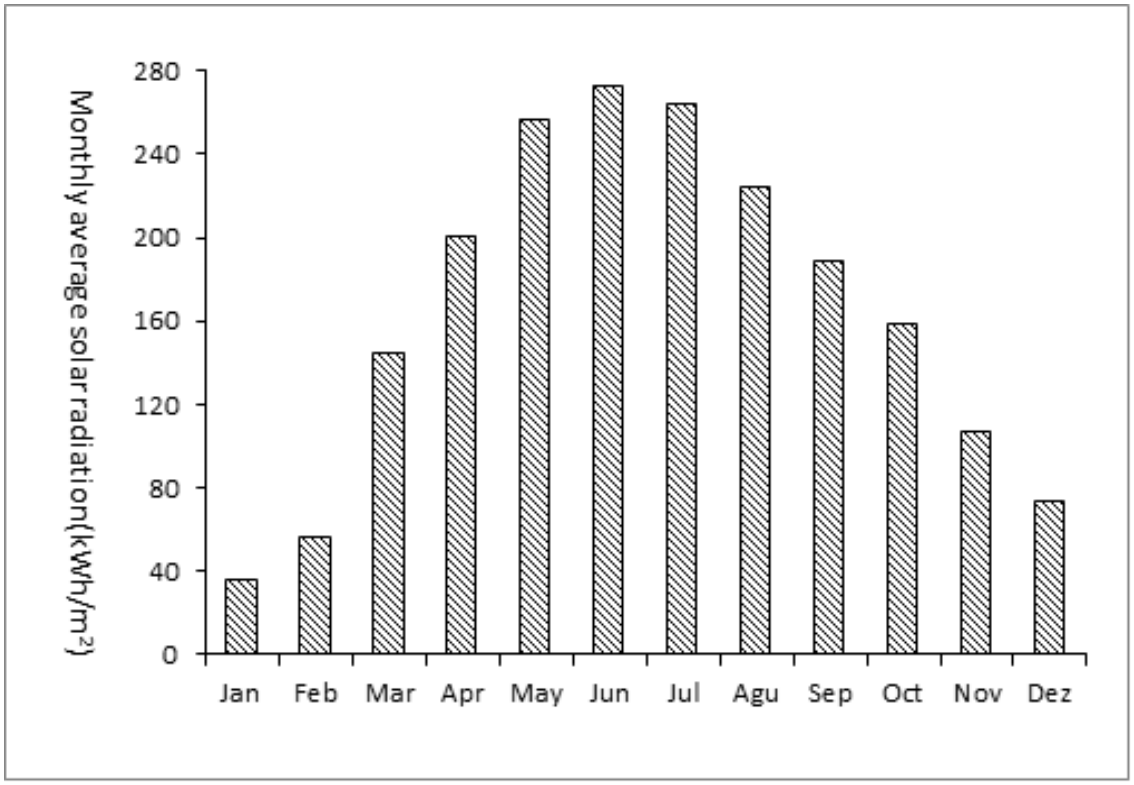

Figure 5.10 Seasonal variability of solar radiation in study area

5.2.2 Geographic solar PV potential

Land cover and the DEM database were used to extract the geographical constraint factors. The appropriate area for PV accounted for 60% of the total area (approximately 130143 km^2), and 226 PWh/year can be obtained from solar radiation in this area. In reality, all suitable areas cannot be covered by PV modules; the author assumed a 10% area factor, based on the research of Charabi& Gastli (2010), in the calculation of the technical potential of solar energy.

The geographical potential of solar energy for each city in this study area is summarised quantitatively in Table 5.2. The difference in the annual average solar radiation between cities is not significant. Zhangjiakou and Chengde have the highest annual average solar radiation and largest available areas for PV. Solar energy resources in these two cities are abundant due to their high elevation.

Table 5.2 Geographical potential of solar energy for each city in study area

Cities	Total area of cities(km^2)	Annual average solar radiation(kWh/m^2)	Available area(km^2)	Geographical potential(TWh/year)
Zhang jia kou	36695	1863	19617	36619
Cheng de	39462	1896	12315	23350
Cang zhou	14105	1678	13238	22270
Bao ding	22294	1719	12536	21418
Xing tai	12481	1724	10051	17306
Tang shan	13018	1649	10021	16366
Tian jin	11613	1611	9930	15996
Han dan	12063	1741	8795	15177
Shi jia zhuang	14062	1680	8772	14800
Heng shui	8825	1745	8121	14173
Bei jing	16376	1792	6616	11695
Lang fang	6410	1688	6080	10260
Qin huang dao	7758	1685	3997	6611

5.2.3 Technical solar PV potential

The spatial distribution of annual PV electricity production in each 1 by 1 km grid, calculated according to the formula in section 4.2.3, is shown in Figure 5.11. The total technical potential is estimated to be 2379 TWh for large-scale PV plants, and in 2012, total electricity consumption in the study area exceeded 467.47 TWh. Technical potential in this study area is five times that of electricity consumption in 2012.

The climate conditions, especially solar radiation; the conversion efficiency of PV modules; and the suitability of the area determine the annual electricity production in a given area. Technical potential in each city is influenced directly by geographical potential, and cities with high geographical potential have high technical potential. The technical PV potential of each city is shown in Figure 5.12. Zhangjiakou is ranked first at 384 TWh/year.

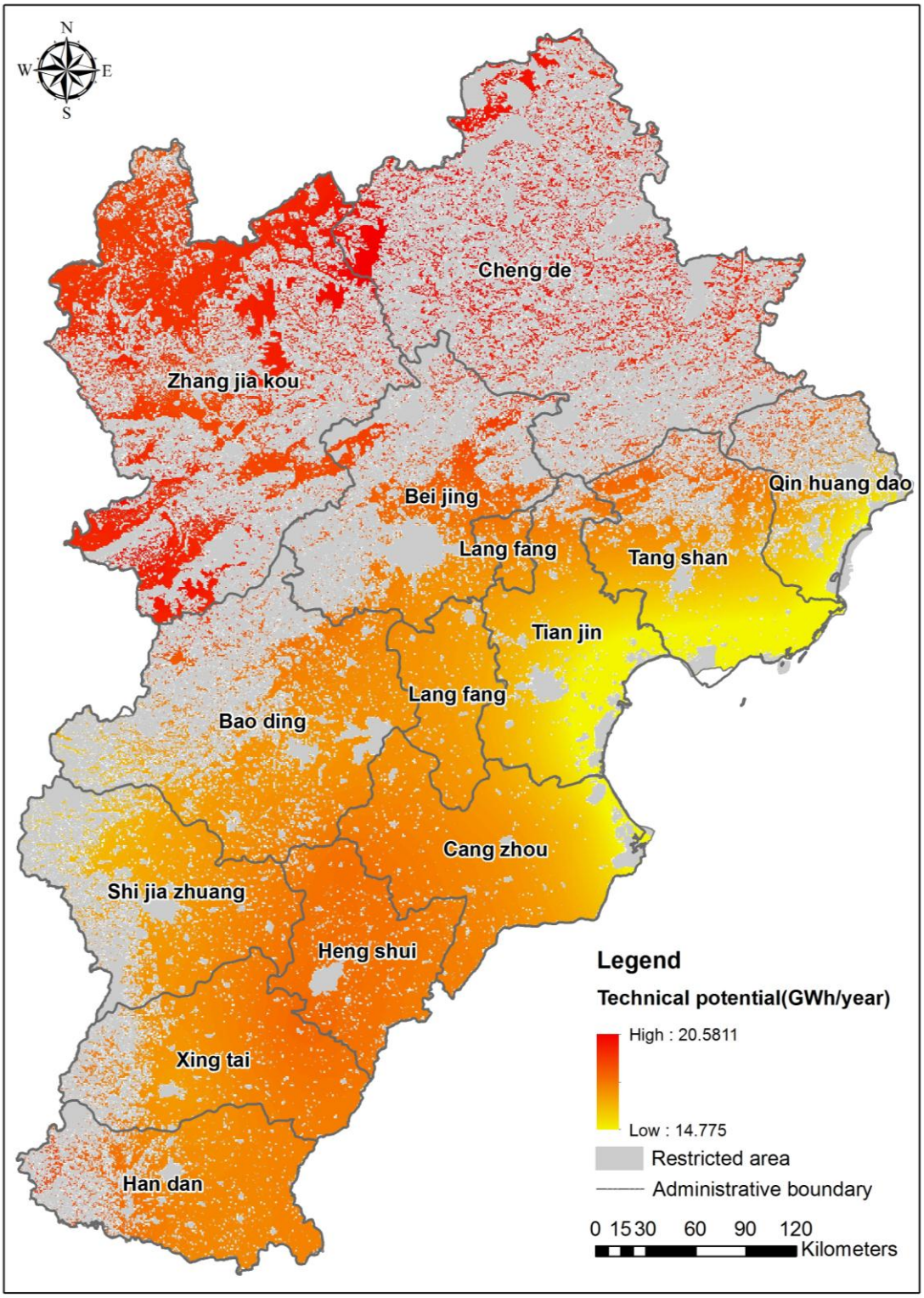

Figure 5.11 Spatial distribution of PV electricity production

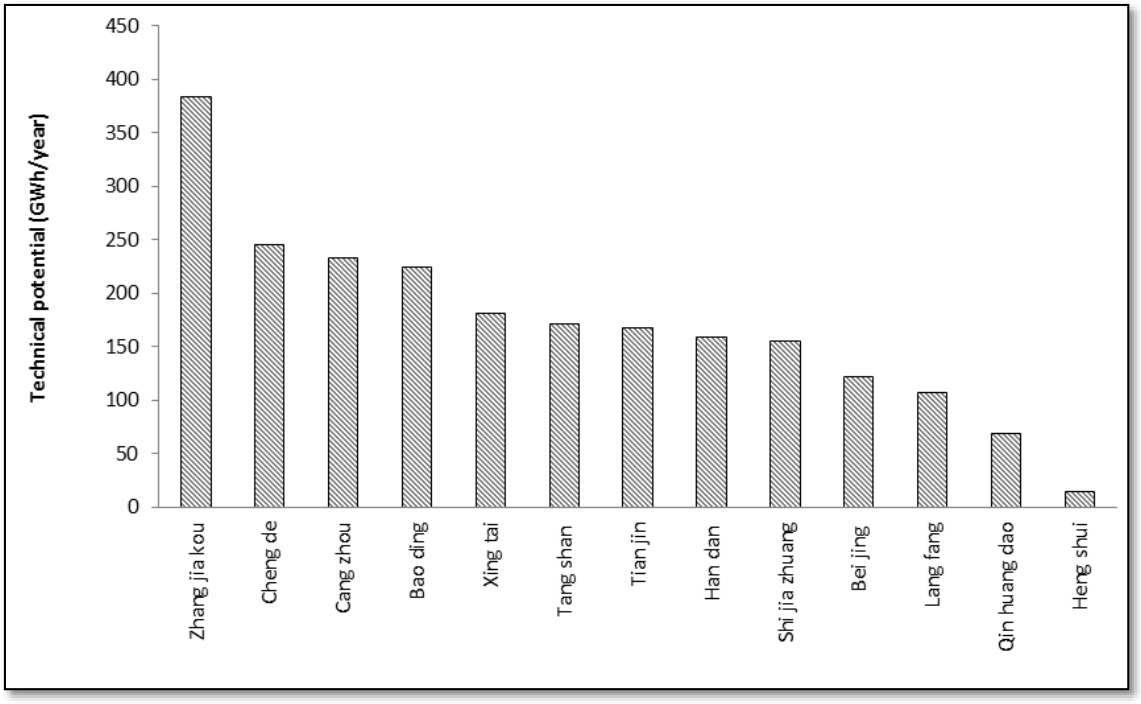

Figure 5.12 Technical PV potential among cities

5.2.4 Economic solar power potential

Figure 5.13 shows the spatial distribution of PV production cost, which is calculated based on the formula in section 4.2.4. It ranges from 0.16 $/kWh to 0.23 $/kWh. The unit production cost is related closely to annual electricity production and the price of PV modules. Figure 5.14 displays the supply cost curve of PV electricity in this study area. In light of the current feed-in-tariff (0.16 $/kWh), even the lowest unit of PV electricity generation cost is higher than the current tariff. At present, the average tariff of electricity from coal power plants is approximately 0.069 $/kWh, thus the unit generation cost of PV electricity is significantly higher than that of conventional energy. Under current national energy policy, there is no economic potential for PV electricity.

To solve these problems, two provinces in China have proposed an explicit tariff: Shandong declared a progressive implementation curve, with FIT decreasing from 0.27 $/kWh in 2010 to 0.22 $/kWh in 2011 and 0.19 $/kWh in 2012. Jiangsu had a similar tariff in 2011 for large-scale PV plants (Sun et al., 2013). Because current FIT cannot cover PV electricity production cost, two future FIT scenarios have been assumed in this study. With a 0.17 $/kWh FIT, economic potential is 403.86 TWh, and with 0.175 $/kWh FIT, economic potential reaches 937.08 TWh.

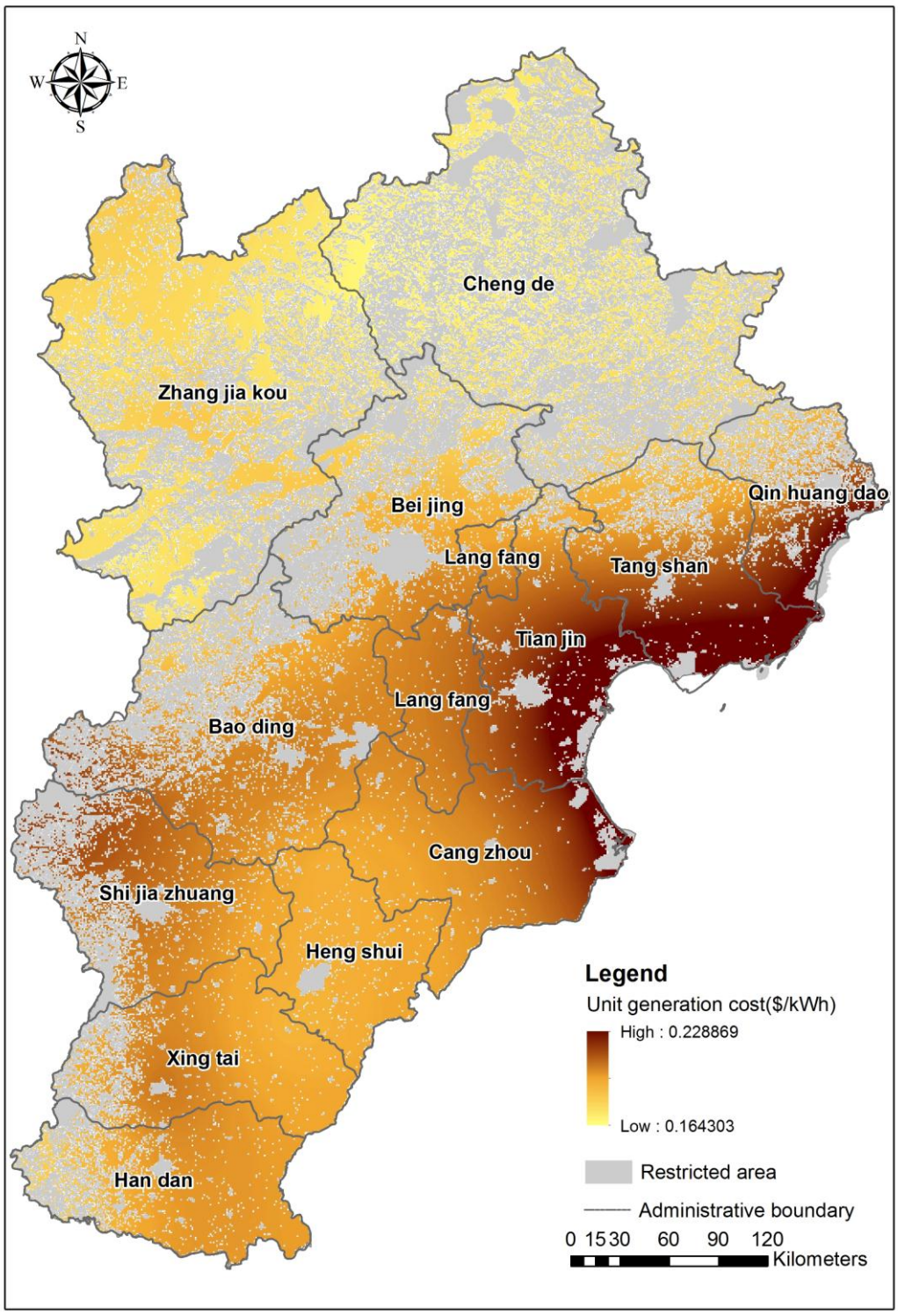

Figure 5.13 Spatial distribution of PV production cost

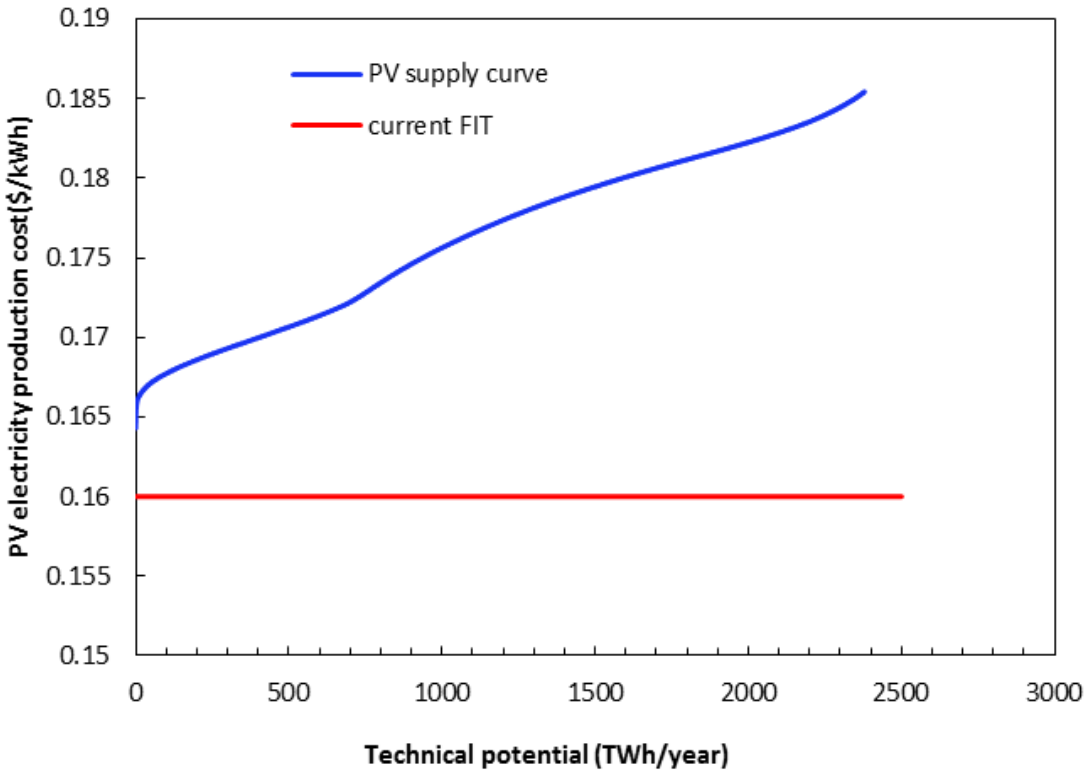

Figure 5.14 Supply cost curve of PV power

In the last decade, the price of PV modules decreased. In 2002, the weighted global average price provided by Solar Buzz was around 6 $/w (Hoogwijk, 2004); in 2013, it is around 1.0 to 1.2 $/w, according to the price information provided by the producer. To determine the influence of solar module price on economic potential, two future scenarios are assumed. If the price of PV modules decreases by 5%, economic potential under the current policy reaches 178.412 TWh/year; with a 10% price decrease, economic potential increases to 1251 TWh/year.

5.2.5 Sensitivity analysis

In the calculation of technical solar energy potential, the efficiency with which solar systems convert sunlight into electricity, η, is an important parameter. Conversion efficiency varies according to PV cell type, and the highest conversion efficiency is between 36 and 41.1% when using high-efficiency tandem cells. The efficiency of multi c-Si cells is between 20 and 24%, while the conversion efficiency of simple c-Si cells is 14 to 18%. For thin film cell technology, efficiency is only 6 to 11%. However, the dilemma is that the cost of PV cells with high conversion efficiency is significantly higher than the cost of cells with lower

conversion. Due to the high price, high-efficiency tandem cells are not used in practical PV solar power plants. One promising tendency that should be noted is that in the last ten years, the price of PV cells decreased, on average, from 6-7 $/w to 1.2 $/w. It is reasonable to conclude that the cost of PV cells with high conversion efficiency will decrease in future and that high efficiency tandem cells will be used in PV solar power plants eventually.

Technical solar energy potential varies as conversion efficiency changes. The relationship is linear, as Figure 5.15 shows. If the conversion efficiency ratio increases by 1%, total technical potential increases 166 TWh/year.

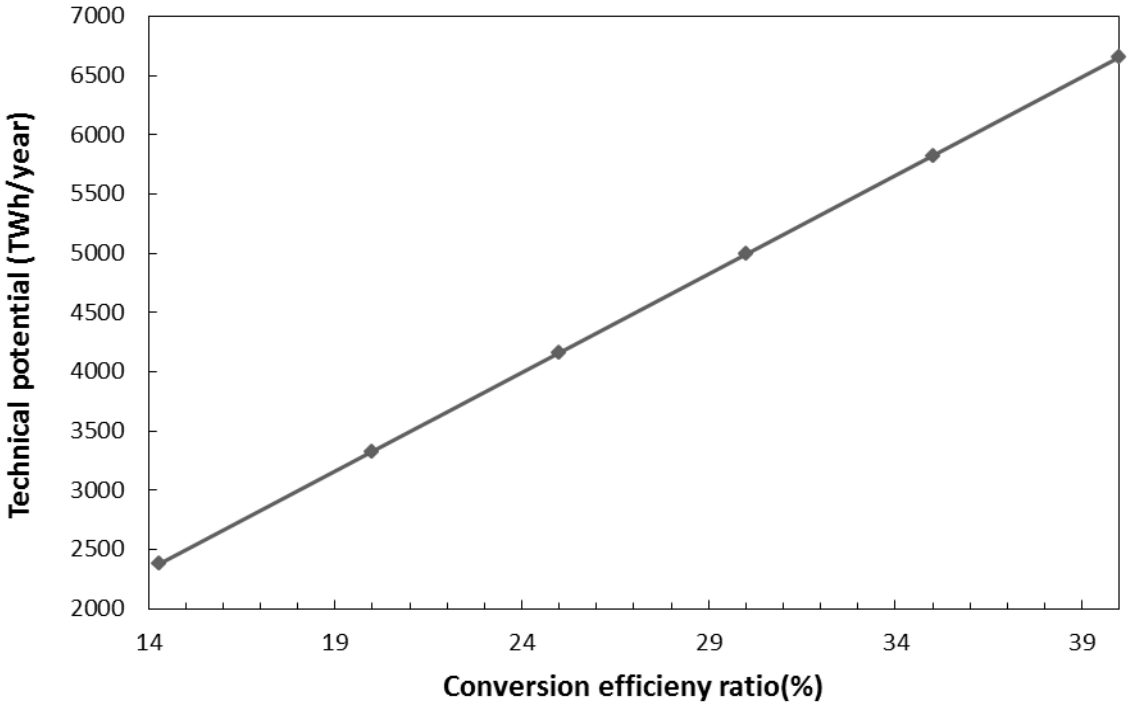

Figure 5.15 Sensitivity of total PV technical potential to the conversion efficiency ratio of PV cells

Another uncertainty input factor when calculating technical PV energy potential is the area factor, A_f. The area factor indicates what fraction of the eligible areas can be covered by solar panels, which is assumed to be 10% in this study. However, in reality, there may not be as much space that can be provided for the development of solar energy due to urban sprawl and other activities; land can be occupied for other purposes other than solar power generation. If the area factor decreases from the assumed value of 10% to 1%, the technical solar

potential decreases as Figure 5.16 shows. Technical solar potential decreases by 238 TWh with every 1% decrease on area factor.

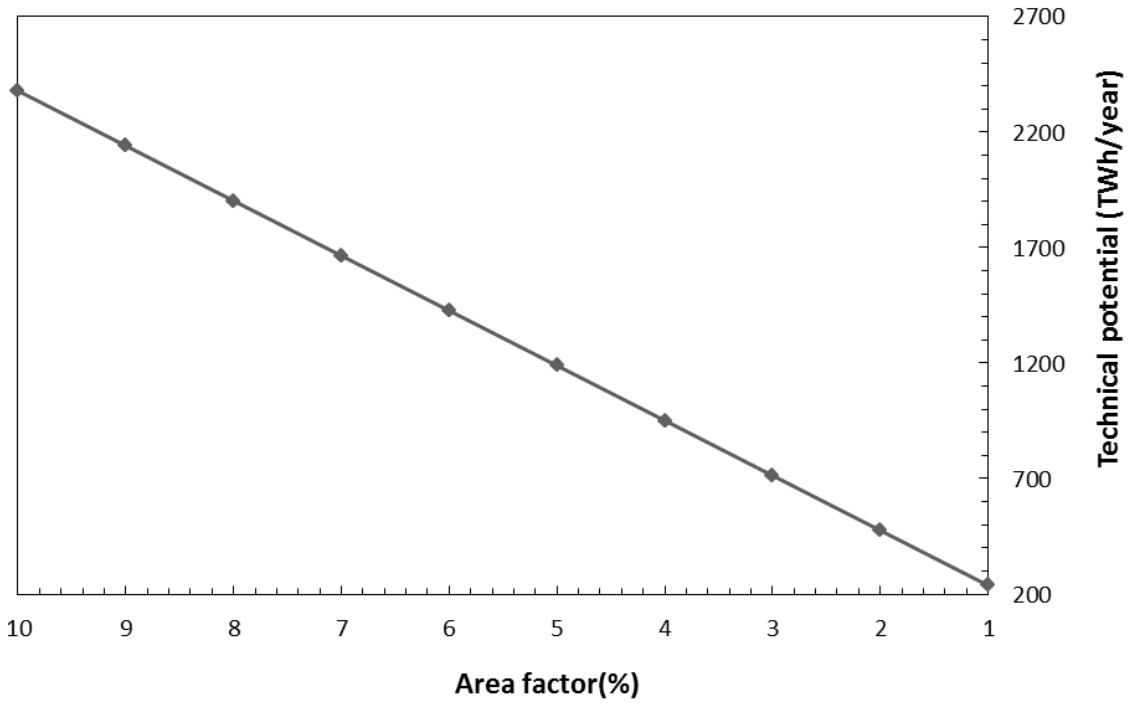

Figure 5.16 Sensitivity of total PV technical potential to the area factor

5.2.6 Land suitability level for solar power plants

Figure 5.17 shows the land suitability level for PV solar power plants based on the multi-criteria method. Regions with scores higher than 8 are classified as very extremely suitable, while areas with score between 7 and 8 are categorized highly suitable. Most of the suitable land is distributed in the north-eastern part of study area, on the Bashang Plateau, and covers 10634 km^2. The sum of the corresponding technical potential in these areas is 200 TWh/year.

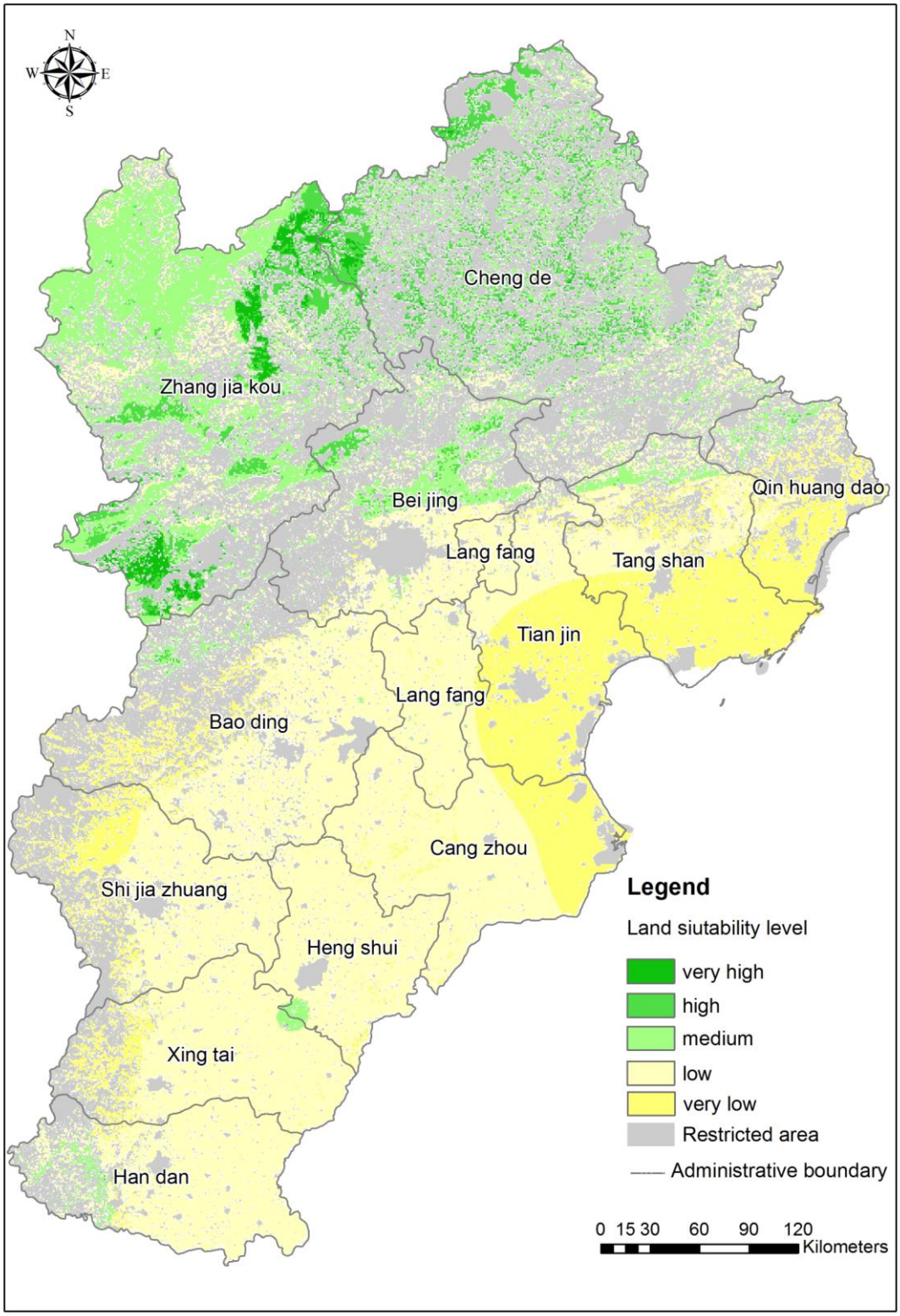

Figure 5.17 Land suitability level of solar power plants

5.3 Bioenergy

5.3.1 Usable biomass power potential

Figure 5.18 shows the spatial distribution of biomass residue in the study area, calculated based on the model described in section 4.3.1. Annual biomass residue varies from 0 t/km^2 to 4008 t/km^2. The amount of biomass residue is related closely to land cover type. Forest occupies the north-western part of study area, thus biomass in this region is abundant. The dominant land cover type in the southern part is farm-land, and the residues from crops provide promising opportunities to develop biomass energy. The total annual amount of biomass in the study area is approximately 214 million tons. A recent report indicates that 1 kWh electricity can be produced from about 1 kg biomass using combustion technology. Based on this transfer parameter, the annual theoretical biomass power potential in this study area is 214 TWh.

Through the spatial statistic function in ArcGIS, the biomass for each county was analysed. Table 5.3 lists the top 20 counties with the largest biomass amounts, and the spatial distribution of these counties is expressed in Figure 5.19. Most of them are distributed in the northern part of the study area. From the viewpoint of usable biomass quantity, the northern area is the preferable location for biomass power plants. However, there are only two existing biomass power plants in this area (Figure 5.19) with others located in the south. This is mainly because of the elevation and population density—the northern area has a lower population and is covered by mountains, while most central and southern parts lie within the North China Plain, where the flat terrain provides superior living conditions and offers more biomass residue from a large number of agricultural products.

In the biomass power plant planning field, numerous factors determine the locations of power plants. Considering only the amount of usable biomass power cannot satisfy demand, and the economic cost of building and operating biomass power plants cannot be neglected. Therefore, not only focused on the quantification of usable biomass but also on economic analysis and considering various during site selection. The results of these two topics are discussed in the sections that follow.

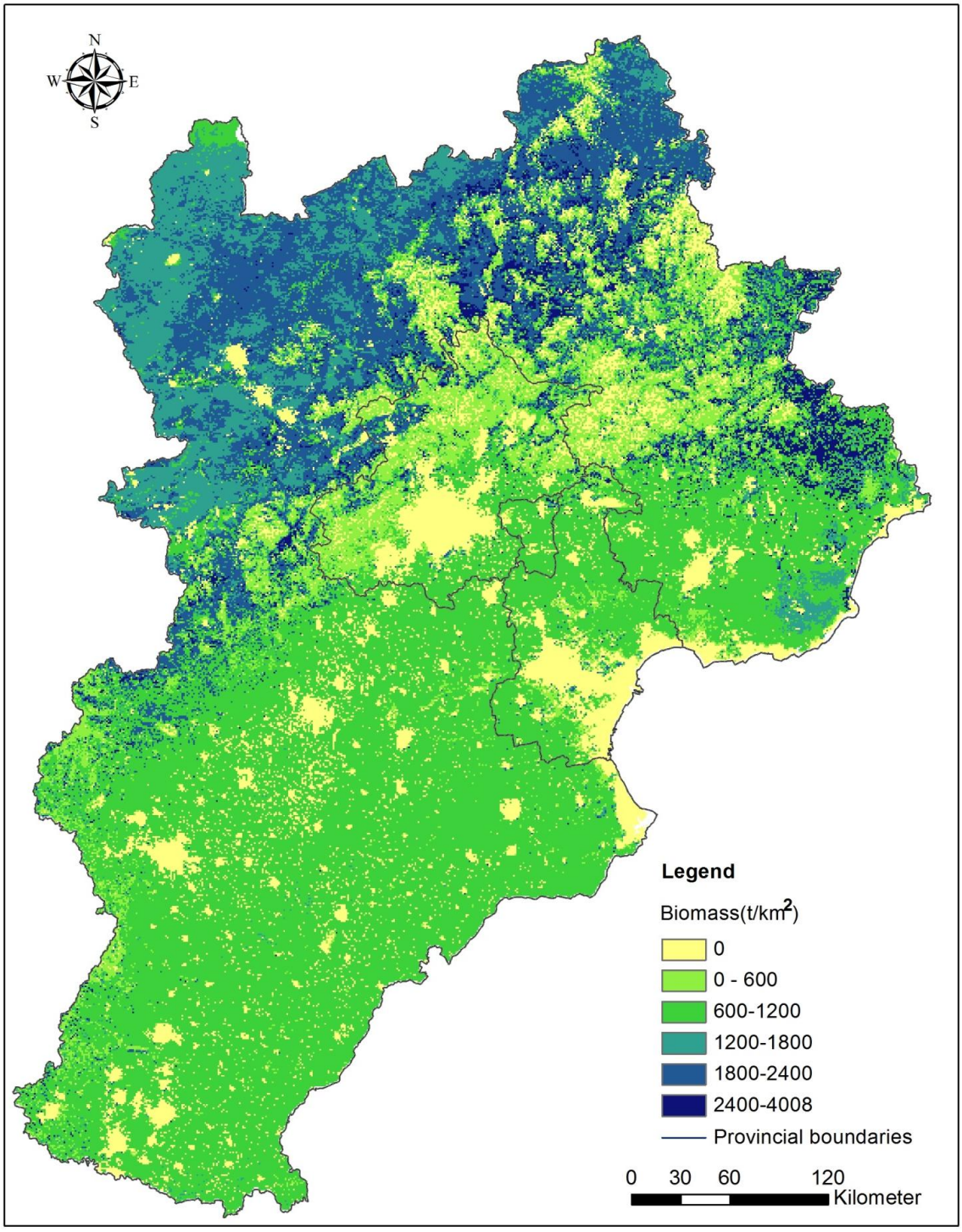

Figure 5.18 Spatial distribution of annual usable biomass

Table 5.3 Table Statistic results of biomass and biomass power potential

Name of county	Area(km^2)	Usable biomass(ton)	Theoretical power potential(GW)
Fengning	10393	15933200	15933.2
Weichang	8813	14414500	14414.5
Chicheng	5274	8097010	8097.01
Zhangbei	4183	7597050	7597.05
Longhua	5431	6882610	6882.61
Guyuan	3523	6241540	6241.54
Qinglong	3516	6063830	6063.83
Kangbao	3288	5022330	5022.33
Pingquan	3231	4387020	4387.02
Shangyi	2559	4091050	4091.05
Wei xian	3159	4025160	4025.16
Chongli	2352	3951830	3951.83
Zhuolu	2767	3930100	3930.1
Xuanhua	2327	3816560	3816.56
Laiyuan	2405	3452250	3452.25
Luanping	3221	2905290	2905.29
Chengdexian	4062	2884270	2884.27
Fuping	2477	2781900	2781.9
Yangyuan	1784	2738440	2738.44
Huanan	1635	2630260	2630.26

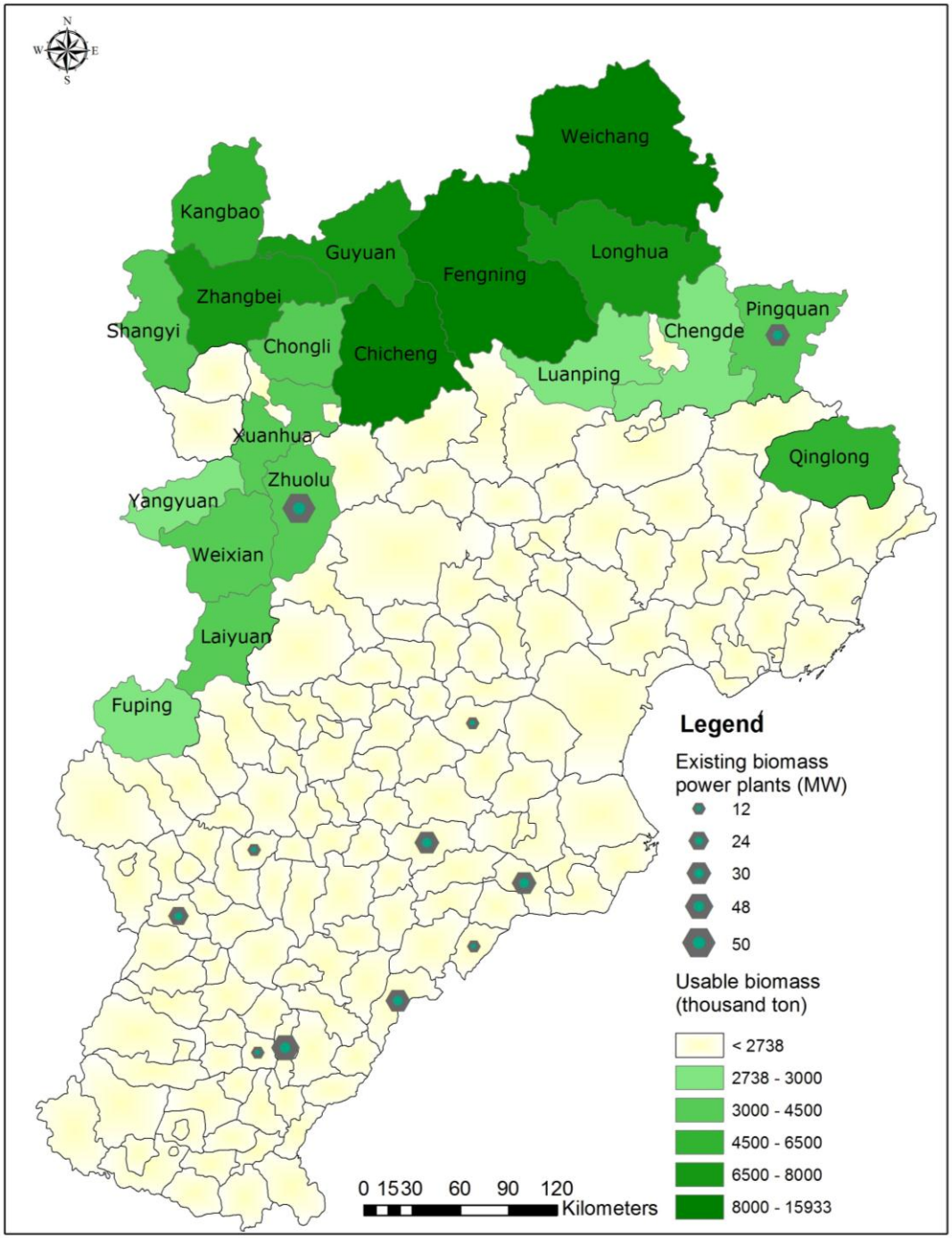

Figure 5.19 Spatial distribution of existing biomass power plants and counties with abundant usable biomass

5.3.2 Economic analysis of biomass power plants

The economic analysis of biomass power plants is based on specific case studies, as economic factors vary with the installed capacity, price of biomass and so forth. To highlight the effects of renewable energy subsidies, two scenarios for each case study are assumed: with a subsidy and without a subsidy. The two case studies examine biomass power plants with 12 MW installed capacity and 30 MW

installed capacity. Operating income includes revenue from power sales and heat sales, and operating costs are composed of fuel costs, loan repayments, and operation and maintenance costs. The pre-tax profile is the operating income minus operating cost.

The average price of power from conventional power plants is 0.45 ¥/kWh, while the subsidy from the government for each kWh of power produced from biomass is 0.3 ¥/kWh. With the subsidy, the price of power from biomass power plants is 0.75 ¥/kWh; without the subsidy, the price is only 0.45 ¥/kWh. Moreover, the Chinese government provides tax support to biomass power plants. Corporate tax usually is 25%, but for biomass power plants, corporate tax is reduced to 15%. In addition, biomass power plants receive VAT (17%) refunds on all machines and office products bought during the construction of the plants. The results of the economic analysis with subsidies are shown in Table 5.4 and Table 5.6 for two cases. Table 5.5 and Table 5.7 contain the economic analysis results without subsidies.

Based on the results calculated, without subsidies, biomass power plants are still profitable. However, in reality, existing biomass power plants are unprofitable. The primary reason is that the supply of biomass residues is not continuous during the year, as the production of biomass is seasonal. Residues are abundant in summer and autumn but lacking in winter and spring. As the study area lies between the 36°N and 43°N latitudes, temperature and precipitation constrains mean that most agricultural products are harvested in summer or autumn. Many biomass power plants stop operating during spring due to the lack of biomass fuels.

Another difficulty is the collection of biomass residue. The price of 1 ton of biomass residue for biomass power plants is around 300 ¥, which includes collection and transportation cost. However, the farmer receives a maximum of 100 ¥/t from the dealer. The farmer has to collect the biomass residues from the farmland and take it to a retrieving points. Compared to the revenue, 100 ¥/t, the physical collection workload for farmers is too heavy. For the farmer, combustion is preferable to collection and sale when dealing with biomass residue. Recently, a possible solution to this problem has emerged— biomass power plants

purchase collection machines to collect residues free of charge and pay farmers less than 100 ¥/ton.

Table 5.4 The income statement of 12MW combustion power heat system

The period(year)	1	2	3	4	5	6	7	8	9	10
Operating income	140525	138417	137433	136759	136351	135944	135536	135129	134721	134314
Power sale revenues(thousand yuan)	74375	73259	72739	72382	72166	71950	71735	71519	71303	71088
Heat sales revenuew(thousand yuan)	66150	65158	64695	64377	64185	63994	63802	63610	63418	63226
Decline of facilities performance	1.000	0.985	0.978	0.973	0.970	0.967	0.965	0.962	0.959	0.956
Operating cost	57161	58001	58858	59732	60623	61532	62460	63406	64371	65355
Fuel cost (thousand yuan)	42000	42840	43697	44571	45462	46371	47299	48245	49210	50194
Loan payment (thousand yuan)	11561	11561	11561	11561	11561	11561	11561	11561	11561	11561
O&M cost(thousand yuan)	3600	3600	3600	3600	3600	3600	3600	3600	3600	3600
Pre-tax operate profit	83364	80416	78576	77027	75728	74411	73076	71723	70351	68959
AVT refund	20400									
Corporate tax(15%)	12505	12062	11786	11554	11359	11162	10961	10758	10553	10344
Net profit (thousand yuan)	91259	68354	66789	65473	64369	63250	62115	60965	59798	58615

The period(year)	11	12	13	14	15	16	17	18	19	20
Operating income	133920	133246	132585	131911	131250	130983	130460	129939	129420	128904
Power sale revenues(thousand yuan)	70879	70522	70173	69816	69466	69325	69048	68772	68498	68224
Heat sales revenuew(thousand yuan)	63041	62723	62413	62095	61784	61658	61412	61167	60923	60679
Decline of facilities performance	0.953	0.948	0.944	0.939	0.934	0.932	0.928	0.925	0.921	0.917
Operating cost	66359	67383	68427	69493	70579	71688	72818	73971	75147	76347
Fuel cost (thousand yuan)	51198	52222	53266	54331	55418	56526	57657	58810	59986	61186
Loan payment (thousand yuan)	11561	11561	11561	11561	11561	11561	11561	11561	11561	11561
O&M cost(thousand yuan)	3600	3600	3600	3600	3600	3600	3600	3600	3600	3600
Pre-tax operate profit	67561	65863	64158	62418	60671	59295	57642	55968	54273	52557
AVT refund										
Corporate tax (15%)	10134	9879	9624	9363	9101	8894	8646	8395	8141	7883
Net profit (thousand yuan)	57427	55984	54534	53056	51570	50401	48996	47573	46132	44673

Table 5.5 The income statement of 12MW combustion power heat system without any subsidy

The period year	1	2	3	4	5	6	7	8	9	10
Operating income	110775	110106	109793	109579	109450	109320	109191	109061	108932	108803
Power sale revenues(thousand yuan)	44625	43956	43643	43429	43300	43170	43041	42911	42782	42653
Heat sales revenuew(thousand yuan)	66150	66150	66150	66150	66150	66150	66150	66150	66150	66150
Decline of facilities performance	1.000	0.985	0.978	0.973	0.970	0.967	0.965	0.962	0.959	0.956
Operating cost	58520	59360	60216	61090	61982	62891	63818	64764	65729	66714
Fuel cost (thousand yuan)	42000	42840	43697	44571	45462	46371	47299	48245	49210	50194
Loan payment (thousand yuan)	11561	11561	11561	11561	11561	11561	11561	11561	11561	11561
O&M cost(thousand yuan)	3240	3240	3240	3240	3240	3240	3240	3240	3240	3240
Pre-tax operate profit	52255	50746	49577	48489	47468	46429	45372	44297	43203	42089
AVT refund	0	0	0	0	0	0	0	0	0	0
Corporate tax (25%)	13064	12686	12394	12122	11867	11607	11343	11074	10801	10522
Net profit	39191	38059	37183	36366	35601	34822	34029	33223	32402	31567

The period year	11	12	13	14	15	16	17	18	19	20
Operating income	108678	108463	108254	108039	107830	107745	107579	107413	107249	107085
Power sale revenues(thousand yuan)	42528	42313	42104	41889	41680	41595	41429	41263	41099	40935
Heat sales revenuew(thousand yuan)	66150	66150	66150	66150	66150	66150	66150	66150	66150	66150
Decline of facilities performance	0.953	0.948	0.944	0.939	0.934	0.932	0.928	0.925	0.921	0.917
Operating cost	67717	68741	69786	70851	71938	73046	74177	75330	76506	77706
Fuel cost (thousand yuan)	51198	52222	53266	54331	55418	56526	57657	58810	59986	61186
Loan payment (thousand yuan)	11561	11561	11561	11561	11561	11561	11561	11561	11561	11561
O&M cost(thousand yuan)	3240	3240	3240	3240	3240	3240	3240	3240	3240	3240
Pre-tax operate profit	40960	39722	38468	37188	35892	34699	33402	32084	30743	29379
AVT refund	0	0	0	0	0	0	0	0	0	0
Corporate tax(25%)	10240	9931	9617	9297	8973	8675	8351	8021	7686	7345
Net profit	30720	29792	28851	27891	26919	26024	25052	24063	23057	22034

Table 5.6 The income statement of 30MW combustion power heat system

The period year	1	2	3	4	5	6	7	8	9	10
Operating income	301125	263364	261493	260209	259434	258659	257883	257108	256332	255557
Power sale revenues(thousand yuan)	159375	156984	155869	155104	154642	154179	153717	153255	152793	152331
Heat sales revenuew(thousand yuan)	141750	106380	105624	105106	104792	104479	104166	103853	103540	103226
Decline of facilities performance	1.000	0.985	0.978	0.973	0.970	0.967	0.965	0.962	0.959	0.956
Operating cost	127903	118337	120173	122045	123956	125904	127891	129918	131986	134095
Fuel cost (thousand yuan)	90000	91800	93636	95509	97419	99367	101355	103382	105449	107558
Loan payment (thousand yuan)	28903	17537	17537	17537	17537	17537	17537	17537	17537	17537
O&M cost(thousand yuan)	9000	9000	9000	9000	9000	9000	9000	9000	9000	9000
Pre-tax operate profit	173222	145028	141320	138164	135478	132755	129992	127189	124346	121462
AVT refund	2981	0	0	0	0	0	0	0	0	0
Corporate tax(15%)	25983	21754	21198	20725	20322	19913	19499	19078	18652	18219
Net profit (thousand yuan)	150220	123274	120122	117439	115157	112841	110493	108111	105694	103243

The period year	11	12	13	14	15	16	17	18	19	20
Operating income	254808	253525	252268	250985	249728	249219	248224	247233	246246	245263
Power sale revenues(thousand	151884	151119	150370	149605	148856	148553	147960	147369	146781	146195
Heat sales revenuew(thousand	102924	102406	101898	101380	100872	100666	100264	99864	99466	99068
Decline of facilities	0.953	0.948	0.944	0.939	0.934	0.932	0.928	0.925	0.921	0.917
Operating cost	136246	138440	140678	142961	145290	147665	150087	152558	155079	157650
Fuel cost (thousand yuan)	109709	111904	114142	116425	118753	121128	123551	126022	128542	131113
Loan payment (thousand yuan)	17537	17537	17537	17537	17537	17537	17537	17537	17537	17537
O&M cost(thousand yuan)	9000	9000	9000	9000	9000	9000	9000	9000	9000	9000
Pre-tax operate profit	118562	115085	111590	108024	104438	101554	98137	94675	91167	87614
AVT refund	0	0	0	0	0	0	0	0	0	0
Corporate tax(15%)	17784	17263	16738	16204	15666	15233	14721	14201	13675	13142
Net profit (thousand yuan)	100778	97822	94851	91820	88773	86321	83416	80474	77492	74472

Table 5.7 The income statement of 30MW combustion power heat system without any subsidy

The period year	1	2	3	4	5	6	7	8	9	10
Operating income	237375	202005	201249	200731	200417	200104	199791	199478	199165	198851
Power sale revenues(thousand yuan)	95625	95625	95625	95625	95625	95625	95625	95625	95625	95625
Heat sales revenuew(thousand yuan)	141750	106380	105624	105106	104792	104479	104166	103853	103540	103226
Decline of facilities performance	1.000	0.985	0.978	0.973	0.970	0.967	0.965	0.962	0.959	0.956
Operating cost	127903	118337	120173	122045	123956	125904	127891	129918	131986	134095
Fuel cost (thousand yuan)	90000	91800	93636	95509	97419	99367	101355	103382	105449	107558
Loan payment (thousand yuan)	28903	17537	17537	17537	17537	17537	17537	17537	17537	17537
O&M cost(thousand yuan)	9000	9000	9000	9000	9000	9000	9000	9000	9000	9000
Pre tax- operate profit	109472	83668	81076	78685	76462	74200	71900	69559	67179	64756
AVT refund	0	0	0	0	0	0	0	0	0	0
Corporate tax(25%)	27368	20917	20269	19671	19115	18550	17975	17390	16795	16189
Net profit (thousand yuan)	82104	62751	60807	59014	57346	55650	53925	52170	50384	48567

The period year	11	12	13	14	15	16	17	18	19	20
Operating income	198549	198031	197523	197005	196497	196291	195889	195489	195091	194693
Power sale revenues(thousand	95625	95625	95625	95625	95625	95625	95625	95625	95625	95625
Heat sales revenuew(thousand	102924	102406	101898	101380	100872	100666	100264	99864	99466	99068
Decline of facilities performance	0.953	0.948	0.944	0.939	0.934	0.932	0.928	0.925	0.921	0.917
Operating cost	136246	138440	140678	142961	145290	147665	150087	152558	155079	157650
Fuel cost (thousand yuan)	109709	111904	114142	116425	118753	121128	123551	126022	128542	131113
Loan payment (thousand yuan)	17537	17537	17537	17537	17537	17537	17537	17537	17537	17537
O&M cost(thousand yuan)	9000	9000	9000	9000	9000	9000	9000	9000	9000	9000
Pre tax- operate profit	62303	59590	56845	54043	51207	48627	45802	42931	40012	37044
AVT refund	0	0	0	0	0	0	0	0	0	0
Corporate tax(25%)	15576	14898	14211	13511	12802	12157	11451	10733	10003	9261
Net profit (thousand yuan)	46727	44693	42633	40533	38405	36470	34352	32198	30009	27783

5.3.3 Site selection for biomass power plants

Once the evaluation of usable biomass power potential and economic analysis for specific biomass power plants have been completed, the next important issue is the location of the plants, which is affected by multi-factors. The transportation cost of biomass residue from retrieving points to biomass power plants and usable biomass potential are considered the two most important factors because of the high cost of residue transportation. The location-allocation method in network analysis can search optimal sites while considering these two factors simultaneously. Figure 5.20 shows the top 10 sites derived using the location-allocation model described in section 4.3.3. Considering only these two factors is inadequate when sitting a biomass power plant— existing power plants and population density also have unavoidable influences on the locations of biomass power plants. The existing coal power plants and population density are illustrated in Figure 5.20. The planned biomass power plant should supply power for more people and not be clustered with existing power plants. To avoid competition for resources, the NDRC has declared that each county can have only one biomass power plant. Based on these planning rules, four sites have been selected as shown in Figure 5.21. The first site is given higher priority, then the second, the third and the fourth, as the numbers show.

Table 5.8 lists the statistical results of the four optimal sites. As mentioned previously, 100 km was chosen as the transport cost threshold. Once the four optimal sites were identified, supply areas with 30 km, 50 km, 80 km and 100 km buffer were established by the network analysis tools. The biomass in each buffer was calculated using the spatial analysis tool in ArcGIS. Table 5.8 lists the biomass in the entire supply area and each buffer zone. The total distance refers to the sum distance between each biomass retrieval point and the biomass power plants. The biomass demand for specific biomass power plants and the capacity of the trucks used for transport, should be considered to calculate the total transport distance. In this study, the specific data, such as how much biomass is needed for biomass power plants, and which type of truck is used for transport, are not defined, thus the exact transport distance is not examined. The land cover of the four optimal sites is all cropland. Presently, a biomass power plant with 30 MW installed capacity requires 300,000 t of biomass residues annually.

Therefore, the quantity of biomass residues in the supply areas within 30 km can provide enough biomass residue for power plants with installed capacity to 80 MW.

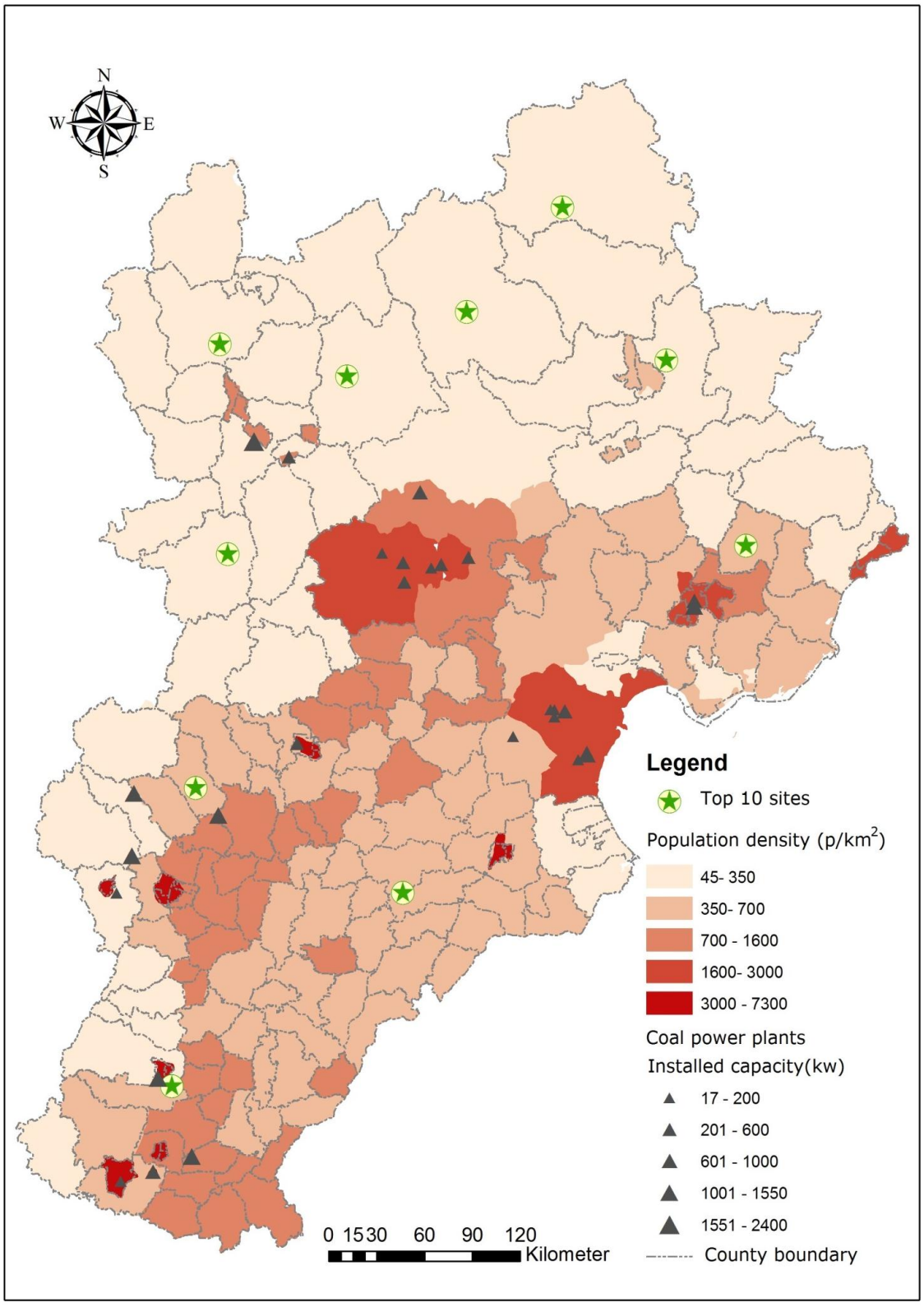

Figure 5.20 Top 10 sites for biomass power plants and existing coal power plants

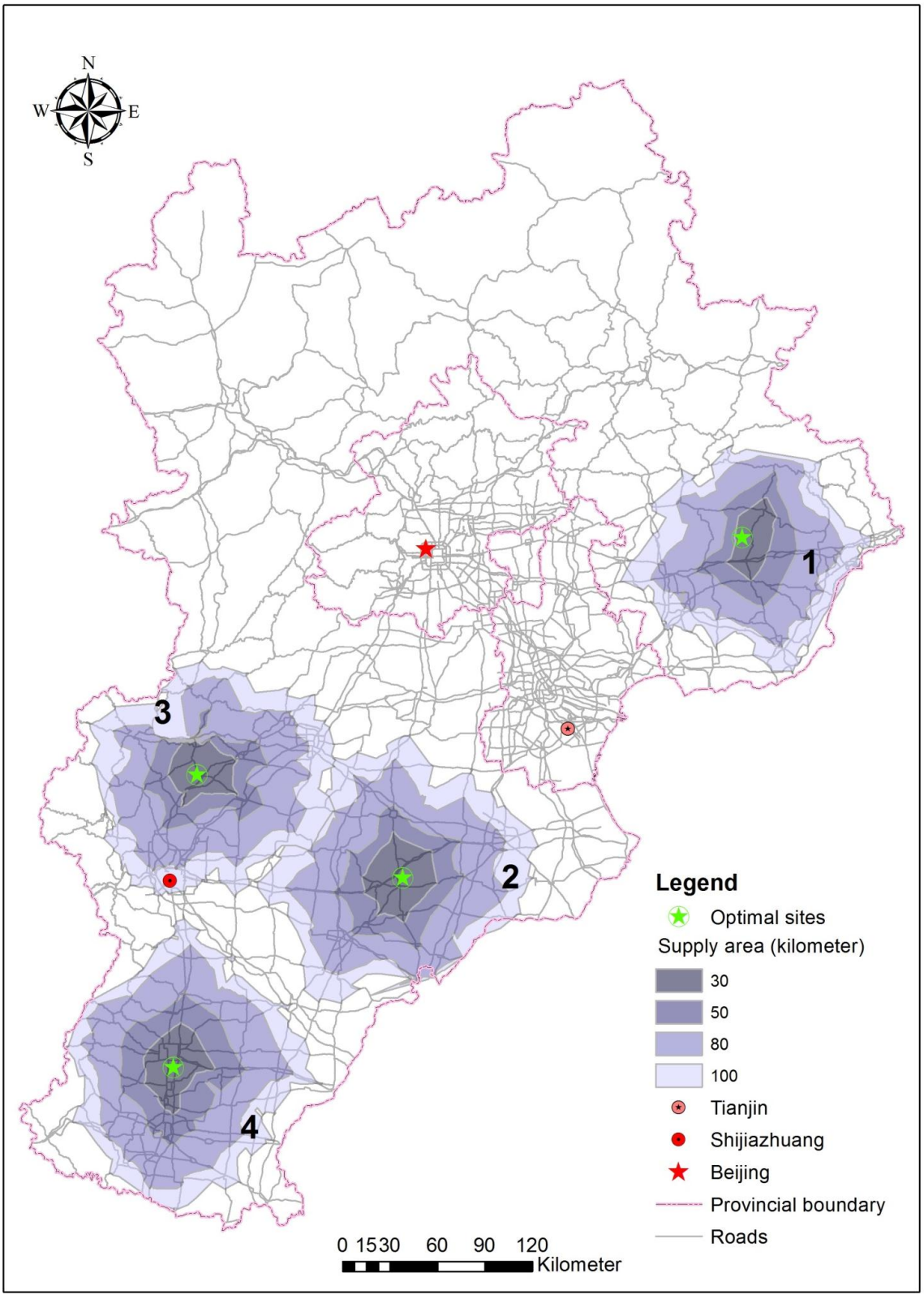

Figure 5.21 Four optimal sites of biomass power plants

Table 5.8 Statistical results of the optimal sites for biomass plats

		Site 1	Site 2	Site 3	Site 4
Biomass in each buffer of supply area (t)	30 km	851,824	1,300,380	950,318	996,159
	50 km	2,198,395	2,165,025	1,803,247	2,508,792
	80 km	6,080,394	6,219,125	5,721,685	6,050,118
	100 km	4,932,790	4,785,208	4,904,004	3,995,847
Total biomass (t)		14,063,403	14,469,738	13,379,254	13,550,916
Total transport distance (m)		38,836,891	51,281,211	48,384,518	51,265,827
Land cover type		cropland	cropland	cropland	cropland

This section showed the results of the study, namely renewable energy potential and land suitability analysis for renewable energy power plants. However, some assumptions have to be assumed in the calculation of renewable energy potential, such as the percentage of area used for solar power plants and interest rate, and some parameters are from empiric, such as energy transfer coefficient. Sensitivity analysis is conducted for major unfixed factors, but not for the all unfixed factors. These assumptions and parameters mentioned above could affect the accuracy of the results.

In the calculation of theoretical wind and solar energy potential, only 48 meteorological stations' wind speed data and daily temperature data are used for such a large study area. Therefore, the limited data affected the quality of results. Based on the previous study from other researches and published academic researches, the author defined the criteria for restricted areas of renewable energy plants without public participation and local survey. The calculation of technical wind energy potential is based on a specific type of wind turbine, and

thus the results vary with other types of wind turbine. Although these limitations of study are inevitable, the results of the study are plausible for renewable energy potential planning at regional level.

6 Conclusion and outlook

In this chapter, the conclusions derived from the key findings of the study area are presented. Based on the results and current research situation, further steps or research ideas are provided in the Outlook section.

6.1 Conclusion

The researcher presented a methodology to assess wind, solar and biomass energy potential at regional scale with the aid of GIS and RS. The methodology integrates climate resources, geographical conditions, technology characteristics, and economic variables in the evaluation of these three types of renewable energy potential from a theoretical level to the economic level. Additionally, renewable energy policy was considered because it has a significant effect on the development of renewable energy. Hebei Province, Beijing and Tianjin have been analyzed as a reference case to present this methodology. Policy makers, investors and utility companies involved in renewable energy projects can use the research to inform their decision. Based on the results and the current situation of renewable energy development in the study area, suggestions and advice are provided for renewable energy planning in the future.

Wind speed and wind power density, as the indicators used to express theoretical wind energy potential, have been spatialized and quantified. Wind speed differs over the region from 2.6 to 6.0 m/s at 80 m above the ground. Wind power density, which indicates theoretical wind power potential, varies from 4.5 to 210 w/m^2. The north-western area (the Bashang Plateau) and the eastern area near the sea are endowed with excellent wind energy resources. The area of the restricted region that is unsuitable for erecting wind turbines is 80,189 km^2, accounting for 36.9% of the total area. Taking the Vestas 82 (V82 1.65 MV) wind turbine as the reference turbine, annual wind energy yield can reach 307 TWh, whereas in 2012, total electricity consumption in the study area exceeded 467.47 TWh. Therefore, consumption far exceeds the entire technical potential of wind energy. The economic potential under the current FIT is 34 TWh, and the economic installed capacity is 32 GW. Based on the result of cost analysis, unit generation cost of power ranges from 0.07 $/kWh to more than 1 $/kWh.

The current alternative energy policy defines four wind FIT levels based on the estimated regional wind resource, ranging from 0.08 to 0.1 $/kWh. The north-western part of study area lies at the level of 0.09 $/kWh, while other regions are at the 0.1 $/kWh level. The incentive policy is critical to promote the further development of wind energy; as such, FIT policy is still required. Another opportunity for wind energy development is the reduction of wind turbine price. With the 15% and 30% reductions in cost, economic potential increases to 70 TWh/year and 122 TWh/year respectively.

Land suitability analysis for wind power plants indicates that the area defined as extremely suitable occupies 21,543 km^2, which is enough for 108 GW of installed wind power capacity. Thus, the eligible area for wind projects is adequate. In 2013, the installed wind power capacity of the study area was only around 8.96 GW. Compared to the estimated results of this study, much potential still can be exploited, as only approximately 27.8% of economic wind power potential has been exploited.

During the estimation process in this study, adjusted parameters were introduced due to the lack of adequate transmission lines and supporting infrastructure. Only 5.3 GW of the total 8.96 GW installed wind power capacity in the study area was connected to the local grid in 2013. To make full use of wind energy, supporting infrastructure and electricity grids should receive attention, especially in this study area, as the grid-connected ratio of wind- installed capacity is lower than national average level (88%). The rapid development of wind power in China increasingly is restricted by the capacity of the local grids and transmission lines, which have not kept pace with the accelerating growth in installed wind capacity. The energy planners and policy makers need to plan implementation to improve supporting infrastructure, local grids and transmission lines.

Annual solar radiation simulated through the Bristow and Campbell model ranges throughout the region from 1406 kWh/m^2 to 1960 kWh/m^2. The northern mountains area is endowed with excellent solar energy resources, and terrain largely determines the spatial distribution of solar radiation in this study area. Based on the geographical constraints defined in the study, the appropriate area for PV, where 226 PWh/year can be obtained from the solar radiation, accounted

for 60% of the total area (about 130,143 km^2). In reality, not all suitable areas can be covered by PV module; thus, a 10% area factor was considered in the calculation of the technical potential of solar energy.

The total technical potential over the region is estimated to be 2379 TWh/year for large-scale PV plants, 5 times the total electricity consumption in 2012. However, based on the supply cost curve in this study, current FIT cannot cover PV electricity generation costs. Stronger energy policy incentives are essential to stimulate the development of large-scale PV. In the assumed 0.17 $/kWh FIT scenario, economic potential would be 403.86 TWh/year; with 0.175 $/kWh, economic potential would reach 937.08 TWh/year. Hence, FIT should be increased slightly or the decentralization of small-scale PV development, such as PV modules for households or blocks of flats, should be prioritized. Moreover, a reduction in the price of PV modules can stimulate the development of large-scale PV plants. Under current FIT policy, a 5% decrease in PV module price in the study area would produce economic potential of 178.412 TWh/year, while a 10% price decrease would increase economic potential to 1251 TWh/year. Most of the extremely suitable areas are distributed in the north-eastern part of the study area, covering 10,634 km^2. The sum of the corresponding technical potential of this lands is 200 TWh/year.

Annual usable biomass residues range from 0 to 4008 t/km^2, and the amount of biomass residue is related closely to land cover type. Forest occupies the north-western part of the study area, hence biomass is abundant. The dominant land cover type in the southern part is farm land, and the residues from crops provide promising opportunities for developing biomass energy. The total annual amount of biomass available in the study area is approximately 214 million tons. According to a recent technical report, 1 kWh electricity can be produced from about 1 kg biomass by combustion technology. Therefore, the annual technical biomass power potential in this study area is 214 TWh.

The economic analysis results based on 12 MW installed capacity and 30 MW installed capacity case studies indicate that biomass power plants can be profitable without subsidy. However, all existing biomass power plants in China are unprofitable. Interruptions to biomass residue supply and difficulties with

biomass residue collection are the principal reasons. Most biomass power plants have to stop operations due to a lack of biomass residues, especially from February to July. In contrast, during August and January, biomass residues from farmland is abundant. To solve these two problems, some biomass power plants have entered into agreements with farmers to guarantee continuous biomass residue supply and purchase biomass collection machine to collect biomass residues in order to reduce the workload of collection for farmers. The issue about biomass power plants is biomass residues, such as a continuous supply, quality of biomass residues. Incentive energy policy at present is sufficient to stimulate biomass energy development.

Siting biomass power plants differ from siting wind and solar power plants, and their locations rely on the availability of resources. Biomass residue needs to be transported from retrieval points to power plants, thus optimal sites can reduce transportation costs. Once restricted areas have been excluded, the location-allocation analysis model coupled with road network information is adopted to search for optimal sites. After considering population density and existing biomass and coal power plants, the author retained only four optimal sites.

Land use for renewable energy production includes direct land use by wind turbine, solar panel and biomass plants and indirect land use. Indirect land use includes access roads, related infrastructure and other purposes. Compared to traditional energy generation, which requires land for mining and transport, renewable energy consumes less land. The land use consumption and renewable energy research from NREL in the United States shows that the average total land use requirement for PV is 3.6 acres/GWh/year (NREL, 2013). According to the existing PV power plants in China, 1 MW installed capacity needs on average more than 2.9 acres (Statistic data from Beijixing Website). Research regarding land use consumption for other renewable energy generation in China is lacking. Land use consumption by renewable energy can be reduced through deploying distributed generation technologies or brownfield development. Not all renewable energy plants occupy public open space and, for example, brownfield in an urban area can provide space for a distributed PV system. Another advantage of utilizing brownfield for renewable energy development is the usage of existing infrastructure, which can reduce investment costs.

Most of the existing research on renewable energy estimation in China estimated only theoretical or geographic renewable energy potential. Few researchers have estimated technological and economic renewable energy potential under current energy policy. Although renewable energy policies have an unavoidable influence on the development of renewable energy, few researchers have considered their effects. In this study, the researcher combined renewable energy policy and renewable energy potential and calculated economic renewable energy potential in several assumed scenarios. In addition, the problems in renewable energy development have been pointed out for wind, solar and biomass energy separately, and possible solutions have been provided. The methodology presented in this study does not have spatial limitations; policy makers, renewable energy project investors and developers, as well as energy planners in other study areas, can apply it. Policy makers can define different parameters (such as restricted areas and energy incentive policy) to analyse their effects on power generation, while energy project developers can quickly identify new profitable areas based on the land suitability analysis results in this study.

6.2 Outlook

With the presented GIS method, the researcher has achieved the three major research objectives, namely (1) to quantify and map wind energy, solar energy and bioenergy potential, (2) to define the social and environmental restrictions for wind, photovoltaic and biomass power plants, and (3) to analyse land suitability for wind, and photovoltaic power plants and to find the optimal locations for biomass power plants. Based on the research results, suggestions for renewable energy development in the future have been proposed. Nevertheless, the research still has some limitations that could be improved with further study.

The wind speed data used to estimate wind energy potential and the temperature data used to simulate solar resources are from meteorological stations, but the meteorological data from 48 national meteorological stations are available free of charge. To improve the precision of the output, more meteorological data from provincial meteorological stations or municipal meteorological stations should be obtainde.

USGS provides land cover data, and the primary land cover scheme identifies 17 land cover classes that include 11 natural vegetation classes, 3 developed and mosaicked land classes, and three non-vegetated land classes (NASA Land Data Products and Services, 2014). Although these land cover data provide detailed information about vegetation classes, detailed information about farmland classes, specifically identifying fertile and barren land, should have been classified in this study, as renewable energy power plants should avoid fertile farmland. The lack of farmland classification leads to imprecise land suitability analysis results.

PV technology and direct combustion were selected to evaluate solar energy potential and biomass potential respectively, but other technologies exist in addition to these. As the technical potential of renewable energy varies with the technologies used, identifying the type of technology that maximises renewable energy potential is an open research question for future study.

In the economic potential assessment, transmission line cost is not included due to the lack of current transmission line data. However, in renewable energy projects, transmission line costs account for a large percentage of the investment cost. For further study, transmission line costs should be considered in the economic potential assessment.

Combining renewable energy with conventional energy offers additional opportunities for utilising renewable energy. Solar power plants can be built with coal power plants. During winter, coal power can supplement solar power. Similarly, biomass power plants could be combined with coal power plants to solve the problems of interruptions biomass residues supply.

This research is the first effort to assess renewable energy potential based on GIS in this study area. The study includes the development of an overall method of estimating renewable energy potential while considering climate resources, geographical conditions, technology characteristics, economic factors and renewable energy policies. With enhanced data quality, various renewable energy technologies and combinations with conventional energy, further studies in the field could bring a greater number of promising benefits for the country and contribute to the study context.

Reference

Ahmed, M., Ahmad, F., & Akhtar, M. (2006). Assessment of wind power potential for coastal Areas of Pakistan. *Turkish Journal of Physics*, *30*, 127–136.

Akash, B. A., Mamlook, R., & Mohsen, M. S. (1999). Multi-criteria selection of electric power plants using analytical hierarchy process. *Electric Power Systems Research*, *52(1),* 29-35.

Allen, R. (1997). Self-calibrating method for estimating solar radiation from air temperature. *Journal of Hydrologic Engineering, 2,* 56–57.

Ångström A. (1924). Solar and terrestrial radiation. Report to the international commission for solar research on actinometric investigations of solar and atmospheric radiation. *Quarterly Journal of the Royal Meteorological Society*, *50*(210), 121-126.

Arán Carrión, J., Espín Estrella, A., Aznar Dols, F., Zamorano Toro, M., Rodríguez, M., & Ramos Ridao, A. (2008). Environmental decision-support systems for evaluating the carrying capacity of land areas: Optimal site selection for grid-connected photovoltaic power plants. *Renewable and Sustainable Energy Reviews*, *12*, 2358–2380.

Archer, C. L., & Jacobson, M. Z. (2005). Evaluation of global wind power. *Journal of Geophysical Research: Atmospheres*, *110*(D12).

ArcGIS Help 10.1 - Understanding solar radiation analysis. (n.d.). Retrieved from http://resources.arcgis.com/en/help/main/10.1/009z/009z000000t8000000.html Accessed 15.06.2013.

Arnette, A. N., & Zobel, C. W. (2011). Spatial analysis of renewable energy potential in the greater southern Appalachian mountains. *Renewable Energy*, *36*, 2785–2798.

Baccini, A., Fruedl, M., Woodcock, C., & Warbington, R. (2004). Forest biomass estimation over regional scales using multisource data. *Geophysical research letters, 31(10).*

Ball, R. A., Purcell, L. C., & Carey, S. k. (2004). Evaluation of solar radiation prediction models in North America. *Agronomy Journal*, *96*(2), 391-397.

Beijixing's website. http://guangfu.bjx.com.cn/news/20151211/690651-41.shtml Accessed 25.09.2014

Ben Salah, C., Chaabene, M., & Ben Ammar, M. (2008). Multi-criteria fuzzy algorithm for energy management of a domestic photovoltaic panel. *Renewable Energy*, *33*, 993–1001.

Bennui, A., Rattanamanee, P., Puetpaiboon, U., Phukpattaranont, P., & Chetpattananondh, K. (2007). Site selection for large wind turbine using GIS. In PSU-UNS International Conference on Engineering and Environment, 561-566.

Bi, Y., Gao, C., Wang, Y., & Li, B. (2009). Estimation of straw resources in China, *Transactions of the Chinese Society of Agricultural Engineering, 25(12)*, 211–217.

Bristow, K. L., & Campbell, G. S. (1984). On the relationship between incoming solar radiation and daily maximum and minimum temperature. Agricultural and Forest Meteorology, 31, 159–166.

Brown, S., & Gaston, G. (1995). Use of forest inventories and geographic information systems to estimate biomass density of tropical forests: Application to tropical Africa. *Environmental Monitoring and Assessment*, *38*(2-3), 157-168.

Buflasa, H., Infield, D., & Thomson, M. (2008). Wind resource assessment for the Kingdom of Bahrain. *Wind Engineering, 32*(5), 439-448.

China Statistical Bureau. (2013). China statistical yearbook. Beijing.

Cadenas, E., & Rivera, W. (2007). Wind speed forecasting in the South Coast of Oaxaca, México. *Renewable Energy*, *32*, 2116–2128.

Chang, T. J, Wu, Y. T., Hsu, H. Y., Chu, C. R. & Liao, C. M. (2003). Assessment of wind characteristics and wind turbine characteristics in Taiwan. *Renewable Energy* 28(6), 851–871

Charabi, Y., & Gastli, A. (2010). GIS assessment of large CSP plant in Duqum, Oman. *Renewable and Sustainable Energy Reviews*, *14*, 835–841.

Charabi, Y., & Gastli, A. (2011). PV site suitability analysis using GIS-based spatial fuzzy multi-criteria evaluation. *Renewable Energy*, *36*, 2554–2561.

Cheng, E. W. L., & Li, C. (2005). Analytic network process applied to project selection. *Journal of construction engineering and management, 131(4), 459-466.*

Chen, R., Ersi, K., Yang, J., Lu, S., & Zhao, W. (2004). Validation of five global radiation models with measured daily data in China. *Energy Conversion and Management*, *45*, 1759–1769.

China Electricity Council, 2013 http://english.cec.org.cn/ Accessed 25.05.2014

Coskun, C., Oktay, Z., & Dincer, I. (2011). Estimation of monthly solar radiation distribution for solar energy system analysis. *Energy*, *36*, 1319–1323.

Dai, L., Li, J., & Overend, R. MOA/DOE Project Expert Team (1998). Biomass Energy Conversion Technologies in China: Development and Assessment.

Domínguez Bravo, J., García Casals, X., & Pinedo Pascua, I. (2007). GIS approach to the definition of capacity and generation ceilings of renewable energy technologies. *Energy Policy*, *35*, 4879–4892.

EIA, U. (2011). International energy outlook 2011. US Energy Information Administration

Elamouri, M., & Ben Amar, F. (2008). Wind energy potential in Tunisia. *Renewable Energy*, *33*, 758–768.

Furlan, C., Oliveira, A. P. de, Soares, J., Codato, G., & Escobedo, J. F. (2012). The role of clouds in improving the regression model for hourly values of diffuse solar radiation. *Applied Energy*, *92*, 240–254.

Gastli, A., & Charabi, Y. (2010). Solar electricity prospects in Oman using GIS-based solar radiation maps. *Renewable and Sustainable Energy Reviews*, *14*, 790–797.

Gillespie, A. J., Brown, S., & Lugo, A. E. (1990). Tropical forest biomass estimation from truncated stand tables. *Forest Ecology and Management, 48*(1), 69-87.

Grady, D.O. (2002). Public Attitudes Toward Wind Energy in Western. http://energy.appstate.edu/sites/energy.appstate.edu/files/wnc_pubsurvey.pdf. Accessed 15.06.2014.

Graham, R., Liu, W., & Jager, H. (1996). A regional scale GIS-based modeling system for evaluating the potential costs and supplies of biomass from biomass crops. *InProceedings of BIOENERGY,15-20*

Grassi, S., Chokani, N., & Abhari, R. S. (2012). Large scale technical and economical assessment of wind energy potential with a GIS tool: Case study Iowa. 03 GIS and Wind. *Energy Policy*, *45*, 73–85.

Greening, L. A., & Bernow, S. (2004). Design of coordinated energy and environmental policies: use of multi-criteria decision-making. *Energy Policy*, *32*, 721–735.

Gurel, A. E., & Ergun, A. (2012). Estimation of global solar radiation on horizonal surface using meteorological data. *Energy Education Science and Technology Part A: Energy Science and Research*, *28*, 947–954.

Haaren, R., & Fthenakis, V. (2011). GIS-based wind farm site selection using spatial multi-criteria analysis (SMCA): Evaluating the case for New York State. Renewable and Sustainable Energy Reviews, 15, 3332–3340.

Hammer, A., Heinemann, D., Hoyer, C., Kuhlemann, R., Lorenz, E., Müller, R., & Beyer, H. G. (2003a). Solar energy assessment using remote sensing technologies. Remote Sensing of Environment, 86, 423–432.

Hammer, A., Heinemann, D., Hoyer, C., Kuhlemann, R., Lorenz, E., Müller, R., & Beyer, H. G. (2003b). Solar energy assessment using remote sensing technologies. *Remote Sensing of Environment*, *86*, 423–432.

Hellmann, G. (1914). *Über die Bewegung der Luft in den untersten Schichten der Atmosphäre*. Reimer: Akademie der Wissenschaften.

He, Y., Xia, T., Liu, Z., Zhang, T., & Dong, Z. (2013). Evaluation of the capability of accepting large-scale wind power in China. *Renewable and Sustainable Energy Reviews*, *19*, 509–516.

Hofierka, J., & Kaňuk, J. (2009). Assessment of photovoltaic potential in urban areas using open-source solar radiation tools. *Renewable Energy*, *34*, 2206–2214.

Hoogwijk, M. M. (2004). On the global and regional potential of renewable energy sources. *University of Utrecht PhD Thesis*.

Hossain, J. (1989). Estimation of specific annual energy generation from wind in Antarctica. *Solar & Wind Technology*, *6*, 91–95.

Hossain, J., Sinha, V., & Kishore, V. (2011). A GIS based assessment of potential for windfarms in India. *Renewable Energy*, *36*, 3257–3267.

Intergovernmental Panel on Climate Chang.(2013). http://www.accuweather.com/en/weather-blogs/climatechange/key-points-from-the-latest-ipc/18226513 Accessed 12.11.2013

Izquierdo, S., Dopazo, C., & Fueyo, N. (2010). Supply-cost curves for geographically distributed renewable-energy resources. *Energy Policy*, *38*, 667–672.

Janjai, S., Pankaew, P., & Laksanaboonsong, J. (2009). A model for calculating hourly global solar radiation from satellite data in the tropics. *Applied Energy*, *86*, 1450–1457.

Janjai, S., Sricharoen, K., & Pattarapanitchai, S. (2011). Semi-empirical models for the estimation of clear sky solar global and direct normal irradiances in the tropics. *Applied Energy*, *88*, 4749–4755.

Janke, J. R. (2010). Multicriteria GIS modeling of wind and solar farms in Colorado. *Renewable Energy*, *35*, 2228–2234.

Jiang, B., Zhao, S., Ma, Z., Hou, P., & Xu, H. (2010). Temporal spatial distribution of the wind energy in Liaoning littoral. *Marine Science*, *35*, 56–62.

Justus, C., Hargraves, W., Mikhail, A., & Graber, D. (1978). Methods for estimating wind speed frequency distributions. *Journal of Applied Meterology*, *17*, 350–353.

Kaldellis, J. (2005). Social attitude towards wind energy applications in Greece. *Energy Policy*, *33*, 595–602.

Kasten, F., & Czeplak, G. (1980). Solar and terrestrial radiation dependent on the amount and type of cloud. *Solar energy, 24(2), 177-189.*

Katiyar, A. K., & Pandey, C. K. (2013). A Review of Solar Radiation Models—Part I. *Journal of Renewable Energy*, *2013*, 1–11.

Klinge, H., Rodrigues, W. A., Brunig, E., & Fittkau, E. J. (1975). *Biomass and structure in a central amazonian rain forest*: Springer Berlin Heidelberg.

Korachagaon, I. (2012) Estimating Global Solar Radiation Potential for Brazil by Iranna-Bapat's Regression Models. International journal of Emerging Technology and Advanced Engineering, 2(2).

Kose, R., Ozgur, M. A., Erbas, O., & Tugcu, A. (2004). The analysis of wind data and wind energy potential in Kutahya, Turkey. *Renewable and Sustainable Energy Reviews*, *8*, 277–288.

Kreith, F., & Kreider, J. F. (1978). Principles of solar engineering. Washington, DC, Hemisphere Publishing Corp., 1978. 790 p., 1.

Stoddard, L. E., Abiecunas, J., & O'Connell, R. (2006). Economic, energy, and environmental benefits of concentrating solar power in California. National Renewable Energy Laboratory.

Liao, C., Yan, Y., Wu, C., & Huang, H. (2004). Study on the distribution and quantity of biomass residues resource in China. *Biomass and Bioenergy*, *27*, 111–117.

Lima, L. d. A., & Filho, C. R. B. (2012). Wind resource evaluation in São João do Cariri (SJC) – Paraiba, Brazil. *Renewable and Sustainable Energy Reviews*, *16*, 474–480.

Liu, F. (2012). *Case-study on biomass combustion power generation in China*. *Master Thesis,* Göteborg, Sweden.

Liu,Y.J. & Pan, T. (2012).Spatial simulation of China's land surface solar radiation resources. *Journal of Natural Resources, 8, 014.*

Lu, D. (2006). The potential and challenge of remote sensing‐based biomass estimation. *International Journal of Remote Sensing*, *27*, 1297–1328.

Lu, D., & Batistella, M. (2005). Exploring TM image texture and its relationships with biomass estimation in Rondonia, Brazilian Amazon. *Acta Amazonica, 35*(2), 249-257.

Luo, L., Hamilton, D., & Han, B. (2010). Estimation of total cloud cover from solar radiation observations at Lake Rotorua, New Zealand. *Solar Energy*, *84*, 501–506.

Madlener, R., Antunes, C. H., & Dias, L. C. (2009). Assessing the performance of biogas plants with multi-criteria and data envelopment analysis. *European Journal of Operational Research*, *197*, 1084–1094.

Madlener, R., & Stagl, S. (2005). Sustainability-guided promotion of renewable electricity generation. *Ecological Economics*, *53*, 147–167.

Ma, J., Scott, N. R., DeGloria, S. D., & Lembo, A. J. (2005). Siting analysis of farm-based centralized anaerobic digester systems for distributed generation using GIS. *Biomass and Bioenergy*, *28*, 591–600.

Mamlook, R., Akash, B. A., & Nijmeh, S. (2001). Fuzzy sets programming to perform evaluation of solar systems in Jordan, *Energy Conversion and Management, 42(14),* 1717-1726.

Maxwell, E. (1998). METSTAT—The solar radiation model used in the production of the National Solar Radiation Data Base (NSRDB). *Solar Energy*, *62*, 263–279.

MCD12Q1 | LP DAAC :: NASA Land Data Products and Services. (n.d.).Retrieved from https://lpdaac.usgs.gov/products/modis_products_table/mcd12q1

Mendoza, G. (1997). A GIS-based multicriteria approach to land suitability assessment and allocation. United States Department Of Agriculture Forest Service General Technical Report NC, 89-94.

Mikhail, A. S. (1985). Height extrapolation of wind data. *Journal of Solar Energy Engineering, 107(1),* 10-14.

Miller, A. E. (2008). Patterns of avian and bat mortality at a utility scaled wind farm on the southern high plains. http://gods001.rw.ttu.edu/boal/CWBoal%20web/Web%20PDFs/Miller%20Thesis.pdf. Accessed 15.06.2014.

Montague, L., Slayton, A., & Lukas, J. (2002). Lignocellulosic biomass to ethanol process design and economics utilizing co-current dilute acid prehydrolysis and enzymatic hydrolysis for corn stover. *NREL Technical Report 2002.*

Moon, J.-H., Lee, J.-W., & Lee, U.-D. (2011). Economic analysis of biomass power generation schemes under renewable energy initiative with Renewable Portfolio Standards (RPS) in Korea. *Bioresource Technology*, *102*, 9550–9557.

Mortensen, N. G., Landberg, L., Troen, I., & Lundtang Petersen, E. (1993). *Wind Atlas Analysis and Application program*: Risø National Laboratory.

National development and reform commission (2005). Renewable energy generated electrical pricing and fee sharing management rules. http://www.gov.cn/ztzl/2006-01/20/content_165910.htm Accessed 10.06.2014

Nedaei, M. (2012). Wind energy potential assessment in chalus county in Iran.International Journal of Renewable Energy Research , 2(2), 338-347.

Netherlands Environmental Assessment Agency (2013). Trends in global CO2 emissions report. See

http://edgar.jrc.ec.europa.eu/news_docs/pbl-2013-trends-in-global-co2-emissions-2013-report-1148.pdf (accessed on 08. 04.2014)

Nguyen, H., & Pearce, J. (2010). Estimating potential photovoltaic yield with r.sun and the open source Geographical Resources Analysis Support System. *Solar Energy*, *84*, 831–843.

National Renewable Energy Laboratory. (2013). Land-Use Requirements for Solar Power Plants in the United States. See http://www.nrel.gov/docs/fy13osti/56290.pdf (accessed on 8th April 2015)

Oberschmidt, J., Geldermann, J., Ludwig, J., & Schmehl, M. (2010). Modified PROMETHEE approach for assessing energy technologies. *International Journal of Energy Sector Management*, *4*, 183–212.

Odo, F., Offiah, S. U., & Ugwuoke, P. (2012). Weibull distribution-based model for prediction of wind potential in Enugu, Nigeria. *Adv Appl Sci Res, 3(2),* 1202-1208.

Overman, J. P. M., Witte, H. J. L., & Saldarriaga, J. G. (1994). Evaluation of regression models for abover ground biomass determination in Amazon Rainforet. *Journal of tropical Ecology, 10(02),* 207-218.

Pan, T., Wu, S., Dai, E., & Liu, Y. (2013). Estimating the daily global solar radiation spatial distribution from diurnal temperature ranges over the Tibetan Plateau in China. *Applied Energy*, *107*, 384–393.

Perpiñá, C., Alfonso, D., Pérez-Navarro, A., Peñalvo, E., Vargas, C., & Cárdenas, R. (2009). Methodology based on Geographic Information Systems for biomass logistics and transport optimisation. *Renewable Energy*, *34*, 555–565.

Pinard, J., Benoit, R., & Yu, W. (2005). A WEST Wind Climate Simulation of the Mountainous Yukon. *ATMOSPHERE-OCEAN*, *43*, 259–282.

Pohekar, S., & Ramachandran, M. (2004). Application of multi-criteria decision making to sustainable energy planning—A review. *Renewable and Sustainable Energy Reviews*, *8*, 365–381.

Qin, J., Chen, Z., Yang, K., Liang, S., & Tang, W. (2011). Estimation of monthly-mean daily global solar radiation based on MODIS and TRMM products. *Applied Energy*, *88*, 2480–2489.

Ramanathan, R., & Ganesh, L. S. (1993). A multiobjective programming approach to energy resource allocation problems. International journal of energy research, *17*(2), 105-119.

Ranta, T. (2005). Logging residues from regeneration fellings for biofuel production–a GIS-based availability analysis in Finland. Biomass and Bioenergy, *28*(2), 171-182.

Renne, D. S., Perez, R., Zelenka, A., Whitlock, C. H., & DiPasquale, R. C. (1999). Use of weather and climate research satellites for estimating solar resources. BIOPROCESS TECHNOLOGY, 13, 171-240.

Rio, J., Simões, T., & Estanqueiro, A. (2006). Monthly Forecasts of the average wind speed in Portugal. *In: Proceedings of the European Wind Energy Conference 2006, Athens, Greece*.

Saaty, T. L. (1980). The analytic hierarchy process: planning, priority setting, resources allocation. *New York: McGraw*

Saaty, T. L. (1996). Decision making with dependence and feedback: The analytic network process. *Pittsburgh: RSW publications.*

Saaty, T. L., & Vargas, L. G. (2006). Decision making with the analytic network process. *Springer Science+ Business Media, LLC.*

Şenkal, O., & Kuleli, T. (2009). Estimation of solar radiation over Turkey using artificial neural network and satellite data. *Applied Energy*, *86*, 1222–1228.

Serwan M.J. Baban, T. P. (2001). Developing and applying a GIS-assisted approach to locating wind farms in the UK. *Renewable Energy*, 59–71.

Shi, X., Elmore, A., Li, X., Gorence, N. J., Jin, H., Zhang, X., & Wang, F. (2008). Using spatial information technologies to select sites for biomass power plants: A case study in Guangdong Province, China. *Biomass and Bioenergy*, *32*, 35–43.

Simao, A., Densham, P. J., & Haklay, M. M. (2009). Web-based GIS for collaborative planning and public participation: An application to the strategic planning of wind farm sites. *Journal of Environmental Management*, *90*(6), 2027-2040.

Scanlan, R. H., & Simiu, E. (1996). Wind Effects on Structures: Fundamentals and Applications to Design. *Wiley*

Sisterson, D. L., & Frenzen, P. (1978). Nocturnal boundary-layer wind maxima and the problem of wind power assessment. *Environmental Science & Technology, 12*(2), 218-221.

Sliz-Szkliniarz, B., & Vogt, J. (2011). GIS-based approach for the evaluation of wind energy potential: A case study for the Kujawsko–Pomorskie Voivodeship. *Renewable and Sustainable Energy Reviews*, *15*, 1696–1707.

Storm, B., Dudhia, J., Basu, S., Swift, A., & Giammanco, I. (2009). Evaluation of the Weather Research and Forecasting model on forecasting low-level jets: implications for wind energy. *Wind Energy*, *12*, 81–90.

Sun, G., Ranson, K. J., & Kharuk, V. I. (2002). Radiometric slope correction for forest biomass estimation from SAR data in the Western Sayani Mountains, Siberia. *Remote Sensing of Environment, 79*(2), 279-287.

Sun, Y.-w., Hof, A., Wang, R., Liu, J., Lin, Y.-j., & Yang, D.-w. (2013). GIS-based approach for potential analysis of solar PV generation at the regional scale: A case study of Fujian Province. *Energy Policy*, *58*, 248–259.

Šúri, M., & Hofierka, J. (2004). A new GIS‐based solar radiation model and its application to photovoltaic assessments. *Transactions in GIS, 8*(2), 175-190.

Šúri, M., Huld, T. A., & Dunlop, E. D. (2005). PV-GIS a web based solar radiation database for the calculation of PV potential in Europe. *International journal of sustainbale energy*, *24*, 55–67.

Šúri, M., Huld, T. A., Dunlop, E. D., & Ossenbrink, H. A. (2007). Potential of solar electricity generation in the European Union member states and candidate countries. *Solar Energy*, *81*, 1295–1305.

Taha, R. A., & Daim, T. (2013). Multi-criteria applications in renewable energy analysis, a literature review. In Research and Technology Management in the Electricity Industry (pp. 17-30). Springer London.

Takle, E. S. & Brown, J. M. (1978). Note on the use of Weibull statistics to characterize wind-speed data, Journal of Applied Meteorology, 17,556-559

Tao, Y. X., & Rayegan, R. (2011). Solar Energy Applications and Comparisons.Energy and Power Generation Handbook, Editor: KR Rao, Publisher: ASME Press.

Thek, G. (2004). Techno-economic evaluation of selected decentralised CHP applications based on biomass combustion in IEA partner countries. Graz, Austria: Bioenergiesysteme GmbH.

Thenkabail, P. S., Stucky, N., Griscom, B. W., Ashton, M. S., Diels, J., Van Der Meer, B., & Enclona, E. (2004). Biomass estimations and carbon stock calculations in the oil palm plantations of African derived savannas using IKONOS data. *International Journal of Remote Sensing, 25*(23), 5447-5472.

Thinh, N. X., & Vogel, R. (2007). Application of the analytic hierarchy process in the multiple criteria decision analysis of retention areas for flood risk management. *Environmental Informatics and Systems Research*. *EnviroInfo Warsaw*, 675-682

Thornton, P. E., & Running, S. W. (1999). An improved algorithm for estimating incident daily solar radiation from measurements of temperature, humidity, and precipitation. *Agricultural and Forest Meteorology*, *93*, 211–228.

Tiwari, A. K., & Singh, J. S. (1984). Mapping forest biomass in India through aerial photographs and nondestructive field sampling. *Applied Geography*, *4*(2), 151-165.

Tomberlin, G., & Mosey, G. (2013). *Feasibility Study of Economics and Performance of Biomass Power Generation at the Former Farmland Industries Site in Lawrence, Kansas*.

Troen, I. E. L. P., & Petersen, E. L. (1989). *European wind atlas*.

US Department of Energy (1997). Renewable Energy Technology Characterizations: Topical Report TR-109496. http://infohouse.p2ric.org/ref/36/35405.pdf. Accessed 05.06.2014.

USGS. Land cover type yearly L3 global 500m SIN Grid. https://lpdaac.usgs.gov/products/modis_products_table/mcd12q1. Accessed 04.05.2013.

USGS. Terra/MODIS Net Primary Production Yearly L4 Global 1km. https://lpdaac.usgs.gov/products/modis_products_table/mod17a3. Accessed 04.03.2013.

Vestas's website. https://www.vestas.com/ Accessed 15.08.2013

Voivontas, D. (2001). Assessment of biomass potential for power production: a GIS based method. 01 Biomass and GIS. *BIOMASS & BIOENERGY*, *20*, 101–112.

Voivontas, D. (1998). Evaluation of renewable energy potential using a gis decision support system. 01 GIS and Wind. *Renewable Energy*, *13*, 333–344.

Walmsley, J., & Salmon, J. (1989). *MS-Micro/2 User's Manual: Second Ed:*. Ontario, Canada: Canadian Climate Centre.

Wang, J.-J., Jing, Y.-Y., Zhang, C.-F., & Zhao, J.-H. (2009). Review on multi-criteria decision analysis aid in sustainable energy decision-making. *Renewable and Sustainable Energy Reviews*, *13*, 2263–2278.

Wang, M., Lin, S. J., & Lo, Y. C. (2010, December). The comparison between MAUT and PROMETHEE. In Industrial Engineering and Engineering Management (IEEM), *2010 IEEE International Conference on* (pp. 753-757). IEEE.

Wang, Z., Ding, L., Huang, T., & Zhi, S. (2012). Using 10m wind speed to calculate average wind power density at wheel height of wind turbines. *Meteorological Science and Technology*, *40*, 680–684.

Wijk, A. J. M., & Coelingh, J. P. (1993). Wind power potential in the OECD Countries, Utrecht University, Department of Science, Technology and Society, pp: 35

World energy council. (2013). World energy resource http://www.worldenergy.org/wpcontent/uploads/2013/09/Complete_WER_2013_Survey.pdf (online pdf)

WRF(http://www.wrf-model.org/index.php) Accessed 14.04.2014

Wu, C. Z., Huang, H. A. I. T. A. O., Zheng, S. P., & Yin, X. L. (2002). An economic analysis of biomass gasification and power generation in China. *Bioresource Technology*, *83*(1), 65-70.

Wu, C., Yin, X., Yuan, Z., Zhou, Z., & Zhuang, X. (2010). The development of bioenergy technology in China. *Energy*, *35*, 4445–4450.

Yim, S. H. L., Fung, J. C. H., Lau, A. K. H., & Kot, S. C. (2007). Developing a high-resolution wind map for a complex terrain with a coupled MM5/CALMET system. *Journal of Geophysical Research*, *112*.

Yue, C.-D., & Wang, S.-S. (2006). GIS-based evaluation of multifarious local renewable energy sources: a case study of the Chigu area of southwestern Taiwan. *Energy Policy*, *34*, 730–742.

Yu, W., Benoit, R., Girard, C., Glazer, A., Lemarquis, D., Salmon, J., & Pinard, J. P. (2006). Wind Energy Simulation Toolkit (WEST): A wind mapping system for use by the WindEnergy Industry. *Wind Engineering*, *30*(1), 15-33.

Zadeh, L. A. (1965). Fuzzy sets. *Information and control*, *8*(3), 338-353.

Zarzo, M., & Martí, P. (2011). Modeling the variability of solar radiation data among weather stations by means of principal components analysis. *Applied Energy*, *88*, 2775–2784.

ZHAN, F., CHEN, X., NOON, C., & WU, G. (2005). A GIS-enabled comparison of fixed and discriminatory pricing strategies for potential switchgrass-to-ethanol conversion facilities in Alabama. *Biomass and Bioenergy*, *28*, 295–306.

Zhang, D., Xiong, W., Tang, C., Liu, Z., & Zhang, X. (2014). Determining the appropriate amount of subsidies for wind power: The integrated renewable power planning (IRPP) model and its application in China. *Sustainable Energy Technologies and Assessments*, *6*, 141–148.

Zhang, S., & He, Y. (2013). Analysis on the development and policy of solar PV power in China. *Renewable and Sustainable Energy Reviews*, *21*, 393–401.

Zheng, D., Rademacher, J., Chen, J., Crow, T., Bresee, M., Le Moine, J., & Ryu, S.-R. (2004). Estimating aboveground biomass using Landsat 7 ETM+ data across a managed landscape in northern Wisconsin, USA. *Remote Sensing of Environment*, *93*, 402–411.

Zhou, W., Yang, H., & Fang, Z. (2006). Wind power potential and characteristic analysis of the Pearl River Delta region, China. *Renewable Energy*, *31*, 739–753.

Zhuang, D., Jiang, D., Liu, L., & Huang, Y. (2011). Assessment of bioenergy potential on marginal land in China. *Renewable and Sustainable Energy Reviews*, *15*, 1050–1056

EIDESSTATTLICHE VERSICHERUNG

Hiermit versichere ich an Eides statt, dass ich die vorliegende Dissertationsschrift zum Thema

"Assessment of renewable energy potentials based on GIS and RS-

A case study in China"

selbstständig verfasst und keine anderen als die angegebenen Quellen benutzt habe. Alle Stellen, die wörtlich oder sinngemäß aus Quellen entnommen wurden, habe ich als solche gekennzeichnet.

Des Weiteren erkläre ich an Eides statt, dass diese Arbeit weder in gleicher noch in ähnlicher Fassung einer akademischen Prüfung vorgelegt wurde.

Dortmund, 19.05.2015 Jie Zhang